

Patterns of Astragalar Fibular Facet Orientation in Extant and Fossil Primates and Their Evolutionary Implications

Doug M. Boyer^{1*} and Erik R. Seiffert²

¹Department of Evolutionary Anthropology, Duke University, Durham, NC 27708

²Department of Anatomical Sciences, Stony Brook University, Health Sciences Center T-8, Stony Brook, NY 11794-8081

KEY WORDS astragalus; talus; fibula; haplorhine; strepsirrhine; ancestral states; *Cantius*; *Teilhardina*

ABSTRACT A laterally sloping fibular facet of the astragalus (=talus) has been proposed as one of few osteological synapomorphies of strepsirrhine primates, but the feature has never been comprehensively quantified. We describe a method for calculating fibular facet orientation on digital models of astragali as the angle between the planes of the fibular facet and the lateral tibial facet. We calculated this value in a sample that includes all major extant primate clades, a diversity of Paleogene primates, and nonprimate euarchontans ($n = 304$). Results show that previous characterization of a divide between extant haplorhines and strepsirrhines is accurate, with little overlap even when individual data points are considered. Fibular facet orientation is conserved in extant strepsirrhines despite major differences in locomotion and body size, while extant anthropoids are more variable (e.g., low values for

catarrhines relative to non-callitrichine platyrrhines). Euprimate outgroups exhibit a mosaic of character states with *Cynocephalus* having a more obtuse strepsirrhine-like facet and sampled treeshrews and plasiadapiforms having more acute haplorhine-like facets. Surprisingly, the earliest species of the adapiform *Cantius* have steep haplorhine-like facets as well. We used a Bayesian approach to reconstruct the evolution of fibular facet orientation as a continuous character across a supertree of living and extinct primates. Mean estimates for crown Primatomorpha (97.9°), Primates (99.5°), Haplorhini (98.7°), and Strepsirrhini (108.2°) support the hypothesis that the strepsirrhine condition is derived, while lower values for crown Anthropoidea (92.8°) and Catarrhini (88.9°) are derived in the opposite direction. *Am J Phys Anthropol* 151:420–447, 2013. © 2013 Wiley Periodicals, Inc.

Beard et al. (1988), Gebo (1988, 1993, 2011), Gebo et al. (1991, 2000, 2001), Dagosto (1993), Dagosto and Gebo (1994), Dagosto et al. (2008), Williams et al. (2009, 2010), Boyer et al. (2010), Maiolino et al. (2012), and many others have assessed trait variation among primates with the goal of determining potential synapomorphies of a monophyletic Strepsirrhini (i.e., the extant primate clade that includes the “toothcombed” lemuriform and loriform primates). The slope of the fibular facet of the astragalus has received considerable attention because astragali are relatively common in the early primate fossil record, and the feature is ostensibly both easy to evaluate and consistently distinguishes strepsirrhines from haplorhines (Beard et al., 1988; Gebo, 1988, 1993, 2011; Gebo et al., 2001). Fibular facet orientation has been particularly important for debates surrounding the phylogenetic position of the earliest crown primates, adapiforms and omomyiforms. Adapiforms have consistently been described as having laterally sloping fibular facets like those of extant strepsirrhines, while omomyiforms have been described as having more acute haplorhine-like fibular facets (e.g., Gebo, 1988, 2011; Gebo et al., 2012). The adapiform-strepsirrhine condition has been interpreted as apomorphic relative to that of the primate common ancestor and supporting the placement of adapiforms as stem members of Strepsirrhini (Beard et al., 1988; Gebo, 1988, 2011; Gebo et al., 2012).

As obvious as this feature would appear to be, debate surrounding the middle Eocene Messel adapiform

Darwinius masillae has exposed ambiguity in the identification and phylogenetic interpretation of fibular facet orientation. *Darwinius* was described as having a straight-sided haplorhine-like facet (Franzen et al., 2009), but other researchers debated the accuracy of this assessment because the astragalar trochlea is not visible in the flattened specimen, and the fibular facet is largely obscured by the articulating fibular malleolus (Seiffert et al., 2009; Williams et al., 2009; Boyer et al., 2010). Therefore, even this linchpin feature has been muddied by differences in perspective in the absence of quantification. This calls into question the reliability of previous subjective assessments of this trait and reveals the need

Grant sponsor: NSF; Grant number: BCS 1317525 (formerly BCS 1125507) and BCS 1231288 (to D.B. and E.S.); Grant sponsor: American Association of Physical Anthropologists Professional Development Grant (in 2009 to D.B.); Grant sponsor: NSF DDIG; Grant number: SBE-1028505 (to S.C.).

*Correspondence to: Doug M. Boyer, Department of Evolutionary Anthropology, Duke University, Durham, NC 27708, USA. E-mail: douglasmb@gmail.com

Received 7 January 2013; accepted 28 March 2013

DOI: 10.1002/ajpa.22283
Published online in Wiley Online Library
(wileyonlinelibrary.com).

for a more objective, quantitative approach to its evaluation. Boyer et al. (2010) measured this angle on a small sample of digital models, and Rose et al. (2011) used the same method to estimate the angle in earliest Eocene *Teilhardina brandti*. This first attempt at quantification of fibular facet orientation is, however, difficult to replicate because of sensitivity to landmark choice.

Here we describe a new method for assessing fibular facet orientation and demonstrate that it has high repeatability (less than 2% error on average). Use of 3D digital models from high-resolution μ CT scans allowed us to obtain data from the largest and smallest primates—ranging in size from approximately 70 g to 200,000 g—with the same measurement control and allowed us to calculate rather than measure fibular facet orientation, further reducing the potential for bias and interobserver error. We present fibular facet orientation for 304 euarchontans, of which 291 are euprimates (probable crown primates/“primates of modern aspect”), and reconstruct the evolutionary history of the trait within a Bayesian framework.

MATERIALS AND METHODS

Materials

Our sample of euarchontan astragali numbers 304 individuals, including 125 anthropoids (110 extant, 15 fossil), 6 extant tarsiiids, 86 extant strepsirrhines, 51 fossil adapiforms, 23 omomyiforms, 4 fossil plesiadapiforms, 3 extant dermopterans, and 6 extant scandentians (Tables 1 and 2; Fig. 1; Appendix).

Institutional abbreviations

AMNH, American Museum of Natural History, New York, NY; CGM, Egyptian Geological Museum, Cairo, Egypt; DPC, Duke Lemur Center Division of Fossil Primates, Durham, NC; CM, Carnegie Museum of Natural History, Pittsburgh, PA; GU, H.N.B. Garhwal University, Srinagar, Uttarakhand, India; HTB, Cleveland Museum of Natural History, Hamann-Todd non-human primate osteological collection, Cleveland, OH; IRSNB, Institut Royal des Sciences Naturelles de Belgique, Brussels, Belgium; IVPP, Institute of Vertebrate Paleontology and Paleoanthropology, Chinese Academy of Sciences, Beijing, China; MCZ, Museum of Comparative Zoology, Harvard University, Cambridge, MA; MNHN, Muséum National d'Histoire Naturelle, Paris, France; NMB, Naturhistorisches Museum Basel, Basel, Switzerland; NMNH, Smithsonian Institution National Museum of Natural History, Washington, D.C.; NYCEP, New York Consortium in Evolutionary Primatology, New York, NY; SBU, Stony Brook University, Stony Brook, NY; SDNHM, San Diego Natural History Museum, San Diego, CA; UCM, University of Colorado Museum of Natural History, Boulder, CO; UF, University of Florida, Florida Museum of Natural History, Gainesville, FL; UM, University of Michigan, Ann Arbor, MI; USGS, U.S. Geological Survey, Denver, CO; UNSM, University of Nebraska Science Museum, Lincoln, NB; USNM, United States National Museum, Smithsonian Institute, Washington, DC.

METHODS

Generation of digital sample

All measurements were taken on 3D digital surface models. These were created by various scanning

modalities. Most specimens were scanned using one of four instruments: at SBU, two different ScancoMedical brand machines were used (VivaCT 75, μ CT 40); at the AMNH Microscopy and Imaging Facility, a Phoenix brand v/tome/x s240 was used; and for specimens of *Nasalis*, *Gorilla*, *Pan*, and *Pongo* a GE eXplore Locus SP machine was used at the Ohio University μ CT Facility. A small subset of specimens was created with a Cyberware 3D scanner. These include the *Homo* sample (from the New York medical collection housed in the AMNH Department of Anthropology), the *Hoolock hoolock* sample, and AMNH 106581 and AMNH 106584 of the *Symphalangus* sample. Specimens were mounted in foam or packed in cotton to prevent movement while scanning. Most specimens were scanned at a resolution of 39 μ m or less. The highest resolutions used were on the order of 3–5 μ m for the very smallest fossil specimens. The scanning resolution was usually high enough to result in an initial polygonal mesh surface with between 1 million and 5 million faces (i.e., the surface resulting from creation of a “label field” representing the boundary between the bone and air in the image stack of raw CT data using the software Avizo 6-7, followed by application of the “Surf-Gen” function with “no smoothing”). All specimens were subsequently downsampled using the “simplify” function in Avizo 6-7 to between 300,000 and 500,000 faces. See Appendix for the original scan resolution of each specimen based on a microCT dataset.

Measurements

Three measurements were taken on the astragalus (Fig. 2): trochlear width and ectal facet area were used to represent overall size. Fibular facet angle was calculated as the minimum angle formed between the plane of the dorsal aspect of the fibular facet and the plane formed by the medial and lateral edges of the lateral tibial facet. Specifically, we used linear regression to model the plane of each facet, as represented by coordinates extracted from a 3D model of the astragalus, followed by trigonometry to find the angle between the planes.

Selecting anatomy for computing fibular facet orientation

Each 3D model was opened in Avizo 7.0 (Fig. 2). Using the surface viewer, the coordinate system of the astragalus model was reoriented according to a particular protocol. Because we use regression analysis to fit planes to surface data by minimizing variance in Z-values at a later stage, this reorientation should be roughly adhered to in subsequent studies using our method to ensure tractability of regression parameters. Starting in the “XY plane” (i.e., that in which the Z-axis of the data frame is parallel to the viewing axis), the surface was reoriented so that the lateral rim of the astragalus trochlea was horizontal, and so that both the fibular facet and lateral tibial facet were visible (i.e., so that neither were perpendicular to the XY plane or parallel to the viewing axis). The astragalus was then checked in the YZ and XZ planes to ensure that these facets were also not exactly parallel to the XY plane. After the astragalus model was reoriented as described above it was resaved so that the coordinate values of the point data representing its surface would reflect this reorientation. Next, the surface regions used to represent the facets of interest for angle calculations were selected on, and isolated from, the complete surface. We begin by describing the

TABLE 1. Extant taxa summary statistics.

Superfamily	Higher taxon	Species	n	Fib (s.d.)	OR Fib	Ect (s.d.)	OR Ectal	Troch (s.d.)	OR Troch
Anthropoidea	Aotidae	<i>Aotus azarae</i>	2	95 (3.87)	92–97	22.55 (3.94)	19.76–25.33	5.33 (0.07)	5.28–5.38
Anthropoidea	Aotidae	<i>Aotus infulatus</i>	1	99 (–)	–	17.66 (–)	–	4.84 (–)	–
Anthropoidea	Aotidae	<i>Aotus trivirgatus</i>	3	95 (3.77)	91–99	20.77 (3.14)	18.35–24.32	5.41 (0.48)	5.1–5.97
Anthropoidea	Atelidae	<i>Alouatta caraya</i>	3	98 (4.15)	95–103	70.37 (13.49)	54.82–78.86	10.25 (0.57)	9.63–10.77
Anthropoidea	Atelidae	<i>Alouatta</i> sp.	3	98 (0.41)	98–98	63.06 (13.26)	51.23–77.39	9.25 (0.89)	8.39–10.16
Anthropoidea	Atelidae	<i>Ateles belzebuth</i>	1	–	–	92.2 (–)	–	12.9 (–)	–
Anthropoidea	Atelidae	<i>Ateles fusciceps</i>	1	108 (–)	–	110.2 (–)	–	12.9 (–)	–
Anthropoidea	Atelidae	<i>Ateles geoffroyi</i>	1	98 (–)	–	118 (–)	–	13.19 (–)	–
Anthropoidea	Atelidae	<i>Ateles</i> sp.	3	97 (2.69)	94–99	82.6 (21.93)	58.83–102.06	11.61 (0.6)	10.93–12.04
Anthropoidea	Atelidae	<i>Lagothrix lagotricha</i>	2	102 (1.73)	101–103	57.78 (8.13)	52.03–63.53	10.47 (0.25)	10.3–10.65
Anthropoidea	Callitrichidae	<i>Callimico goeldii</i>	3	87 (3.94)	84–92	10.02 (3)	5.57–12.15	4.08 (0.66)	3.1–4.5
Anthropoidea	Callitrichidae	<i>Callithrix jacchus</i>	2	90 (0.78)	90–91	5.91 (0.48)	5.57–6.25	3.34 (0.34)	3.1–3.58
Anthropoidea	Callitrichidae	<i>Callithrix pygmaea</i>	2	82 (1.5)	81–83	2.8 (0.14)	2.71–2.9	2.19 (0.09)	2.13–2.26
Anthropoidea	Callitrichidae	<i>Leontopithecus rosalia</i>	1	88 (–)	–	10.54 (–)	–	4.46 (–)	–
Anthropoidea	Callitrichidae	<i>Presbytis midas</i>	3	87 (4.82)	82–91	11.73 (2.31)	9.84–14.3	4.26 (0.38)	3.88–4.64
Anthropoidea	Callitrichidae	<i>Saguinus mystax</i>	3	84 (4.91)	81–90	6.93 (0.51)	6.36–7.32	3.5 (0.1)	3.38–3.58
Anthropoidea	Callitrichidae	<i>Saguinus oedipus</i>	1	86 (–)	–	8.89 (–)	–	3.86 (–)	–
Anthropoidea	Cebidae	<i>Cebus apella</i>	6	91 (3.02)	87–95	37.17 (6.15)	31.62–45.68	7.6 (0.69)	7.04–8.86
Anthropoidea	Cebidae	<i>Saimiri boliviensis boliviensis</i>	3	92 (1.42)	90–93	17.54 (2.88)	15.86–20.86	4.43 (0.27)	4.2–4.73
Anthropoidea	Cebidae	<i>Saimiri sciureus</i>	2	97 (0.3)	96–97	15.48 (1.6)	14.35–16.61	4.46 (0.04)	4.44–4.49
Anthropoidea	Cercopithecoidea	<i>Macaca fascicularis</i>	4	82.15 (3.76)	77–85	57.07 (7.95)	48.13–67.43	9.37 (0.62)	8.64–10.15
Anthropoidea	Cercopithecoidea	<i>Macaca nemestrina</i>	3	84 (1.84)	82–86	77.01 (21.07)	61.77–101.06	10.44 (1.03)	9.57–11.58
Anthropoidea	Cercopithecoidea	<i>Nasalis larvatus</i>	4	82 (3.5)	79–86	173.33 (12.33)	163.86–191.45	14.88 (0.51)	14.18–15.31
Anthropoidea	Cercopithecoidea	<i>Presbytis melalophos</i>	1	88 (–)	–	76.82 (–)	–	10.85 (–)	–
Anthropoidea	Cercopithecoidea	<i>Semnopithecus entellus</i>	1	85 (–)	–	79.92 (–)	–	11.58 (–)	–
Anthropoidea	Cercopithecoidea	<i>Trachypithecus cristatus</i>	4	88 (2.88)	85–91	69.03 (7.02)	60.98–73.86	9.81 (0.79)	9.32–10.72
Anthropoidea	Cercopithecoidea	<i>Trachypithecus obscurus</i>	1	84 (–)	–	61.88 (–)	–	10.46 (–)	–
Anthropoidea	Hominoidea	<i>Hoolock hoolock</i>	7	90 (5.82)	84–102	66.36 (6.1)	58.8–74.6	9.64 (0.5)	8.91–10.3
Anthropoidea	Hominoidea	<i>Gorilla gorilla</i>	5	83 (3.85)	76–85	620.61 (152.31)	423.6–769.57	27.12 (2.5)	24.1–29.6
Anthropoidea	Hominoidea	<i>Homo sapiens</i>	5	97 (3.16)	93–101	661.91 (94.13)	527.7–763.99	30.12 (1.87)	27.14–32.15
Anthropoidea	Hominoidea	<i>Hylobates lar</i>	5	99 (2.87)	94–102	62.3 (8.59)	53.32–74.24	8.67 (1.01)	7.35–9.81
Anthropoidea	Hominoidea	<i>Pan troglodytes</i>	5	88 (4.3)	82–94	343.12 (22.67)	321.03–380.76	18.93 (1.27)	17.7–20.74
Anthropoidea	Hominoidea	<i>Pongo pygmaeus</i>	5	82 (5.85)	73–87	248.67 (17.04)	223.56–271.51	18.82 (1.25)	16.74–20.01
Anthropoidea	Hominoidea	<i>Symphalangus syndactylus</i>	3	94 (5.51)	88–99	83.46 (5.64)	79.47–87.44	11.76 (0.55)	11.25–12.34
Anthropoidea	Pitheciidae	<i>Cacajao calvus</i>	3	99 (4.84)	94–104	40.43 (0.77)	39.8–41.28	7.79 (0.96)	6.83–8.75
Anthropoidea	Pitheciidae	<i>Callicebus donacophilus</i>	2	98 (2.49)	97–100	17.85 (2.08)	16.38–19.32	5.37 (0.07)	5.33–5.42
Anthropoidea	Pitheciidae	<i>Callicebus moloch</i>	3	96 (0.92)	96–97	19.21 (3.49)	15.78–22.77	5.06 (0.46)	4.54–5.43
Anthropoidea	Pitheciidae	<i>Pithecia hirsuta</i>	1	94.9 (–)	–	34.8 (–)	–	7.47 (–)	–
Anthropoidea	Pitheciidae	<i>Pithecia monachus</i>	1	95.95 (–)	–	37.6 (–)	–	7.95 (–)	–
Anthropoidea	Pitheciidae	<i>Pithecia pithecia</i>	1	99.77 (–)	–	26.15 (–)	–	6.33 (–)	–
Tarsiiformes	Tarsiidae	<i>Tarsius bancanus borneanus</i>	2	94 (0.51)	93–94	4.85 (0.05)	4.82–4.88	3.25 (0.15)	3.15–3.36
Tarsiiformes	Tarsiidae	<i>Tarsius spectrum</i>	2	91 (2.18)	90–93	4.64 (0.15)	4.53–4.75	3.11 (0)	3.11–3.11
Tarsiiformes	Tarsiidae	<i>Tarsius syrichta</i>	2	98 (1.45)	97–99	4.78 (0.11)	4.7–4.85	3.2 (0)	3.2–3.2
Lemuriformes	Cheirogaleidae	<i>Cheirogaleus major</i>	1	117 (–)	–	9.69 (–)	–	3.97 (–)	–
Lemuriformes	Cheirogaleidae	<i>Cheirogaleus medius</i>	3	110 (4.65)	105–115	4.14 (0.33)	3.88–4.51	2.79 (0.15)	2.61–2.89
Lemuriformes	Cheirogaleidae	<i>Microcebus griseorufus</i>	11	103 (2.99)	97–106	1.95 (0.21)	1.72–2.41	1.71 (0.09)	1.62–1.96
Lemuriformes	Cheirogaleidae	<i>Mirza coquereli</i>	2	108 (1.98)	107–110	5.75 (0.41)	5.46–6.04	3.2 (0.05)	3.16–3.23
Lemuriformes	Daubentoniidae	<i>Daubentonia madagascariensis</i>	1	110 (–)	–	33.19 (–)	–	6.61 (–)	–
Lemuriformes	Indriidae	<i>Avahi laniger</i>	1	111 (–)	–	21.61 (–)	–	5.1 (–)	–
Lemuriformes	Indriidae	<i>Indri indri</i>	2	113 (3.06)	111–115	60.08 (2.57)	58.26–61.9	9.55 (0.24)	9.38–9.72
Lemuriformes	Indriidae	<i>Propithecus diadema</i>	1	117 (–)	–	73.45 (–)	–	10.93 (–)	–
Lemuriformes	Indriidae	<i>Propithecus verreauxi</i>	6	112 (2.81)	110–117	34.08 (3.2)	28.67–37.76	7.83 (0.43)	7.1–8.3
Lemuriformes	Lemuridae	<i>Eulemur fulvus</i>	7	114 (2.66)	110–117	26.58 (3.25)	21.79–29.23	5.85 (0.48)	5.38–6.71
Lemuriformes	Lemuridae	<i>Eulemur mongoz</i>	1	115 (–)	–	22.46 (–)	–	5.49 (–)	–
Lemuriformes	Lemuridae	<i>Haplemur griseus griseus</i>	3	113 (2.15)	111–115	13.94 (2.34)	11.54–16.22	4.83 (0.17)	4.68–5.02
Lemuriformes	Lemuridae	<i>Lemur catta</i>	3	112 (3.45)	108–115	26.54 (2.75)	24.92–30.65	6.73 (0.73)	6.33–7.83
Lemuriformes	Lemuridae	<i>Varecia variegata</i>	3	111 (0.56)	110–111	37.62 (1.14)	36.41–38.67	7.97 (0.45)	7.55–8.44
Lemuriformes	Lepilemuridae	<i>Lepilemur leucopus</i>	6	114 (3.2)	109–118	11.92 (1.38)	9.9–14.06	4.39 (0.36)	3.84–4.84
Lorisiformes	Galagidae	<i>Euoticus elegantulus</i>	2	104 (2.54)	102–106	7.48 (0.27)	7.29–7.67	3.56 (0.09)	3.49–3.62
Lorisiformes	Galagidae	<i>Galago senegalensis</i>	5	110 (3.34)	105–113	6.29 (0.37)	6.01–6.87	3.25 (0.14)	3.1–3.43
Lorisiformes	Galagidae	<i>Galagoides demidoff</i>	6	113 (3.04)	111–118	3.07 (0.2)	2.77–3.36	2.14 (0.09)	2–2.23
Lorisiformes	Galagidae	<i>Otolemur crassicaudatus</i>	5	109 (1.79)	107–112	17.31 (3.32)	13.8–21.38	4.79 (0.72)	4.23–5.76
Lorisiformes	Lorisidae	<i>Arctocebus calabarensis</i>	2	113 (2.47)	111–114	3.71 (0.25)	3.53–3.88	2.84 (0.11)	2.76–2.91
Lorisiformes	Lorisidae	<i>Loris tardigradus</i>	4	109 (1.51)	108–111	3.9 (1.25)	2.83–5.32	2.76 (0.51)	2.3–3.34
Lorisiformes	Lorisidae	<i>Nycticebus coucang</i>	3	112 (2.83)	109–114	6.29 (0.41)	5.83–6.61	3.67 (0.27)	3.43–3.97
Lorisiformes	Lorisidae	<i>Perodicticus potto</i>	8	112 (3.49)	108–117	10.57 (1.8)	8.61–13.51	4.44 (0.42)	3.77–5.04
Dermoptera	Cynocephalidae	<i>Cynocephalus volans</i>	3	109 (2.14)	107–111	9.43 (4.04)	5.02–12.97	4.11 (0.94)	3.12–5
Scandentia	Ptilocercidae	<i>Ptilocercus lowii</i>	3	96 (1.95)	94–98	1.46 (0.01)	1.45–1.47	1.45 (0.02)	1.43–1.47
Scandentia	Tupaiaidae	<i>Tupaia</i> sp.	3	74 (0.26)	74–74	4.52 (0.35)	4.12–4.77	2.65 (0.08)	2.58–2.74

Abbreviations: Ect, Ectal facet area; Fib, fibular facet angle; n, sample size; OR, observed range; s.d., standard deviation; Troch, astragalus trochlea width.

protocol used to identify and select the region of interest for modeling the plane of the lateral tibial facet. First, the reoriented astragalus model was viewed so that the rims of the lateral tibial facet were visible. The viewer

perspective on the astragalus model (but not the coordinate system) was then rotated in a way that brought the arcs of the trochlear rims into alignment (Fig. 2.1 and 2.2). When aligned as well as possible in lateral view

TABLE 2. Fossil taxa summary statistics.

Superfamily	Higher taxon	Species	n	Fib (s.d.)	OS Fib	Ect (s.d.)	OS Ectal	Troch (s.d.)	OS Troch
Anthropoidea	Stem Platyrrhini	<i>Dolichocebus gaimanensis</i>	1	94 (-)	-	94.4 (-)	-	94.4 (-)	-
Anthropoidea	Eosimiidae	<i>Eosimias</i> sp.	3	95 (2.23)	93-97	3.61 (0.2)	3.5-3.84	2.32 (0.1)	2.2-2.38
Anthropoidea	Propliopithecidae	<i>Aegyptopithecus zeuxis</i>	2	92 (7.31)	86-97	53.15 (-)	-	9.32 (0.42)	9.02-9.62
Anthropoidea	Oligopithecidae	<i>Catopithecus browni</i>	1	96 (-)	-	12.92 (-)	-	4.27 (-)	-
Anthropoidea	Parapithecidae	Parapithecid	1	79 (-)	-	26.64 (-)	-	5.91 (-)	-
Anthropoidea	Parapithecidae	<i>Apidium phiomense</i>	3	85 (6.97)	80-93	16.78 (1.81)	15.5-18.07	4.97 (0.21)	4.74-5.14
Anthropoidea	Parapithecidae	<i>Parapithecus grangeri</i>	1	83 (-)	-	15.15 (-)	-	4.76 (-)	-
Anthropoidea	Proteopithecidae	<i>Proteopithecus sylviae</i>	1	95 (-)	-	8.25 (-)	-	3.69 (-)	-
Anthropoidea	Pitheciidae	<i>Cebupithecia sarmientoi</i>	1	103 (-)	-	21.57 (-)	-	5.3 (-)	-
?	?	<i>Pondaungia</i> (?)	1	93 (-)	-	34.51 (-)	-	7.45 (-)	-
Tarsiiformes	Omomyiformes	<i>Absarokius abbotti</i>	1	104 (-)	-	3.83 (-)	-	2.27 (-)	-
Tarsiiformes	Omomyiformes	<i>Anemorhysis pearcei</i>	3	95.81 (2.91)	93-99	2.2 (0.17)	2.08-2.32	1.69 (0.09)	1.63-1.79
Tarsiiformes	Omomyiformes	<i>Hemiacodon gracilis</i>	4	101 (1.58)	99-103	6.51 (0.6)	6.07-7.4	3.37 (0.19)	3.13-3.56
Tarsiiformes	Omomyiformes	<i>Necrolemur</i> sp.	1	86 (-)	-	6.01 (-)	-	2.59 (-)	-
Tarsiiformes	Omomyiformes	<i>Nomomys carteri</i>	2	98 (1.36)	97-99	4.83 (0.17)	4.71-4.95	2.77 (0.02)	2.76-2.79
Tarsiiformes	Omomyiformes	<i>Ourayia uintensis</i>	2	94 (5.31)	90-98	20.2 (4.69)	16.89-23.52	5.37 (0.67)	4.89-5.84
Tarsiiformes	Omomyiformes	<i>Shoshonius cooperi</i>	3	98 (3.46)	96-102	2.71 (0.55)	2.14-3.23	1.95 (0.13)	1.85-2.09
Tarsiiformes	Omomyiformes	<i>Teilhardina belgica</i>	1	103 (-)	-	1.45 (-)	-	1.63 (-)	-
Tarsiiformes	Omomyiformes	<i>Teilhardina brandti</i>	2	102 (2.49)	100-104	1.42 (0.08)	1.36-1.47	1.84 (0.10)	1.77-1.91
Tarsiiformes	Omomyiformes	<i>Tetonius</i> sp.	2	97 (1.99)	95-99	2.39 (0.39)	2.08-2.83	1.84 (0.2)	1.63-2.03
Tarsiiformes	Omomyiformes	<i>Washakius insignis</i>	2	97 (0.07)	97-97	3.29 (0.09)	3.23-3.35	2.17 (0.11)	2.09-2.24
Adapiformes	Adapinae	<i>Adapis parisiensis</i>	8	109 (2.69)	106-114	15.57 (2.34)	12.6-18.98	4.77 (0.24)	4.46-5.13
Adapiformes	Adapinae	<i>Leptadapis magnus</i>	3	106 (2.16)	104-109	73.25 (9.96)	62.53-82.23	9.76 (0.99)	8.7-10.66
Adapiformes	Asiadapinae	<i>Asiadapis cambayensis</i>	1	100 (-)	-	6.88 (-)	-	3.17 (-)	-
Adapiformes	Asiadapinae	<i>Marcgodinotius indicus</i>	3	107 (2.11)	106-110	3.52 (0.24)	3.25-3.71	2.04 (0.07)	1.96-2.1
Adapiformes	Caenopithecinae	<i>Afradapis longicristatus</i>	1	116 (-)	-	18.96 (-)	-	5.51 (-)	-
Adapiformes	Notharctinae	<i>Cantius abditus</i>	6	102 (5.07)	93-107	31.84 (1.06)	30.86-32.97	6.22 (0.2)	6.03-6.49
Adapiformes	Notharctinae	<i>Cantius frugivorus</i>	1	110 (-)	-	na (-)	-	5.46 (-)	-
Adapiformes	Notharctinae	<i>Cantius mckennai</i>	2	98 (3.48)	94-103	17.9 (4.2)	15.18-22.74	4.53 (0.71)	3.39-5.71
Adapiformes	Notharctinae	<i>Cantius nuniensis</i>	1	118 (-)	-	na (-)	-	6.86 (-)	-
Adapiformes	Notharctinae	<i>Cantius ralstoni</i>	4	100 (3.7)	95-103	15.18 (-)	-	4.08 (0.46)	-4.37
Adapiformes	Notharctinae	<i>Cantius trigonodus</i>	5	98 (4.12)	93-103	20.47 (3.2)	18.21-22.74	5.39 (0.42)	4.85-5.89
Adapiformes	Notharctinae	<i>Pelycodus</i> sp.?	3	102 (6.22)	96-108	40.29 (4.63)	36.89-45.56	7.17 (0.21)	6.94-7.35
Adapiformes	Notharctinae	<i>Pelycodus jarrovi</i>	1	99 (-)	-	na (-)	-	7.96 (-)	-
Adapiformes	Notharctinae	<i>Notharctus tenebrosus</i>	10	108 (3.71)	101-116	34.28 (9.51)	23.61-52.85	7.01 (0.73)	6.12-8.4
Adapiformes	Notharctinae	<i>Smilodectes gracilis</i>	2	108 (1.4)	107-109	29.12 (0.1)	29.06-29.19	6.82 (0.16)	6.71-6.93
Plesiadapiformes	Carpolestidae	<i>Carpolestes simpsoni</i>	1	98 (-)	-	98.2 (-)	-	98.2 (-)	-
Plesiadapiformes	Paromomyidae	<i>Ignacius graybullianus</i>	1	91 (-)	-	2.67 (-)	-	2.07 (-)	-
Plesiadapiformes	Plesiadapidae	<i>Plesiadapis</i> sp.	2	102 (1.62)	100-103	13.27 (5.7)	9.25-17.3	4.46 (0.97)	3.77-5.14

Abbreviations: Ect, Ectal facet area; Fib, fibular facet angle; n, sample size; OR, observed range; s.d., standard deviation; Troch, astragal trochlea width.

(i.e., so that the medial rim is hidden behind the lateral rim), a region where the rims have similar radii of curvature was selected (Fig. 2.3 and 2.4) using a penetrating selection tool in the surface editor menu (i.e., the “pen tool”). The length of the arc of this selection was sometimes modified after comparing it to the mediolateral width of the trochlea. That is, the segment of the trochlear rim that was used to represent the plane of the lateral tibial facet was never allowed to be longer than about one-third the width of the trochlea. As implied above, the radii of curvature of the medial and lateral trochlear rims do not remain equal along their full lengths (i.e., the radius of curvature of one or both rims may be greater or smaller at its proximal end compared to its distal end). Thus a longer selection is rarely possible. Another reason for using this approach is that the radii of curvature of the trochlear rims are typically of a magnitude such that a longer arc will not approximate a planar surface very well and would reduce the correlation coefficient of the planar regression equation fit to the facet rim data. Once an appropriate portion of the tibial facet was selected, the rest of the surface was deleted, the “surface editor” tool was turned off, and the facet was saved as an “ASCII” formatted Avizo surface file with a new name. To begin preparing the fibular facet, the complete, reoriented version of the astragalus was reopened and the viewer perspective was rotated so that the fibular facet was visible. A flat surface was then

cropped out using a nonpenetrating selection tool (i.e., the “paint brush” tool). When selecting this surface, we avoided any area on the lateral shelf of the facet. For the purpose of our measurement protocol, the lateral shelf was identified solely by the presence of a proximodistally oriented concavity on the facet. Therefore, the region tends to be restricted to the dorsal half of the fibular facet, often positioned slightly above the fossa for the posterior astragalofibular ligament. Generally speaking, as long as the region of interest that we selected to represent the fibular facet was relatively flat, and was sampled from close to the rim of the lateral tibial facet (but did not inadvertently include it) instead of more plantarly, the angle calculations were consistent among replicated measures (Table 3). The unselected part of the surface was again deleted away (as was done when isolating the trochlear rims to represent the tibial facet) and the fibular facet was saved as a second “ASCII” file. Within the general specifications given here, the angle calculation is very robust to variation in amount and position of area selected.

Measurement error

Intraobserver error was evaluated for each measurement by replicating them five times on the same specimen, doing this for five different specimens. These specimens were chosen specifically to represent major

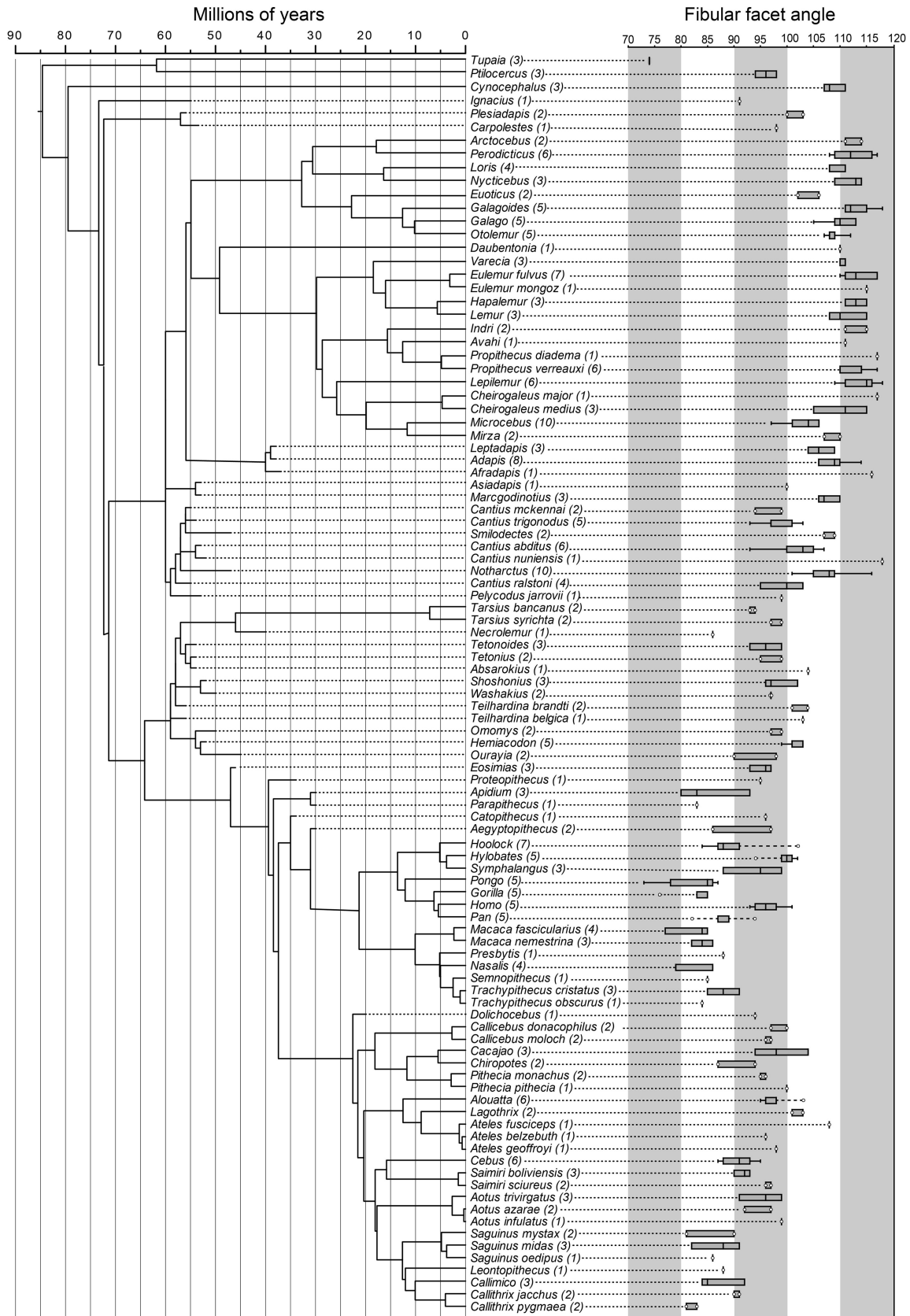


Fig. 1. Summary of data for this article. Left side shows supertree constructed for use in PGLS regressions and ancestral state reconstructions in *BayesTraits* (see Materials and Methods). Number following taxon names is sample size available for each species. Right side gives box plots summarizing data. Boxes include 50% of data. Whiskers encompass 75%. Outliers beyond this are represented by grey circles connected to whiskers by dashed lines. Grey circles represent individual data points in all cases. Not all taxa listed here could be included in standard ANOVAs (Tables 4 and 5; Fig. 5) due to $N < 3$ in many cases.

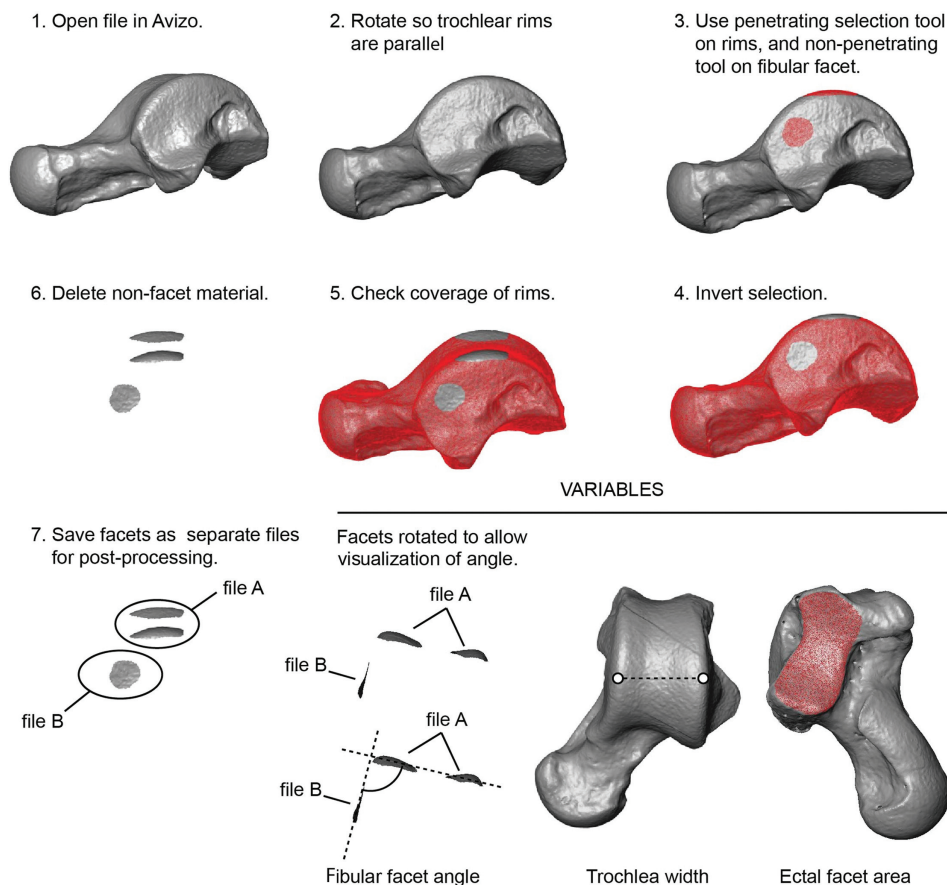


Fig. 2. Measurement protocols illustrated on an astragalus of *Saimiri*. Steps 1–7 allow calculation of fibular facet orientation. Prior to steps 1–7, all meshes were realigned (using Avizo) so that surfaces of interest were oblique to x , y , and z axes. Steps 1–7 were executed in Avizo software but could also be done in other packages designed for mesh editing (e.g., Geomagic and Meshlab). Once files A and B are saved separately, they are imported into SPSS and a plane is fit to each facet surface. The maximum angle of intersection between the two planes is then calculated: the result is the fibular facet orientation. Trochlear width and ectal facet area were both measured with Geomagic but could have been measured in Avizo.

morphological groups in the analysis (Table 3); within those groups they were chosen at random. Angle measurements were replicated by recropping the same surface file and recalculating the angle on the new selection. The other measurements were retaken in Geomagic studio with replications done on separate days. The average percentage error over five replicates was 1.76% for fibular facet angles, 1.65% for ectal facet area, and 1.16% for trochlear width. The lowest errors for any measurement were found among fibular facet trials (less than 0.5% error). However, the measurement error for the fibular facet of a specimen of *Pongo* was 4.48% (this was the highest measurement error of any measurement for any specimen in the analysis) and it brings up the average measurement error for fibular facet angle. We also note that calculating percentage error of an angular measurement is not necessarily the most informative way to assess error because the magnitude of the mean value is not expected to correlate with the magnitude of absolute error. However, comparing absolute levels of error shows a range of 0.39–3.12° (see “dev” column of Table 3).

Interobserver error was investigated less systematically but nevertheless appears to be extremely low for fibular facet slope calculations. We selected 17 specimens. Calculations or averages of calculations from two

or more trials per observer were compared between two different observers. That is, observer #1 calculated the angle for each of these specimens, often more than once, and observer #2 did the same. Percentage error of observer #1 compared to #2 was then calculated. Percentage errors are as follows: AMNH 83299 (0.57%), AMNH 106754 (2.65%), AMNH 106583 (2.01%), AMNH 86898 (3.35%), AMNH 52698 (1.59%), AMNH 131774 (0.15%), AMNH 201384 (0.53%), DPC 24776 (0.65%), DPC 049 (3.14%), GU 747 (0.63%), GU 748 (0.21%), IRSNB M 1235 (0.24%), MaPhQ 1390 (2.70%), SBU NCj1 (0.60%), USGS 4724 (0.71%), USNM 540329 (0.10%), and USNM 488058 (0.01%). See Appendix for more data on these specimens. The average interobserver error of this sample was 1.16% with a standard deviation of $\pm 1.13\%$ and a range 0.01–3.35%. Thus, the assessment of interobserver and intraobserver error yielded similar perspectives on repeatability of fibular facet angle.

Processing files for angle calculation

Once models were reoriented and divided into tibial and fibular facets, the coordinate data were extracted as follows: ASCII files were opened through Excel and the three columns (corresponding to X , Y , and Z) of coordinate data were selected. The points for the tibial and

TABLE 3. Intraobserver error.

Specimen		rep-1	rep-2	rep-3	rep-4	rep-5	Mean	dev	% error
Fibular facet angle									
AMNH 170680	<i>Hapalemur</i>	110	105	109	108	115	109	2.47	2.26
AMNH 133606	<i>Cebus</i>	93	93	94	91	93	93	0.93	1.00
NMNH 145302	<i>Pongo</i>	68	74	65	68	73	70	3.12	4.48
USNM 540329	<i>Teilhardina</i>	104	104	104	102	104	103	0.39	0.38
UNSM 15502	<i>Cynocephalus</i>	107	107	108	110	107	108	0.75	0.70
	Mean %								1.76
Ectal facet area									
AMNH 170680	<i>Hapalemur</i>	16.58	16.35	17.12	17.2	16.22	16.69	0.37	2.24
AMNH 133606	<i>Cebus</i>	43.1	43.63	43.21	43.12	44.18	43.45	0.37	0.84
NMNH 145302	<i>Pongo</i>	243.022	249.9	254.06	261.4	251.70	252.02	4.57	1.81
USNM 540329	<i>Teilhardina</i>	1.315	1.271	1.31	1.283	1.36	1.31	0.02	1.90
UNSM 15502	<i>Cynocephalus</i>	10.676	10.42	10.38	10.70	10.30	10.50	0.15	1.46
	Mean %								1.65
Trochlear width									
AMNH 170680	<i>Hapalemur</i>	4.88	4.88	4.99	4.92	5.02	4.94	0.05	1.08
AMNH 133606	<i>Cebus</i>	8.97	8.68	8.77	8.8	8.86	8.82	0.08	0.90
NMNH 145302	<i>Pongo</i>	18.22	18.79	18.63	18.6	18.94	18.64	0.18	0.99
USNM 540329	<i>Teilhardina</i>	1.76	1.79	1.73	1.74	1.77	1.76	0.02	1.08
UNSM 15502	<i>Cynocephalus</i>	4.30	4.23	4.50	4.28	4.22	4.31	0.08	1.78
	Mean %								1.16

Abbreviations: dev, average deviation from mean; rep, measurement replicate number; %, percent average deviation of a measurement from the mean.

fibular facets were copied into an SPSS spreadsheet. The points were then analyzed as a linear regression with the Z coordinate as a dependent variable on X and Y . The coefficients on X and Y , the constant, and R^2 values were obtained and entered into another spreadsheet. These parameters were used to model the plane of each facet for angular calculation (see below).

Trigonometry for angle calculation

We were interested in calculating the maximum angle formed between the two facet planes that were obtained with SPSS. This required that we find the angle between these planes in a plane perpendicular to them, which we call the angle plane. To do this we started by finding 1) a common point between the two facet planes (i.e., a point lying along their line of intersection) and 2) the vector representing the orientation of the line of intersection of these two planes (which must be perpendicular to the angle plane). We found a first common point between the two facet planes by setting $x = 0$ for each of the original equations from SPSS and then solving the system of two resulting equations $[(-1)C = B_2(y) + B_3(z)]$ and $[(-1)C' = B'_2(y) + B'_3(z)]$ in terms of y (since the form of the original equation from SPSS was $(z) = B_1(x) + B_2(y) + C$, $B_3 = B'_3 = -1$ in all cases): in this process, z cancels out and the solution to $y = [(-1)C - (-1)C'] / (B_2 - B'_2)$. We then input the value we determined for y into either of the original equations with $x = 0$, and solved for z . Next, to determine the orientation of the vector of intersection of the two facet planes, we first took the cross-product of the poles of the two facet planes. The pole vectors are given by the coefficients on the x , y , and z variables when the SPSS equation is rewritten as $(-1)C = B_1(x) + B_2(y) + B_3(z)$ (again, $B_3 = B'_3 = -1$ in all cases). The cross-product of the two vectors $[B_1, B_2, B_3]$ and $[B'_1, B'_2, B'_3]$ gives the vector that is the line of intersection between these planes and is of the form $[(B_2B'_3 - B_3B'_2), (B_3B'_1 - B_1B'_3), (B_1B'_2 - B_2B'_1)]$. Next, we determined the equation for the plane satisfying the condition that it 1) passed

through the common point where $x = 0$, and 2) was perpendicular to the line of intersection of the tibial and fibular facet planes. This was done by multiplying the x , y , z values of the common point (where $x = 0$) by the vector components of the cross-product of the two planes to get the coefficient, C , of this plane (i.e., the angle plane). Next, we determined two more points: one point along the line of intersection between the angle plane and the fibular facet and another between the angle plane and the tibial facet. We did this by arbitrarily choosing $y = 5$ for the y -coordinate of both points. We then solved two systems of equations (with $y = 5$) for x and z (see above for the same procedure used to find the common point between the facet planes using $x = 0$): one system was to find the point on the angle plane and tibial facet and another was for the angle plane and the fibular facet. Once we had two additional points, we calculated the distance between them, as well as the distances between each of these points and the original common point with $x = 0$. This gave us lengths of legs of a triangle lying with an edge along each of the facet planes and within (and parallel to) the angle plane. Finally we used the Pythagorean theorem to determine the angles between the different limbs of this triangle. We checked this calculation several times on different specimens using the 2D angle measurement tool in Avizo and found it to be extremely accurate; this external check on our method was also important because our calculation protocol sometimes returned the complement of the angle between the facet planes, depending on the orientation of the bone in coordinate space.

Phylogenetic methods

We used the continuous module in *BayesTraits* 1.1B (Pagel and Meade, 2011) to reconstruct changes in fibular facet angle throughout the evolutionary history of Euarchonta. First we reconstructed fibular facet orientation at several nodes of interest across a robust, time-scaled molecular phylogeny of the clade that is based on a supermatrix containing 61,199 base pairs from 69

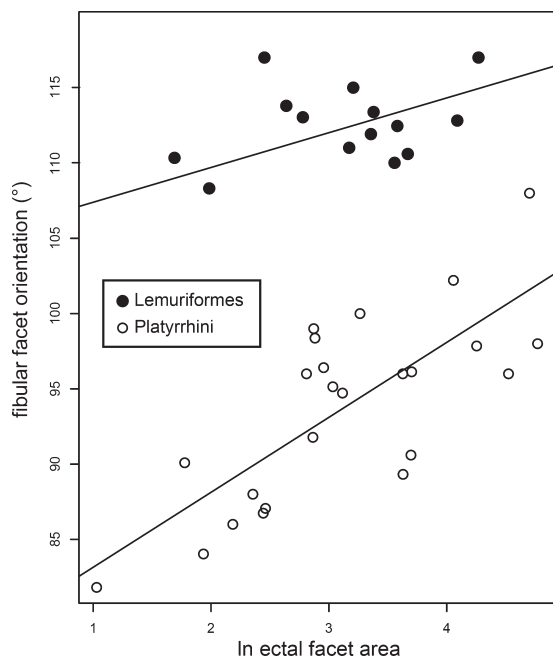


Fig. 3. PGLS regression of fibular facet orientation on one of our body size proxies, \ln ectal facet area, for two of the three primate groups (lemuriforms and platyrrhines) that showed significant relationships. Regression lines are for Lemuriformes and Platyrrhini. Data points are mean values for fibular facet orientation and \ln ectal facet area for each lemuriform and platyrrhine tip in our supertree. The close correspondence between the PGLS line and what would appear to be the TIP distribution of the data is a result.

nuclear genes and 10 mitochondrial genes [(Springer et al., 2012; divergence times calculated using independent rates and soft bounds (their Text S2.4)]. Springer et al.'s analysis did not include the extant scandentian *Ptilocercus*, which is estimated to have shared a common ancestor with tupaiids early in the Paleogene (Janečka et al., 2007; Roberts et al., 2011) and has been interpreted as retaining a more plesiomorphic postcranium than its tupaiid relatives (Sargis, 2004; Bloch et al., 2007). To incorporate the fibular facet angle of this important taxon, we grafted *Ptilocercus* onto Springer et al.'s tree as the sister group of *Tupaia*, with the *Ptilocercus-Tupaia* divergence placed at 61.8 Ma (i.e., the average of the mean molecular divergence estimates calculated by Janečka et al., 2007; Roberts et al., 2011). All species that were not represented in our sample of fibular facet angle measurements were trimmed from this tree, leaving a total of 66 tips. For each operational taxonomic unit (OTU), a mean fibular facet angle (Table 1) was calculated and used as the unit of analysis in *BayesTraits*. Most taxa in our sample were represented in Springer et al.'s supermatrix, but our species of the platyrrhine *Chiropotes* were nonoverlapping; that genus was collapsed into a single OTU in our tree, and its fibular facet angle mean was based on all *Chiropotes* individuals in our sample.

Because the stem lineages of Anthropoidea, Tarsiidae, and Strepsirrhini are all quite long (a combined 107 million years of independent evolution on the Springer et al. tree), and the ancestral crown primate is separated from the extant dermopteran measured for this study (*Cynocephalus*) by a combined ~88 million years of independent evolution along their respective branches, it

was of interest to determine whether incorporation of fibular facet angle measurements from basal fossil crown primates and other fossil euarchontans would or would not suggest a different scenario of fibular facet angle evolution within the clade. We estimated ancestral fibular facet angle values throughout a supertree that included the same 66 extant taxa and an additional 35 extinct taxa that have previously been included in parsimony-based phylogenetic analyses of morphological data. We used matrix representation with parsimony (MRP) to combine Springer et al.'s tree with the morphology-based trees of Tornow (2008, for omomyiforms; his Fig. 10), Rose et al. (2011, for basal omomyiforms, their Fig. 13C), and Bloch et al. (2007, for plesiadapiforms; their Fig. 4). These trees were combined with a tree derived from a new analysis of a matrix most recently used by Patel et al. (2012) that includes several Paleogene primates (including omomyiforms, adapiforms, and basal anthropoids) and which was modified by including a new quantitative character for fibular facet orientation based on the results presented here.¹ We attempted to include Gunnell's (2002) notharctine phylogeny (his Fig. 5) in the MRP analysis, but his taxon sample did not show sufficient taxonomic overlap with the other trees to allow for their resolved placement, so we assumed notharctine monophyly and grafted Gunnell's tree onto the *Cantius abditus* branch.

To create a time-scaled tree that included fossils, we used the same divergence dates as in the analysis of extant taxa described above and minimized ghost lineages for fossil tips by spacing successive extinct clades along stem lineages at 1 Ma intervals, working down from crown nodes. Branch lengths within extinct clades were determined by restricting internodes to be 1 Ma unless adjacent sister taxa were geologically older. The branch connecting *Necrolemur* to Tarsiidae was placed at 46 Ma because there is clear evidence that Tarsiidae was already present at approximately 45 Ma (*Tarsius eocaeus* [Beard et al., 1994]). In light of this, 46 Ma is almost certainly an underestimate of the antiquity of the divergence between microchoerines and tarsiids, but we have no objective basis for placing the divergence older than the oldest known tarsiid. The divergence between *Afradapis* and Adapinae is also probably an underestimate, but relationships among adapids are poorly worked out (i.e., it is not yet clear whether adapines are paraphyletic with respect to caenopithecines), so we have no objective criteria for placing the divergence earlier.

Before reconstructing ancestral values, we tested whether perturbation of certain phylogenetic scaling parameters would provide a better fit of the data to the model than reconstructions that incorporated no such parameters. The phylogenetic scaling factors are delta (δ , a parameter that adjusts overall path lengths in the tree, allowing for the detection of different evolutionary rates through time), kappa (κ , a parameter that adjusts individual branch lengths, revealing whether shorter or longer branches contribute more to trait evolution), and lambda

¹The latter matrix was analyzed in PAUP 4.0b10 (Swofford, 1998) with random addition sequence and TBR branch-swapping across 10,000 heuristic search replicates. Some multistate characters were treated as ordered and were scaled so that transitions between "fixed" states in an ordered morphocline were equal to one step (polymorphisms were assigned their own state, intermediate between fixed states in each morphocline). The analysis was constrained by a molecular scaffold based on the results of Springer et al. (2012).

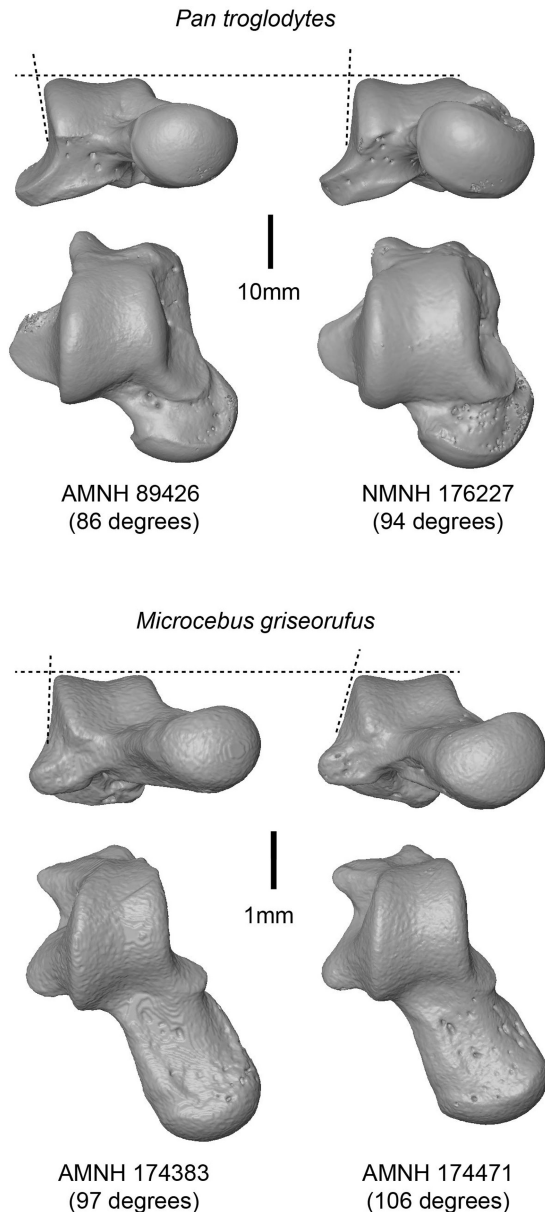


Fig. 4. Illustration of intraspecific variation. Specimens with the minimum and maximum angles for their species samples are illustrated side by side for *Pan* and *Microcebus*. The dashed lines are provided to help guide the viewer to the relevant anatomy. They do not represent actual measurement landmarks and were not used to guide surface selection for angle calculation in any way. Note that the calculated angle differences make sense given the qualitative appearance of the specimens (i.e., the seemingly large amount of intraspecific variation is not an artifact of intraobserver/interobserver error in measurement).

(λ , which tests whether species are phylogenetically independent for a given tree and feature) (e.g., Nunn, 2011). Distributions for each of the three model parameters were generated using Markov Chain Monte Carlo (MCMC) sampling in *BayesTraits*, based on 10,050,000 iterations (first 50,000 discarded as “burn in”) and Model “A” (constant variance random-walk), with the RateDev value individually tuned for each analysis to achieve acceptances between 20% and 40%. The test statistic $2[\log[\text{harmonic}$

$\text{mean}(\text{better model})] - \log[\text{harmonic mean}(\text{worse model})]$ was used to determine which phylogenetic scaling parameter, if any, should be used for the ancestral reconstructions; a value of 2 is considered “positive” evidence and a value of 5 is considered to be “strong” evidence (Pagel and Meade, 2011). We also tested for whether a random-walk or directional model better fit the data evolving on the supertree that included living and extinct taxa (this was not possible for the tree that included only extant taxa because the directional model cannot be used if the input tree(s) is/are ultrametric (i.e., all path lengths are equal). Convergence of independent MCMC chains was evaluated by examining the final harmonic mean likelihoods of the two runs and by examining the traces of the parameters in Tracer 1.5 (Rambaut and Drummond, 2009). For ancestral reconstructions, two longer independent MCMC chains were run (30,050,000 iterations, first 50,000 discarded as burn in, with the DataDev value individually tuned for each analysis to achieve acceptances between 20–40%), using the estimates for the phylogenetic scaling parameters that were calculated in the previous step. Mean values and posterior densities for each reconstruction were taken from the combined results of the two independent MCMC runs [calculated in Tracer 1.5].

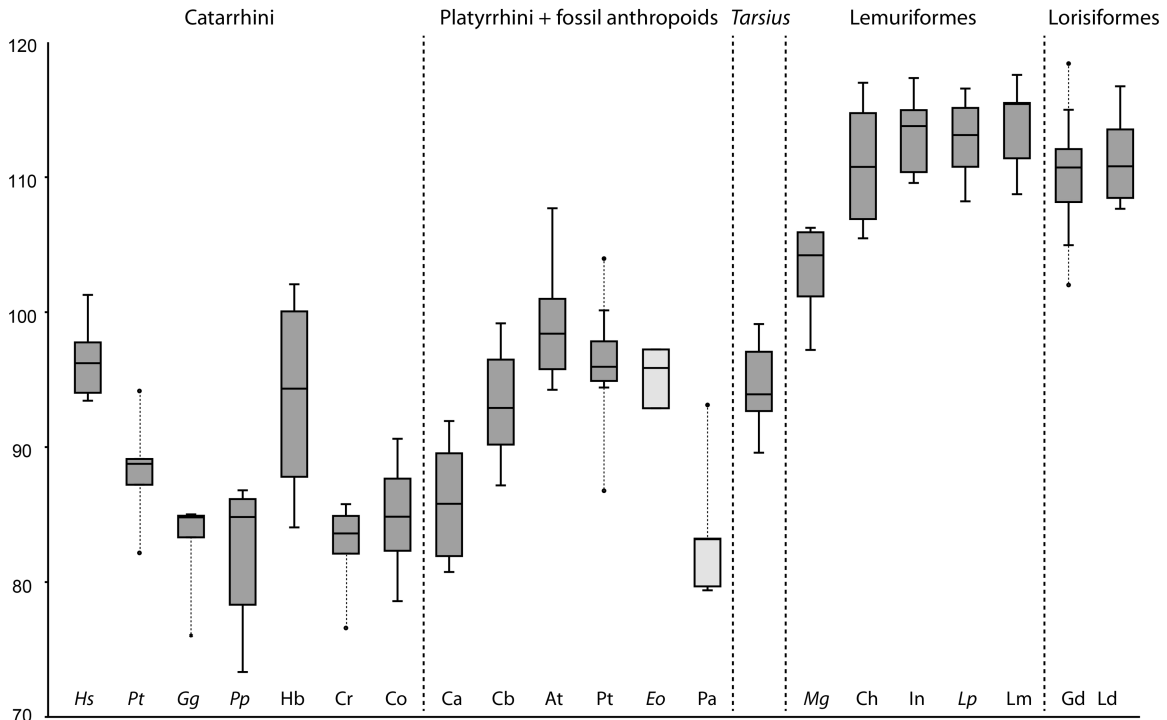
Tests for size-correlated changes in fibular facet orientation

We used the *caper* (Comparative Analysis of Phylogenetics and Evolution in R) package in R (Orme et al., 2011) to calculate phylogenetic generalized least-squares (PGLS) regressions of fibular facet orientation on two size proxies, the natural logarithm of ectal facet area and the natural logarithm of mid-trochlear width, using the maximum-likelihood estimate of lambda. Regressions were calculated using tip means across the entire dataset, as well as in major crown clades within primates [i.e., primates (living and extinct), Strepsirrhini, Lemuriformes, haplorhines (living and extinct), tarsiiiforms (living and extinct), Anthropoidea, Platyrrhini, and Catarrhini], using the MRP supertree that combines living and extinct taxa, and pruning taxa depending on which subclade was being analyzed. For each regression, sample size differed slightly from analysis to analysis because it was not possible to obtain all measurements for all individuals.

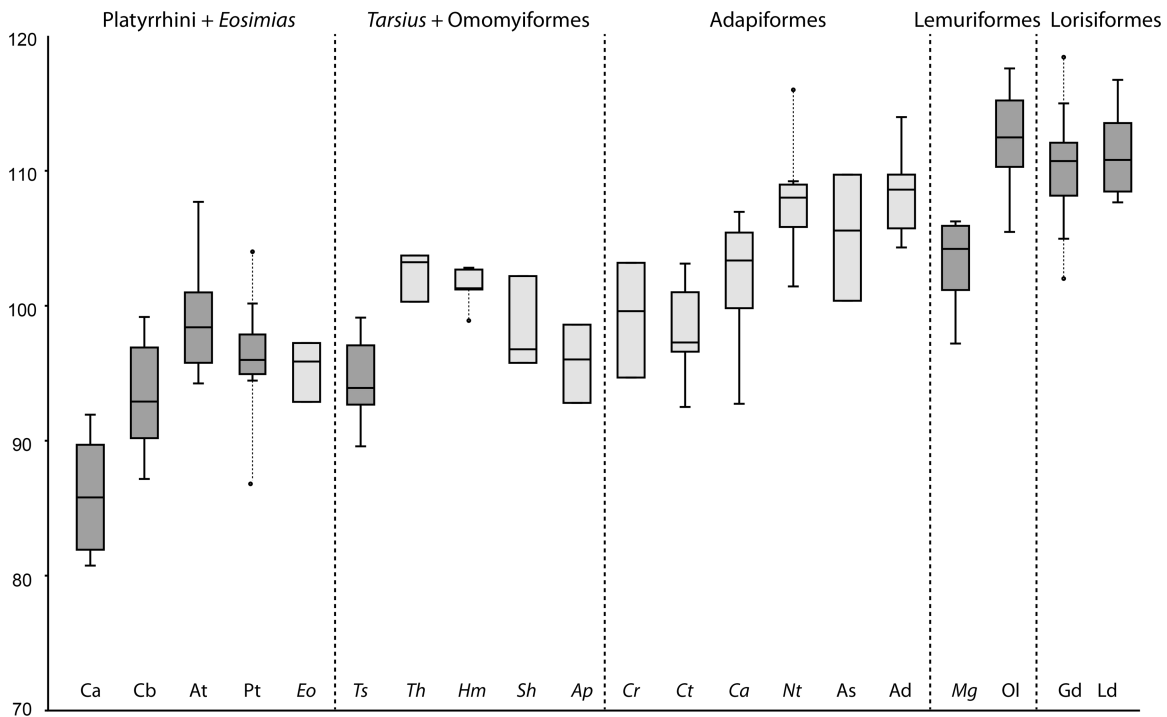
RESULTS

Size-related change in fibular facet orientation

Fibular facet angle is not significantly correlated with either of our proxies for overall size using either GLS or PGLS (natural log of mid-trochlear width [GLS, $r^2 = 0.03$, $P = 0.09$; PGLS, $r^2 = 0.003$, $P = 0.7283$] or ectal facet area [GLS, $r^2 = 0.03$, $P = 0.09$; PGLS, $r^2 = 0.0004$, $P = 0.9652$]) across our sample of 110 euarchontan taxa. Among euarchontan subclades, only platyrrhines (PGLS mid-trochlear width, $r^2 = 0.3664$, $P = 0.0002$; PGLS ectal facet area, $r^2 = 0.5743$, $P = 0.0000005$), strepsirrhines (PGLS mid-trochlear width, $r^2 = 0.2507$, $P = 0.0046$; PGLS ectal facet area, $r^2 = 0.2305$, $P = 0.007$), and lemuriforms (PGLS mid-trochlear width, $r^2 = 0.3756$, $P = 0.0059$; PGLS ectal facet area, $r^2 = 0.3615$, $P = 0.0073$) showed significant relationships between fibular facet orientation and “size,” (with fibular facet angle increasing, or becoming more obtuse, with increases in size) (Fig. 3; Table 4).



A. Groups for ANOVA (see Table 5)



B. Groups for ANOVA (see Table 6)

Fig. 5. ANOVA plots. Groups plotted are those used in a one-way ANOVA (see Tables 4 and 5). Boxes include 50% of data. Whiskers encompass 75%. Outliers beyond this are represented by grey circles connected to whiskers by dashed lines. Dark grey boxes are extant groups. Light grey are fossil groups. Dashed vertical lines separate major taxonomic groups/clades. Part **A** focuses on extant taxa and fossil anthropoids. Part **B** focuses on Eocene taxa mainly. In part B, catarrhines were left out because their comparison to Eocene forms is of limited relevance. As well, to reduce the number of comparisons and improve power, non-*Microcebus* lemuriforms were combined as they did not differ in their pattern of significance in the ANOVA of Figure 5A and Table 4. Significance levels, test statistics, sample sizes, and basic univariate statistics are given in Tables 5 and 6. Abbreviations: *Hs*, *Homo sapiens*; *Pt*, *Pan troglodytes*; *Gg*, *Gorilla gorilla*; *Pp*, *Pongo pygmaeus*; *Hb*, Hylobatidae; *Cr*, Cercopithecinae; *Co*, Colobinae; *Ca*, Callitrichidae; *Cb*, Cebidae and *Aotus*; *At*, Atelidae; *Pt*, Pitheciidae; *Eo*, *Eosimias*; *Pa*, Parapithecidae; *Mg*, *Microcebus griseorufus*; *Ch*, Cheirogaleidae (excluding *Microcebus*); *In*, Indriidae; *Lp*, *Lepilemur*; *Lm*, Lemuridae; *Gd*, Galagidae; *Ld*, Lorisidae; *Ts*, *Tarsius*; *Th*, *Teilhardina* sp.; *Hm*, *Hemia-codon gracilis*; *Sh*, *Shoshonius cooperi*; *Ap*, *Anemorhysis pearcei*; *Cr*, *Cantius ralstoni*; *Ct*, *Cantius trigonodus*; *Ca*, *Cantius abditus*; *Nt*, *Notharctus tenebrosus*; *As*, Asiadapinae; *Ad*, Adapinae; *Ol*, Other lemuriforms (i.e., excluding *Microcebus*).

Taxonomic influence on fibular facet angles

Examination of fibular facet angles for a given species suggests a large amount of intraspecific variation (Tables 1 and 2; Figs. 1 and 4). To assess whether a taxonomic influence on fibular facet angle also exists as previously suggested (e.g., Gebo, 1988), we ran two separate one-way ANOVAs. The first (Table 5, Fig. 5) was designed to assess variation among major extant groups and among fossil anthropoids. The second (Table 6, Fig. 5) was designed to assess patterns of variation among Eocene primates with respect to each other and select extant groups. The first analysis included 21 groups. A one-way ANOVA on these groups shows significant among group variance (mean square error (MSE) = 15.2; $F = 79.65$, $P \ll 0.0001$). Tukey's honestly significant differences (HSD) post hoc comparisons (Table 5) show that the strepsirrhine groups are not significantly different from each other with the exception of *Microcebus*, which is significantly different from Indriidae, Lemuridae, *Lepilemur*, and Lorisiidae. On the other hand, strepsirrhine groups are significantly different from all haplorhines with the exception of *Microcebus*, which is not significantly different from *Homo*, Atelidae, or Pitheciidae. Tarsiers do not differ significantly from *Homo*, *Pan*, Hylobatidae, or non-callitrichid platyrrhines, but they are different from remaining catarrhines and all strepsirrhines. The fossil *Eosimias* and Cebidae+*Aotus* have identical patterns of significance to *Tarsius*. Atelidae and Pitheciidae have similar patterns to the former taxa, but also differ significantly from *Pan*, and do not differ from *Microcebus* among strepsirrhines. Parapitheciidae differ from all strepsirrhines, non-callitrichid platyrrhines, *Eosimias*, *Homo*, and Hylobatidae. They overlap with remaining catarrhines in having a very steep facet.

Next we ran an ANOVA on 20 groups, some of which were also included in the last analysis. Not being immediately concerned with how catarrhines compare with Eocene euprimates, catarrhines were not included. Additionally, having found in the last analysis that all lemuriform groups except *Microcebus* exhibit the same pattern of significance we combined all of them into a single "non-*Microcebus* lemuriform" group. ANOVA on these 20 groups shows significant among-group variance (MSE = 12.2, $F = 59.35$, $P \ll 0.0001$). Tukey's HSD post hoc comparisons (Table 6) show that the four strepsirrhine groups are not different from each other with the exception of *Microcebus*, which differs from other lemuriforms and lorisiids, as before. Non-*Microcebus* strepsirrhines differ from all anthropoids, omomyiforms, and all species of *Cantius* among adapiforms. Other adapiforms included in the analysis do not differ from any strepsirrhine group, including *Microcebus*. Nor does *Cantius*, any omomyiform group (except *Tetonoides*), Atelidae or Pitheciidae differ from *Microcebus*. *Teilhardina* and *Hemiacodon* have identical patterns of significance to one another, differing from Callitrichidae, Cebidae+*Aotus*, and non-*Microcebus* strepsirrhines but not differing from remaining platyrrhines or any adapiforms. *Shoshonius* and *Tetonoides*, with steeper facets, differ from strepsirrhines, non-*Cantius* adapiforms and callitrichids, but no others. Species of *Cantius* show interesting patterns of significance: none differ significantly from *Eosimias*, which, however, differs from remaining adapiforms and strepsirrhines. *Cantius ralstoni* and *Cantius trigonodus* also differ from other adapiforms, while *Cantius abditus* does not. On the other hand, *C.*

ralstoni and *C. trigonodus* do not differ from non-callitrichid platyrrhines or *Tarsius*, whereas *C. abditus* differs additionally from Cebidae+*Aotus* and *Tarsius*, because of its shallower facet slope (more obtuse angle).

Ancestral state reconstructions

For the analysis of extant taxa alone, the phylogenetic scaling parameter λ provided reconstructions with higher mean and harmonic mean log-likelihoods than analyses with δ , κ , or no scaling factors (Table 7, Fig. 7A), so the distribution of estimated λ values was used when reconstructing values at ancestral nodes. $\lambda = 0$ suggests that a trait has evolved completely independent of phylogenetic structure, while a λ of 1 is consistent with a constant variance random-walk model of trait evolution on the tree (e.g., Nunn, 2011). The mean value of λ from all post-burnin iterations sampled along the combined 20 million MCMC iterations was 0.884, indicating that trait variance is phylogenetically structured, and that fibular facet angle did not evolve independently on the tree. The fibular facet angle means calculated from the combined results of the two 30-million-iteration MCMC chains (Table 8, Fig. 8) ranged from 85.9° (crown Cercopithecoidea) to 112.2° (crown Indriidae), with ancestral values of 99.2° for both crown Primatomorpha and crown Primates, 98.5° for crown Haplorhini, and 106° for crown Strepsirrhini. The ancestral value of 99.2° for crown Primates was identical to those for crown Anthropeoidea, crown Catarrhini, and crown Hominoidea.

When extinct taxa were added to the tree, inclusion of the phylogenetic scaling parameter κ provided reconstructions with higher mean and harmonic mean log-likelihoods than analyses with δ , λ , or no scaling factors (Table 7, Fig. 7B). κ values > 1.0 stretch long branches more than short branches, while values < 1.0 compress long branches more than short branches (Pagel and Meade, 2011). The mean value of κ from all post-"burn in" iterations sampled along the combined 20 million iterations of the two independent MCMC chains was 0.296, indicating that shorter branches contribute more to trait evolution than longer branches, and that fibular facet angle did not evolve gradually within Euarchonta. The posterior distribution from model "A" (constant variance random-walk) with parameter κ has a higher mean, higher harmonic mean log-likelihood, and higher point of highest posterior density than the distribution from model "B" (directional) with parameter κ (Table 7; Fig. 7B); the former was accordingly selected as the preferred model for reconstruction of ancestral values throughout the tree. The fibular facet angle means calculated from the combined results of the two 30-million-iteration MCMC chains ranged from 86.0° (crown Cercopithecoidea) to 112.3° (crown Indriidae), with ancestral values of 97.9° for crown Primatomorpha, 99.5° for crown Primates, 98.7° for crown Haplorhini, and 108.2° for crown Strepsirrhini (Table 8). Most of the nodal reconstructions were similar to those in the analysis based on extant taxa alone, aside from those for crown Anthropeoidea (92.8°, a difference of -6.4°), crown Catarrhini (88.9°, a difference of -10.3°), and crown Hominoidea (88.6°, a difference of -10.6°) (Fig. 9A). For almost all nodes, inclusion of fossils decreased the size of the 95% highest posterior density (HPD) for the ancestral reconstructions, with the most dramatic examples being Platyrrhini and Hominae, and the only exceptions

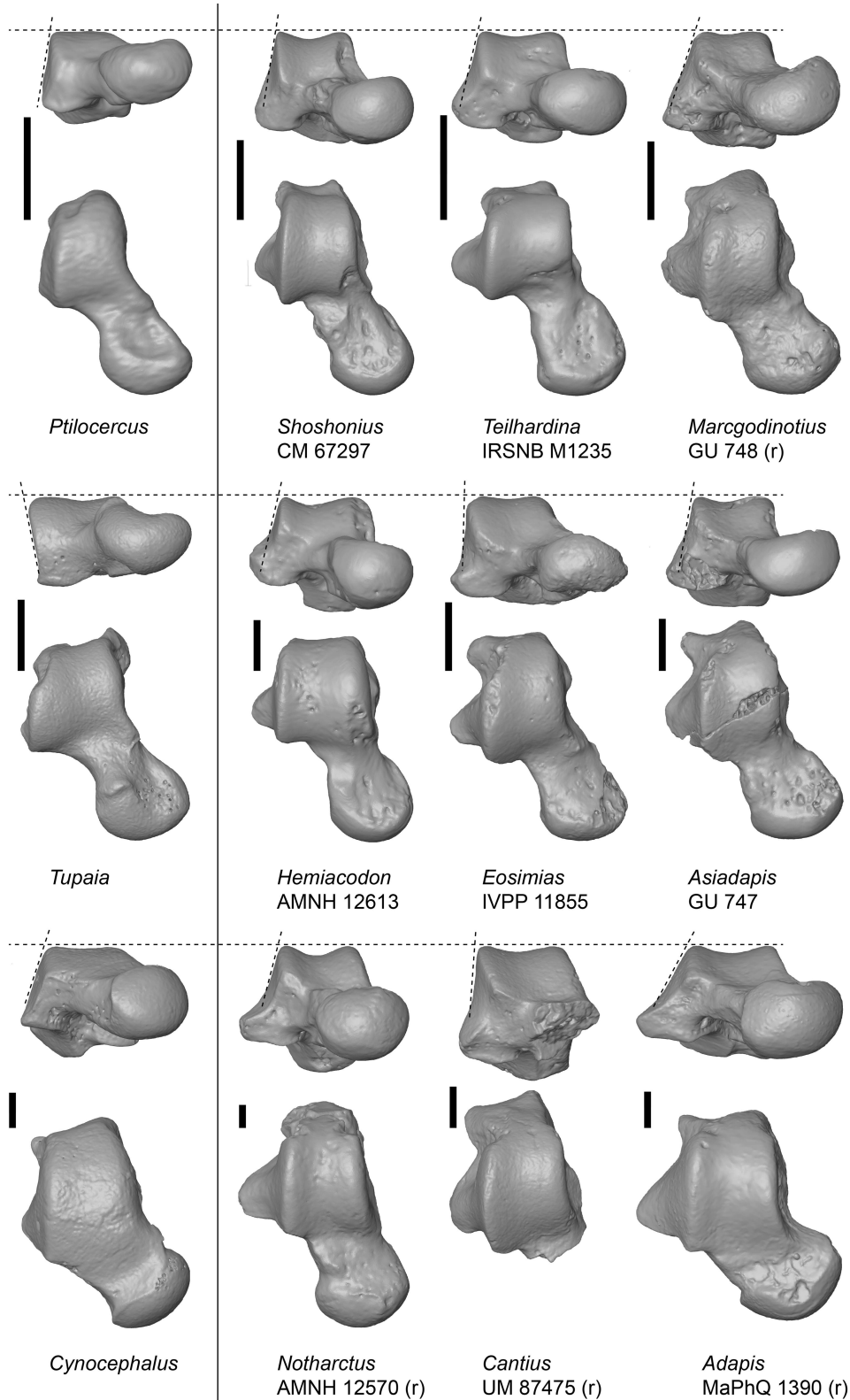


Fig. 6. Illustrations of key example specimens in distal (above) and dorsal (below) views. The dashed lines are provided to help guide the viewer to the relevant anatomy. They do not represent actual measurement landmarks and were not used to guide surface selection for angle calculation in any way. Specimens are scaled to same proximodistal length, except specimens with extremely shortened necks (e.g., *Adapis*) which are scaled to others based on trochlea length. Scale bars equal 2 mm. **A** (left page), Exemplars of nonprimates (left-most column) and fossil euprimates (right three columns). **B**, (right page) of extant examples. Scale bars equal 2 mm. Specimens have been reversed to facilitate comparison if “(r)” follows the specimen number.

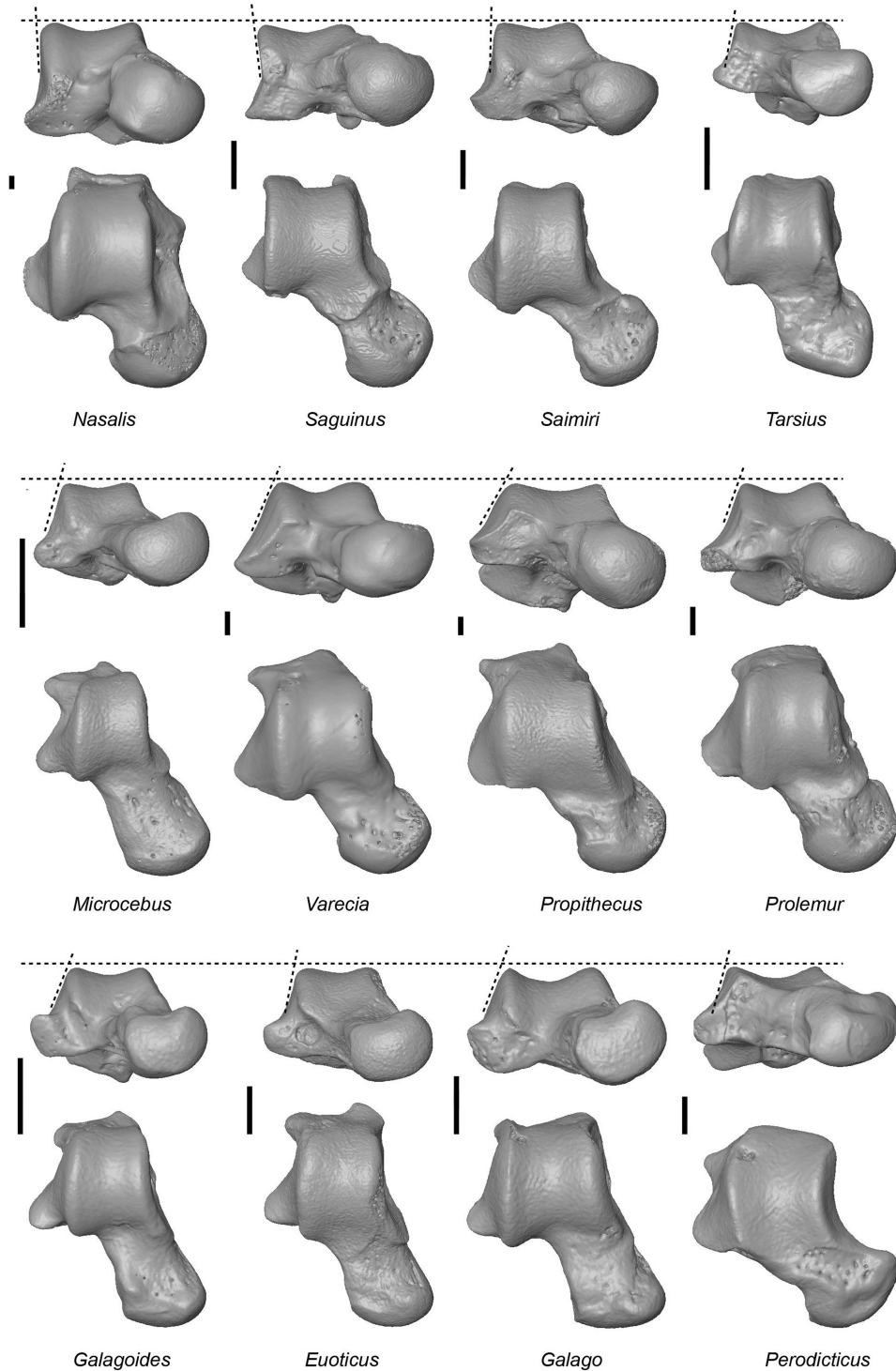


Fig. 6. (Continued)

being Primatomorpha and Catarrhini (Tables 8 and 9; Fig. 9B).

DISCUSSION AND CONCLUSIONS

Using a new method for quantifying fibular facet orientation, we have confirmed that the orientation of this

facet in extant strepsirrhines is significantly different from that in extant haplorhines as described qualitatively by previous authors, and that there is in fact almost no overlap between these clades even at the level of individual specimens. Our ancestral reconstructions incorporating extinct taxa further support the contention that the relatively “steep-sided” condition of the ancestral crown haplorhine (mean of 98.7°) is very close to

TABLE 4. Results of PGLS regressions of fibular facet orientation on ln ectal facet area (-E) and ln mid-trochlear width (-T).

Groups	Lambda	Adj R ²	slope	t-value	P (>t)	RSE (DF)	F-value (DF)	P
Euarchonta-E	0.868	0.010	-0.14	-0.19	0.851	12.22 (95)	0.035 (2.95)	0.965
Euarchonta-T	0.781	0.007	0.84	0.56	0.574	11.68 (97)	0.32 (2.97)	0.728
Crown Primates-E	0.857	0.002	-0.66	-0.86	0.387	12.85 (89)	0.76 (2.89)	0.472
Crown Primates-T	0.827	0.009	-0.61	-0.41	0.684	11.97 (89)	0.17 (2.89)	0.847
Strepsirrhines-E	0.000	0.194	1.633	2.51	0.020	4.13 (21)	6.29 (2.21)	0.007
Strepsirrhines-T	0.000	0.215	3.61	2.65	0.015	4.08 (21)	7.02 (2.21)	0.005
Lemuriforms-E	0.000	0.312	2.07	2.71	0.018	4.10 (13)	7.36 (2.13)	0.007
Lemuriforms-T	0.000	0.328	4.33	2.80	0.015	4.06 (13)	4.33 (2.13)	0.006
Haplorhines-E	0.913	0.003	-1.16	-1.07	0.288	15.08 (55)	1.15 (2.55)	0.323
Haplorhines-T	0.909	0.012	-1.31	-0.578	0.566	14.89 (55)	0.33 (2.55)	0.718
Tarsiiforms-E	0.000	0.158	-3.26	-1.80	0.099	16.37 (11)	3.25 (2.11)	0.078
Tarsiiforms-T	0.000	0.0003	-4.43	-0.99	0.339	17.84 (11)	0.99 (2.11)	0.401
Crown Anthropoids-E	0.746	0.008	1.07	0.83	0.408	11.49 (36)	0.701 (2.36)	0.503
Crown Anthropoids-T	0.748	0.014	1.82	0.69	0.495	11.54 (36)	0.476 (2.36)	0.625
Crown Platyrrhines-E	0.000	0.555	4.98	5.45	<0.0001	8.98 (22)	29.68 (2.22)	<0.000001
Crown Platyrrhines-T	0.243	0.338	8.59	53.57	0.002	9.68 (22)	12.72 (2.22)	0.0002
Crown Catarrhines-E	0.634	0.050	-1.38	-0.617	0.549	13.56 (12)	0.381 (2.12)	0.691
Crown Catarrhines-T	0.000	0.0003	-4.44	-0.998	0.339	17.84 (12)	0.996 (2.12)	0.401

Greyed cells show significance at $P < 0.05$. Note that when lambda is 0.000, regressions are equivalent to TIPS data (internal branch lengths = 0). Abbreviations: Adj, adjusted; DF, degrees of freedom; P, probability; RSE, residual standard error.

that of the primitive condition of euprimates (99.5°), while the ancestral condition for crown strepsirrhines (108.2°) is specialized.

This aspect of strepsirrhines' early rearrangement of their cruro-pedal functional morphology—whatever the original adaptive basis (see below)—clearly had an enduring impact. Despite their ancient origin, broad geographic distribution, and dramatic intragroup differences in body mass and locomotion, strepsirrhines show remarkably little variation in fibular facet orientation (being about as variable as crown Platyrrhini (Fig. 4b), a clade that is about two-fifths the age of Strepsirrhini). What little variation exists in fibular facet orientation among strepsirrhines shows a significant relationship with body size (Table 6). There is apparently no relationship between facet angle and frequency of leaping either, given that the differences between the ancestral reconstructions of groups as behaviorally different as Lorisiidae and Galagidae are almost within our range of measurement error.²

Gebo (2011) reviewed the osteological features that distinguish extant strepsirrhines from extant haplorhines, synthesizing his and others' previous work on this topic (Beard et al., 1988; Gebo, 1988, 1993, 2011; Dagosto, 1993; Gebo et al., 1991, 2000, 2001; Dagosto et al., 2008). He concluded that strepsirrhine hind limb anatomy reflects an ancestral dependence on the types of abducted and inverted foot postures that would be required by the use of small-diameter vertical supports. Gebo argued that there are a series of features—including the shape and orientation of the tibiofibular mortise, the orientation of the tibial malleolus, the orientation of the astragalar fibular facet, the position of the groove for the tendon of flexor hallucis longus relative to the astragalar trochlea, and the morphology of the tibial plateau—that are all functionally related to this strategy. He specifically explained the strepsirrhines' laterally sloping fibular facet as functioning to “add(s) a bony surface that actually provides support for the lower limb” (p. 326) (specifically support for a

more “vertically oriented” fibula while the foot is grasping a vertical support). How does this work, and why is it necessary in strepsirrhines, but not haplorhines? Gebo has suggested that vertical postures put a greater percentage of the body weight on the hind limb, which could explain a reconfiguration of the astragalus to support more weight while maintaining similar stress levels. However, it is unclear whether the premise that vertical postures put more stress on the hind limb than do pronograde postures is generally true. The electromyographic study of *Varecia variegata* and *Eulemur rubriventer* conducted by Boyer et al. (2007) provided evidence against this premise; they observed that recruitment of leg musculature related to grasping and maintaining foot posture was actually lower in vertical postures than in pronograde postures. The authors explained this phenomenon by noting that during vertical postures the forelimbs can potentially support up to 100% of the body weight (i.e., bimanual suspension), whereas they cannot in pronograde postures.

Regardless of whether force transmission requirements on the ankle typically increase or decrease during vertical support use (static and dynamic situations likely differ), we agree that a more sloping facet (more obtuse angle) can help resist body weight better than a vertical one (more acute angle). Furthermore, as we understand it, increased slope of the fibular facet increases the degree to which the foot can be inverted by lateral rotation of the crurotarsal joint (i.e., the leg and upper ankle together: see Fig. 10) before the facet ceases to be loaded in compression, relative to the steep-sided condition. In the steep-sided condition, the astragalar-fibular contact may be parallel to the force of gravity even when the foot is not inverted by leg rotation, but if the foot is typically everted at the lower ankle joint, the calcaneus may be available as a stop (as revealed by a distinct fibular facet on the calcaneus of some African ape individuals and various terrestrial mammals including soricids, lagomorphs, ungulates, and many others); however, if the foot is inverted, the calcaneus rotates under the astragalus. The impressively large lateral shelf on the astragalar fibular facet of some anthropoids (see *Pan* in Fig. 3) is likely to imbue a weight-bearing function

²In fact, when the relatively specialized *Euoticus* is excluded, galagids and lorisids have the same mean value for fibular facet orientation (111°).

TABLE 5. Post hoc comparison of extant higher taxonomic groups after significant ANOVA.

Group	1	2	3	4	5	6	7	8	9	10	11	12	13	14	15	16	17	18	19	20	21
1-Homo		**	****	****	1.00	****	****	****	0.98	1.00	1.00	1.00	1.00	****	****	0.13	****	****	****	****	****
2-Pan	5.81		0.44	0.16	0.42	0.46	0.96	1.00	0.69	****	**	0.26	0.06	0.78	****	****	****	****	****	****	****
3-Gorilla	9.65	3.85		1.00	****	1.00	1.00	1.00	****	****	****	****	****	1.00	****	****	****	****	****	****	****
4-Pongo	10.31	4.50	0.65		****	1.00	1.00	0.93	****	****	****	****	****	1.00	****	****	****	****	****	****	****
5-Hylobatidae	1.92	3.88	7.73	8.38		****	****	0.01	1.00	0.54	1.00	1.00	1.00	****	****	****	****	****	****	****	****
6-Cercopithecini	9.61	3.80	0.05	0.70	7.68		1.00	1.00	****	****	****	****	****	1.00	****	****	****	****	****	****	****
7-Colobinae	8.40	2.59	1.26	1.91	6.47	1.21		1.00	**	****	****	**	****	1.00	****	****	****	****	****	****	****
8-Callitrichidae	7.52	1.71	2.13	2.79	5.60	2.09	0.88		*	****	****	**	****	1.00	****	****	****	****	****	****	****
9-Cebid. + Aotus	2.43	3.38	7.22	7.88	0.51	7.18	5.97	5.09		****	****	****	****	****	****	****	****	****	****	****	****
10-Atelidae	1.73	7.54	11.39	12.04	3.66	11.34	10.13	9.26	4.16		1.00	0.71	0.96	****	****	0.90	****	****	****	****	****
11-Pitheciidae	0.06	5.75	9.60	10.25	1.87	9.55	8.34	7.46	2.37	1.79		1.00	1.00	****	****	0.11	****	****	****	****	****
12-Tarsius	1.61	4.20	8.05	8.70	0.32	8.00	6.79	5.91	0.82	3.34	1.55		1.00	****	****	****	****	****	****	****	****
13-Eosimias	0.86	4.95	8.80	9.45	1.07	8.75	7.54	6.67	1.58	2.59	0.80	0.75		****	****	*	****	****	****	****	****
14-Parapithecidi.	9.02	3.21	0.63	1.29	7.09	0.59	0.62	1.50	6.59	10.75	8.96	7.41	8.16	****	****	****	****	****	****	****	****
15-Other Cheir.	10.00	15.81	19.65	20.30	11.92	19.60	18.39	17.52	12.43	8.26	10.05	11.61	10.85	19.01		*	1.00	1.00	1.00	1.00	1.00
16-Microcebus	4.61	10.42	14.26	14.92	6.54	14.22	13.01	12.13	7.04	2.88	4.67	6.22	5.47	13.63	5.39		****	****	****	0.08	****
17-Indriidae	11.46	17.27	21.12	21.77	13.39	21.07	19.86	18.98	13.89	9.73	11.52	13.07	12.32	20.48	1.47	6.85		1.00	1.00	1.00	1.00
18-Lemuridae	11.41	17.22	21.06	21.72	13.34	21.02	19.81	18.93	13.84	9.68	11.47	13.02	12.27	20.43	1.42	6.80	0.05		1.00	1.00	1.00
19-Lepilemur	12.13	17.93	21.78	22.43	14.05	21.73	20.52	19.65	14.56	10.39	12.18	13.73	12.98	21.14	2.13	7.52	0.66	0.71		0.95	1.00
20-Galagidae	9.44	15.25	19.09	19.75	11.36	19.05	17.84	16.96	11.87	7.71	9.50	11.05	10.30	18.46	0.56	4.83	2.02	1.97	2.69		1.00
21-Lorisidae	10.33	16.14	19.98	20.64	12.26	19.94	18.73	17.85	12.76	8.60	10.39	11.94	11.19	19.35	0.33	5.72	1.13	1.08	1.80	0.89	
N	5	5	5	5	15	7	10	14	18	14	13	6	3	5	6	10	10	18	6	18	15
Mean	97	88	83	82	94	83	85	86	93	99	96	94	95	84	111	103	113	113	114	110	111
Standard error	1.41	1.92	1.72	2.62	1.62	1.13	1.20	1.09	0.97	0.98	1.10	1.38	1.29	2.49	1.81	0.95	0.91	0.62	1.31	0.90	0.77
Median	96	89	85	85	94	84	85	85	93	98	96	94	96	83	110	103	112	113	115	110	111
Min	93	82	76	73	84	77	79	81	87	94	87	90	93	79	105	97	110	108	109	102	108
Max	101	94	85	87	102	86	91	92	99	108	104	99	97	93	117	106	117	117	118	118	117

Tukey's pairwise comparisons: Q below diagonal, p(same) above diagonal.

*P ≤ 0.05.

**P ≤ 0.01.

***P ≤ 0.001.

****P ≤ 0.0001. (See Fig. 5A.)

despite an acute angle between the lateral tibial facet and fibular facet.

In addition to a weight-bearing function, Gebo (1993, 2011) has proposed that a more sloping facet creates a

more open crurotarsal joint that facilitates adduction–abduction mobility. Why do abduction–adduction and inversion correlate with use of small diameter vertical supports (e.g., Gebo, 2011)? Given our understanding of

TABLE 6. Post hoc comparison of extant higher taxonomic groups after significant ANOVA.

Group	1	2	3	4	5	6	7	8	9	10	11	12	13	14	15	16	17	18	19	20
1-Callitrichidae		**	****	****	****	**	****	****	****	****	****	****	****	****	****	****	****	****	****	****
2-Cebid. + Aotus	5.07		0.32	0.99	1.00	1.00	****	**	0.60	1.00	0.13	0.66	**	****	****	****	****	****	****	****
3-Atelidae	9.11	4.04		1.00	0.95	0.68	0.98	1.00	1.00	0.99	1.00	1.00	1.00	**	0.10	****	0.89	****	****	****
4-Pitheciidae	7.34	2.25	1.81		1.00	1.00	0.24	0.61	1.00	1.00	0.98	1.00	0.46	****	****	****	0.10	****	****	****
5-Eosimias	6.51	1.44	2.60	0.80		1.00	0.05	0.22	1.00	1.00	0.79	1.00	0.13	****	****	****	*	****	****	****
6-Tarsius	5.75	0.68	3.35	1.56	0.76		**	*	0.91	1.00	0.39	0.93	*	****	****	****	****	****	****	****
7-Teilhardina	11.51	6.44	2.40	4.22	5.00	5.76		1.00	0.87	0.11	1.00	0.83	1.00	0.45	0.99	0.28	1.00	****	*	****
8-Hemicodon	10.78	5.71	1.67	3.49	4.27	5.03	0.73		0.99	0.37	1.00	0.99	1.00	0.14	0.84	0.07	1.00	****	*	****
9-Shoshonius	8.57	3.50	0.54	1.27	2.06	2.82	2.94	2.21		1.00	1.00	1.00	0.97	****	*	****	0.64	****	****	****
10-Anemorhysis	6.85	1.78	2.26	0.46	0.34	1.09	4.66	3.93	1.72		0.91	1.00	0.24	****	****	****	*	****	****	****
11-C. ralstoni	9.65	4.58	0.54	2.35	3.14	3.90	1.86	1.13	1.08	2.80		1.00	1.00	*	0.27	**	0.98	****	****	****
12-C. trigonodus	8.46	3.40	0.64	1.16	1.96	2.71	3.05	2.32	0.10	1.62	1.19		0.96	****	*	****	0.59	****	****	****
13-C. abditus	11.06	5.99	1.95	3.77	4.55	5.31	0.45	0.28	2.49	4.21	1.41	2.60		0.23	0.93	0.13	1.00	****	*	****
14-Notharctus	15.29	10.22	6.19	8.02	8.78	9.54	3.78	4.51	6.72	8.45	5.64	6.83	4.23		1.00	1.00	0.71	0.64	1.00	0.98
15-Asiadapinae	13.78	8.72	4.68	6.51	7.28	8.03	2.28	3.01	5.22	6.94	4.14	5.32	2.73	1.51		1.00	1.00	0.06	0.82	0.36
16-Adapinae	15.63	10.56	6.53	8.36	9.12	9.88	4.12	4.85	7.06	8.79	5.98	7.17	4.57	0.34	1.85		1.00	0.53	0.81	1.00
17-Microcebus	11.99	6.93	2.89	4.71	5.49	6.24	0.48	1.22	3.43	5.15	2.35	3.53	0.94	3.30	1.79	3.64		****	0.07	*
18-other lemurs	18.73	13.66	9.62	11.47	12.22	12.97	7.22	7.95	10.16	11.88	9.08	10.26	7.67	3.43	4.94	3.10	6.73		1.00	1.00
19-Galagidae	16.84	11.77	7.73	9.58	10.33	11.09	5.33	6.06	8.27	9.99	7.19	8.38	5.78	1.55	3.06	1.21	4.85	1.89		1.00
20-Lorisidae	17.73	12.67	8.63	10.47	11.23	11.98	6.23	6.96	9.17	10.89	8.09	9.27	6.68	2.44	3.95	2.10	5.74	0.99	0.89	
N	15	17	14	13	3	6	3	5	3	3	4	5	6	10	4	11	10	40	18	15
Mean	86	93	99	96	95	94	102	101	98	96	100	98	102	108	106	108	103	113	110	111
Standard error	1.05	0.90	0.98	1.10	1.29	1.38	1.07	0.71	2.00	1.68	1.85	1.84	2.07	1.17	1.96	0.83	0.95	0.49	0.90	0.77
Median	86	93	98	96	96	94	103	101	97	96	101	97	103	108	106	109	103	113	110	111
Min	81	87	94	87	93	90	100	99	96	93	95	93	93	101	100	104	97	105	102	108
Max	92	99	108	104	97	99	104	103	102	99	103	103	107	116	110	114	106	118	118	117

Tukey's pairwise comparisons: Q below diagonal, p(same) above diagonal.

*P ≤ 0.05.

**P ≤ 0.01.

***P ≤ 0.001.

****P ≤ 0.0001. (See Fig. 5B.)

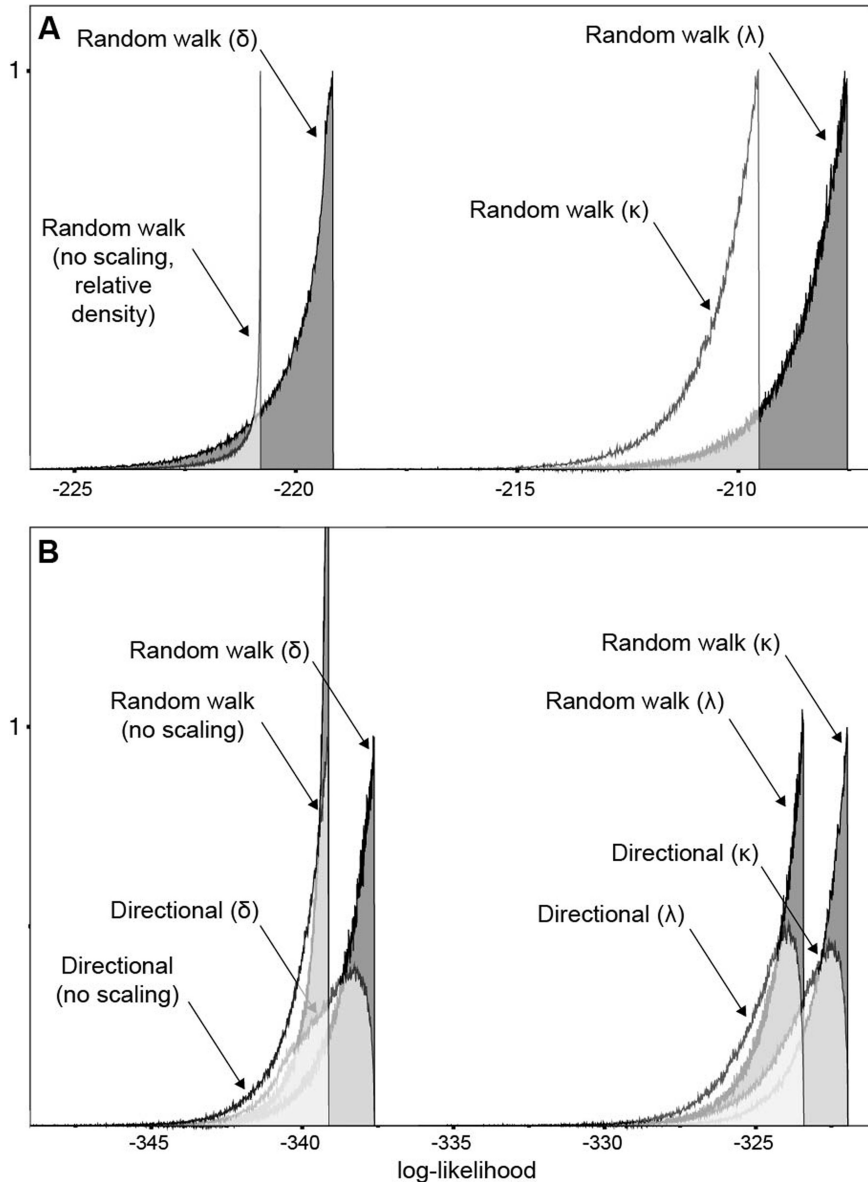


Fig. 7. Densities of likelihoods from initial MCMC analyses (10,050,000 iterations, first 50,000 discarded as burn in), testing the effects of different phylogenetic scaling parameters for **(A)** extant euarchontans alone and **(B)** living and extinct euarchontans.

the movements involved, astragalar features that facilitate weight bearing of the fibula and mobility in abduction–adduction should be important when climbing on horizontal or vertical supports, as long as the support diameter is relatively small: Dagosto (1988) suggested accordingly that as larger bodied taxa are likely to encounter relatively smaller supports, the suite of features recognized as characteristic of strepsirrhine ankles may have been adaptations acquired in a common ancestor that obtained relatively large body size early in the Paleogene, while early haplorhines (omomyiforms) remained small.

Below we describe how locomotion on both horizontal and vertical small diameter supports results in inversion and is facilitated by mobility in abduction–adduction. Observing lemurs walking on small diameter supports, it is clear that they tend to lead with hallux, which is “hooked” over the substrate, so that the tip of the hallucal

digit is on the contralateral side of the branch, while the rest of the foot and digits wrap around the ipsilateral side (e.g., Gebo, 1993; Boyer et al., 2007). When a primate grasps a relatively small support (horizontal or vertical)

TABLE 7. Averages of log-likelihoods from initial MCMC runs (10,050,000 iterations, first 50,000 discarded as burn in) in *BayesTraits*.

Scaling parameter	Extant taxa only	Extant and fossil taxa (A)	Extant and fossil taxa (B)
None	–221.3137	–339.6401	–340.1458
δ	–220.1335	–338.6271	–339.3157
κ	–210.5601	–322.9551	–323.5681
λ	–208.5736	–324.4050	–324.9054

“A” refers to the constant-variance random walk model; “B” is the directional model. See also Figure 6.

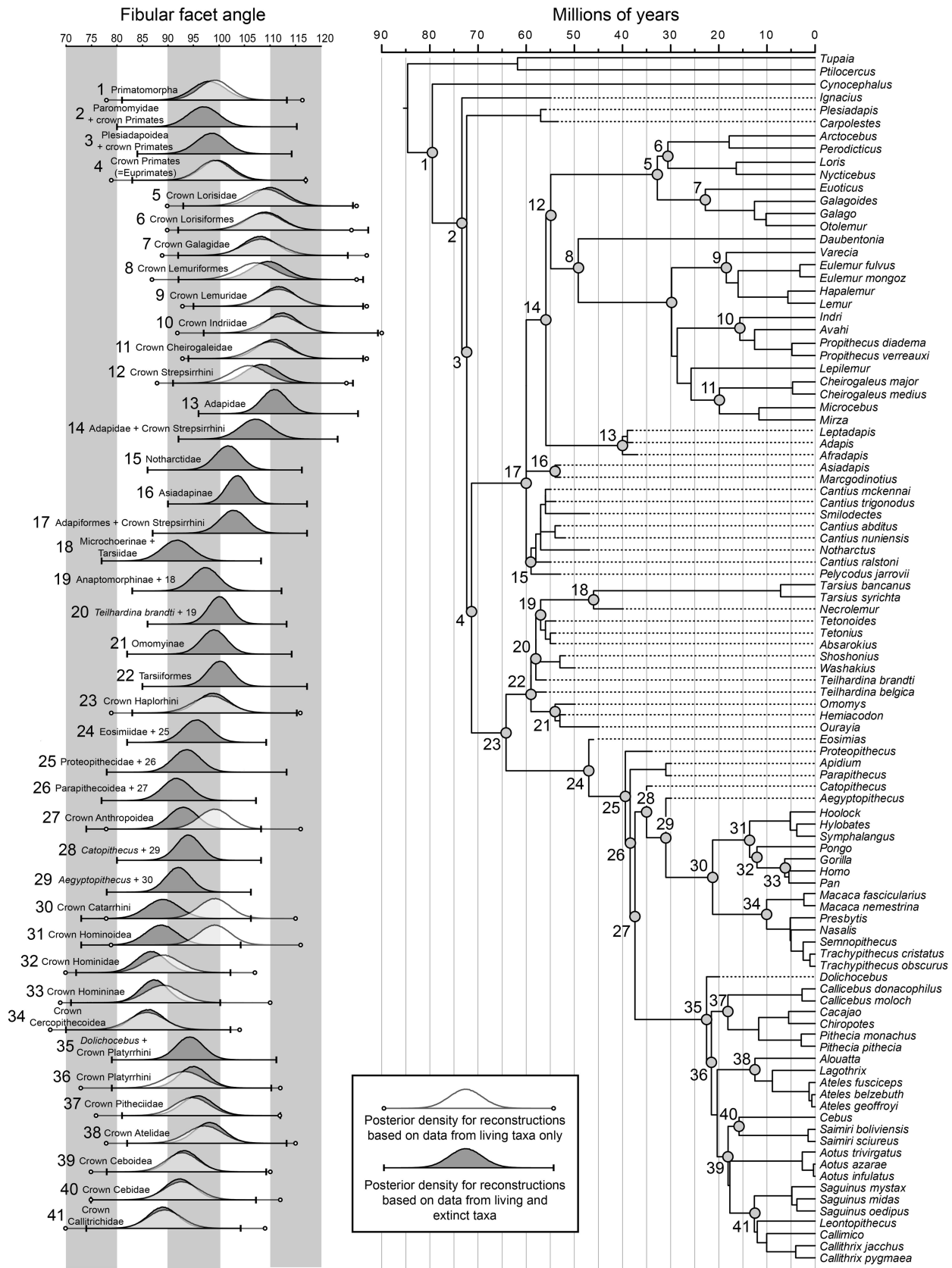


Fig. 8. On right, time-scaled supertree used for Bayesian ancestral reconstructions of living and extinct euarchontans. On left, the 95% densities for each ancestral reconstruction of fibular facet orientation for selected clades (numbers to the left correspond to the numbered nodes on the cladogram) based on combined results of two independent MCMC chains (each of 30,050,000 iterations, first 50,000 discarded as burn in) in *BayesTraits*. Densities colored white and slightly translucent are for reconstructions based on extant taxa alone (i.e., the tree provided by Springer et al. (2012), pruned to only include those taxa represented in our dataset); grey densities are reconstructions based on the entire tree shown here.

TABLE 8. Mean ancestral reconstructions and 95% HPD, calculated in Tracer 1.5 (Rambaut and Drummond, 2007), for major primate crown clades.

Node (crown clades)	Reconstruction with extant taxa only Phylogenetic scaling parameter λ			Reconstruction with extant and fossil taxa Phylogenetic scaling parameter κ		
	Mean	Lower 95% HPD	Upper 95% HPD	Mean	Lower 95% HPD	Upper 95% HPD
Primateomorpha	99.20	92.98	105.34	97.91	91.35	104.38
Primates	99.20	92.92	105.27	99.52	93.33	105.60
Haplorhini	98.47	91.22	105.67	98.70	92.43	104.95
Anthropoidea	99.20	93.00	105.35	92.83	87.11	98.51
Platyrrhini	93.24	85.75	100.57	94.86	89.18	100.64
Aotidae + Cebidae	92.83	86.41	99.29	93.03	87.20	98.86
Atelidae	97.23	90.16	104.31	98.01	92.10	103.92
Callitrichidae	89.41	82.73	96.09	88.89	83.11	94.70
Cebidae	92.67	85.89	99.49	92.18	86.35	98.10
Pitheciidae	94.78	87.93	101.54	95.68	89.45	101.84
Catarrhini	99.20	93.06	105.41	88.90	82.50	95.31
Cercopithecoidea	85.91	78.77	92.91	85.99	79.88	92.11
Hominoidea	99.20	93.05	105.40	88.55	82.39	94.75
Hominidae	88.95	82.09	96.09	86.56	80.74	92.34
Homininae	89.03	82.02	96.17	87.14	81.72	92.48
Strepsirrhini	105.97	98.86	112.95	108.22	101.68	114.72
Lemuriformes	107.27	99.98	114.66	109.52	102.76	116.33
Cheirogaleidae (Che.)	110.32	103.12	117.63	110.62	104.20	117.02
Indriidae (Ind.)	112.23	104.90	119.58	112.32	106.17	118.40
Lemuridae (Lem.)	111.77	104.50	118.97	111.59	105.37	117.89
Lepilemuridae (Lep.)+Che.	110.85	103.93	117.81	111.77	105.34	118.03
Che. + Ind. + Lem. + Lep.	110.77	103.89	117.47	111.11	104.51	117.76
Lorisiformes	108.79	101.53	115.92	108.95	102.15	115.70
Galagidae	108.45	100.95	116.05	107.87	101.41	114.31
Lorisidae	109.15	101.96	116.48	109.92	103.35	116.65

For each analysis [(1) extant taxa only, and (2) extant and fossil taxa combined] values are averages from 60,000,000 post-burnin MCMC iterations in *BayesTraits* (each analysis included two independent MCMC chains run for 30,050,000 generations).

in this way during locomotion, the lateral aspect of the foot collapses around the ipsilateral side of the support, bringing the array of the metatarsal heads approximately in line with the animal's sagittal plane and thereby into inversion (note that in lemurids, the foot is already pre-configured in this way to some degree by the form of the tarso-metatarsal complex: Gebo, 1985, 1993).

Dagosto (1985), Dagosto et al. (2008), and Gebo (2011), among other papers by these authors, describe how the curvilinear paths of the astragalotibial joint facets and the rotated medial malleolus of strepsirrhines result in conjunct abduction during dorsiflexion, and adduction during plantar flexion. Abduction during dorsiflexion is useful during swing phase and just prior to touch down when locomoting on small diameter supports because it 1) shifts the digits lateral to the crurotarsal joint and reduces the amount of contralateral projection of the physiologically abducted hallux (Boyer et al., 2007; Jacobs et al., 2009), and 2) prepositions the nonhallucal digits lateral to (instead of in-line with) the narrow, midline support they are about to engage. Once touch-down and grasping occurs, as support phase progresses, and the ankle begins to plantar flex as the leg moves forward, conjunct adduction will guide the crurotarsal joint away from the midline, such that modifications in foot posture via inversion–eversion movements at the subtalar and transverse tarsal joints can maintain an effective grasp for longer. Alternatively, if the foot is placed on a large diameter support (including flat ground), the array of the metatarsal heads will be at approximately 90° to the sagittal plane, and the foot can maintain a more everted posture. Furthermore, a wide foot stance can be used, negating the need for shifting the lateral position of the foot through abduction–adduction movements.

In our dataset, limited support for this hypothesis comes from our finding that some of the lowest values among strepsirrhines are found in the galagid *Euoticus* (mean of 104°), which uses its claws to cling to large-diameter supports (Charles-Dominique, 1974). The only anthropoids that use this strategy (Callitrichidae) similarly have the lowest values for fibular facet orientation within their radiation (Platyrrhini). Unfortunately, we were not able to measure the astragalus of the only other strepsirrhine that similarly clings to large-diameter supports (*Phaner*); this would be an important test of the hypothesis. Other possible sources of evidence for this hypothesis include our findings that 1) the lemuriforms and platyrrhines with the steepest fibular facets are all small-bodied (for instance *Microcebus* with a mean of 103°) and 2) there is a correlation between body size and facet angle in these groups. The significant relationship between our size proxies and fibular facet orientation in platyrrhines and strepsirrhines (and particularly within lemuriforms) might reflect the fact that smaller lemurs such as *Microcebus* are forced to more frequently use relatively large supports despite a preference for smaller branches (Gebo, 1987), thus requiring more frequent use of everted foot postures. The supports encountered by larger monkeys and lemurs are more often relatively small compared to foot size, requiring relatively abducted and inverted foot postures and greater mobility of the joints between the tibia, fibula, and astragalus.

Note that the functional association between a sloping facet and inverted foot postures is predicated on the assumption that inverted postures are used during pronograde and/or orthograde locomotion. For instance, anti-pronograde *Pongo* uses inverted postures but lacks a sloping facet: its inversion is accomplished partly by

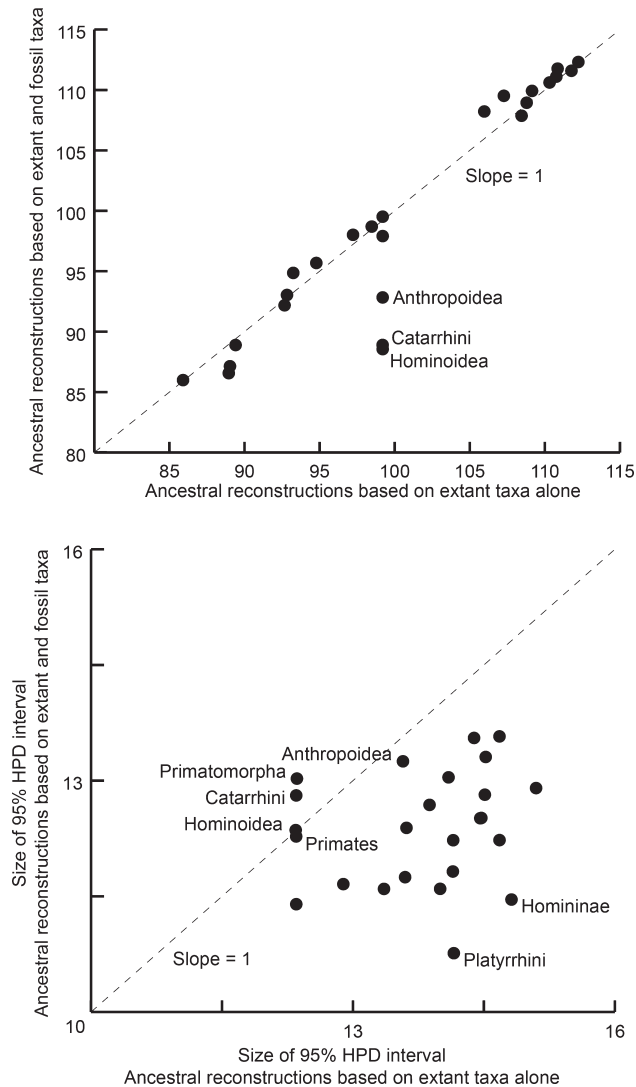


Fig. 9. Above, plot of mean ancestral reconstructions derived from analysis of extant taxa alone against mean ancestral reconstructions derived from analysis of living and extinct taxa. Below, plot of the absolute range of the 95% HPD for each ancestral reconstruction derived from analysis of extant taxa alone against the absolute range of the 95% HPD for each ancestral reconstruction derived from analysis of living and extinct taxa. Essentially the plot shows the effect of including fossils on mean and variance of ancestral state reconstructions (ASR). If there had been *NO* effect, both plots would have been a perfect straight line of points ($y = x$). The fact that this did not happen means the fossil data are affecting the ASRs (see text).

increasing the inequality of the height of astragalar rims (and consequently results in a highly acute fibular facet angle). Humans have a more sloping facet, but this reflects more buttressing of the medial rim of the lateral tibial facet needed to reduce medio-inferior shear that would result during bipedal locomotion if they exhibited the configuration of their relatives.

The recently rekindled debate surrounding the higher-level relationships of the extinct adapiform primates has led some researchers to recite the “established” synapomorphies linking adapiforms to strepsirrhines (Williams et al., 2009, 2010; Gebo, 2011) or to haplorhines (Franzen et al., 2009; Gingerich et al., 2010). Although a laterally sloping

fibular facet has usually been regarded as a feature present in adapiforms and linking them to extant strepsirrhines (e.g., Gebo, 1988), Franzen et al. (2009) argued that *Darwinius masillae* has a “steep-sided” facet and that this is a haplorhine apomorphy. Gingerich et al. (2010) maintained that the fibular facet of *Darwinius* is steep-sided but argued that the condition is plesiomorphic within primates. Our study supports Gingerich et al.’s assessment of the polarity of this trait, but as of this writing, no attempt has been made to quantify the orientation of the fibular facet in *Darwinius*. We contend that it will not be possible to do so without micro-CT imaging and digital extraction of the element, because the astragalar trochlea is obscured by the articulating tibia. Importantly, however, the established close relative of *Darwinius*, *Afradapis* (Seiffert et al., 2009) has an astragalus attributed to it with a facet measured as lemuriform-like (Boyer et al., 2010); it is, in fact, one of the most obtuse angles that we observed among living and extinct primates. In light of this, we predict that, when

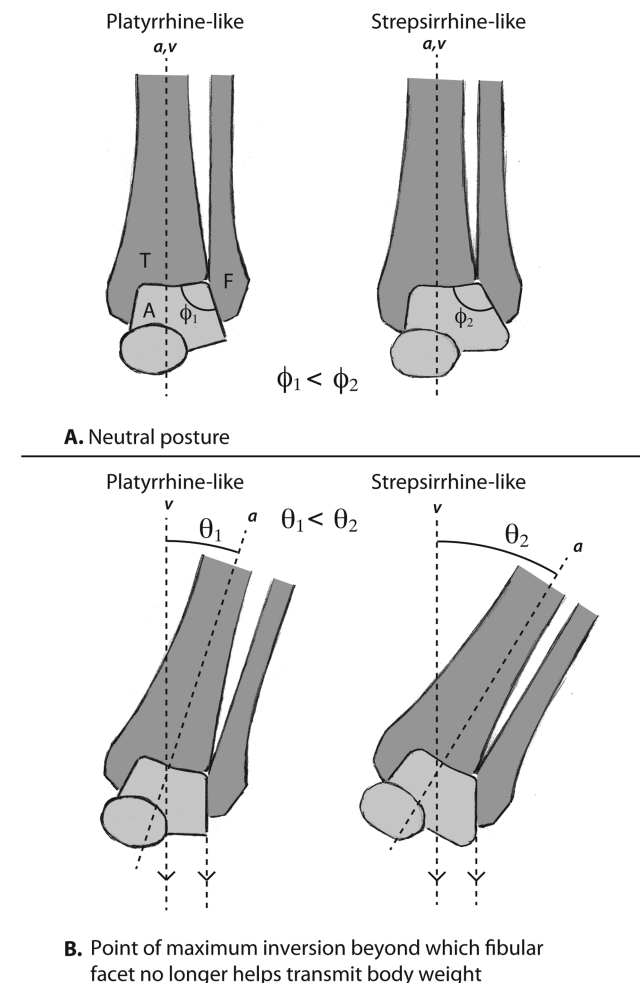


Fig. 10. Schematic diagram showing how a sloping fibular facet (greater ϕ) of strepsirrhines allows the weight-bearing function of the facet to be maintained under higher angles of inversion (greater θ) accomplished by external rotation of the leg (ultimately probably accomplished by abduction of a flexed hip in combination with flexed knees). Such postures are expected to be required by taxa using relatively small diameter supports. A, astragalus; a, anatomical axis of leg; T, tibia; F, fibula; v, vertical axis.

TABLE 9. Mean ancestral reconstructions and 95% HPD, calculated in Tracer 1.5 (Rambaut and Drummond, 2007), for extinct clades and clades that include extinct stem members.

Node	Clade on Fig. 8	Reconstruction with extant and fossil taxa Phylogenetic scaling parameter κ		
		Mean	Lower 95% HPD	Upper 95% HPD
Adapiformes + crown Strepsirrhini	17	102.70	97.31	108.07
Notharctinae	15	101.64	96.54	106.78
Asiadapinae	16	103.44	98.98	107.80
Adapidae + crown Strepsirrhini	14	107.07	100.86	113.21
Adapidae	13	110.75	105.58	115.87
Adapinae	–	108.69	104.40	113.02
Omomyinae	21	98.89	93.84	103.99
Microchoerinae + Tarsiidae [1]	18	91.64	85.74	97.57
Anaptomorphinae + 1 [2]	19	97.21	91.92	102.54
<i>T. brandti</i> + 2	20	100.00	95.46	104.52
Tarsiiformes (omomyiforms + Tarsiidae)	22	100.03	95.07	104.92
<i>Dolichocebus</i> + crown Platyrrhini	35	94.16	88.82	99.59
<i>Aegyptopithecus</i> + crown Catarrhini [3]	29	91.91	86.88	96.91
<i>Catopithecus</i> + 3	28	93.87	88.92	98.79
Parapithecidae + crown Anthropoidea [4]	26	91.58	86.02	97.13
Proteopithecidae + 4 [5]	25	93.55	88.10	99.04
Eosimiidae + 5	24	95.50	90.04	100.97
Plesiadapoidea	–	96.80	90.72	102.78
Plesiadapoidea + crown Primates [6]	3	98.42	92.39	104.33
Paromomyidae + 6	2	96.86	90.70	102.89

quantified using the approach described here, the fibular facet of *Darwinius* will be similarly strepsirrhine-like.

The orientation of the fibular facet in early fossil primates generally fits well with an evolutionary scenario in which this feature tracks an early divergence of

strepsirrhines from haplorhines, with the most basal stem strepsirrhines being early Eocene adapiforms. When the ancestral reconstructions are plotted against geological time (Fig. 11A), the slopes of lines connecting adjacent nodes in the phylogeny generally have very

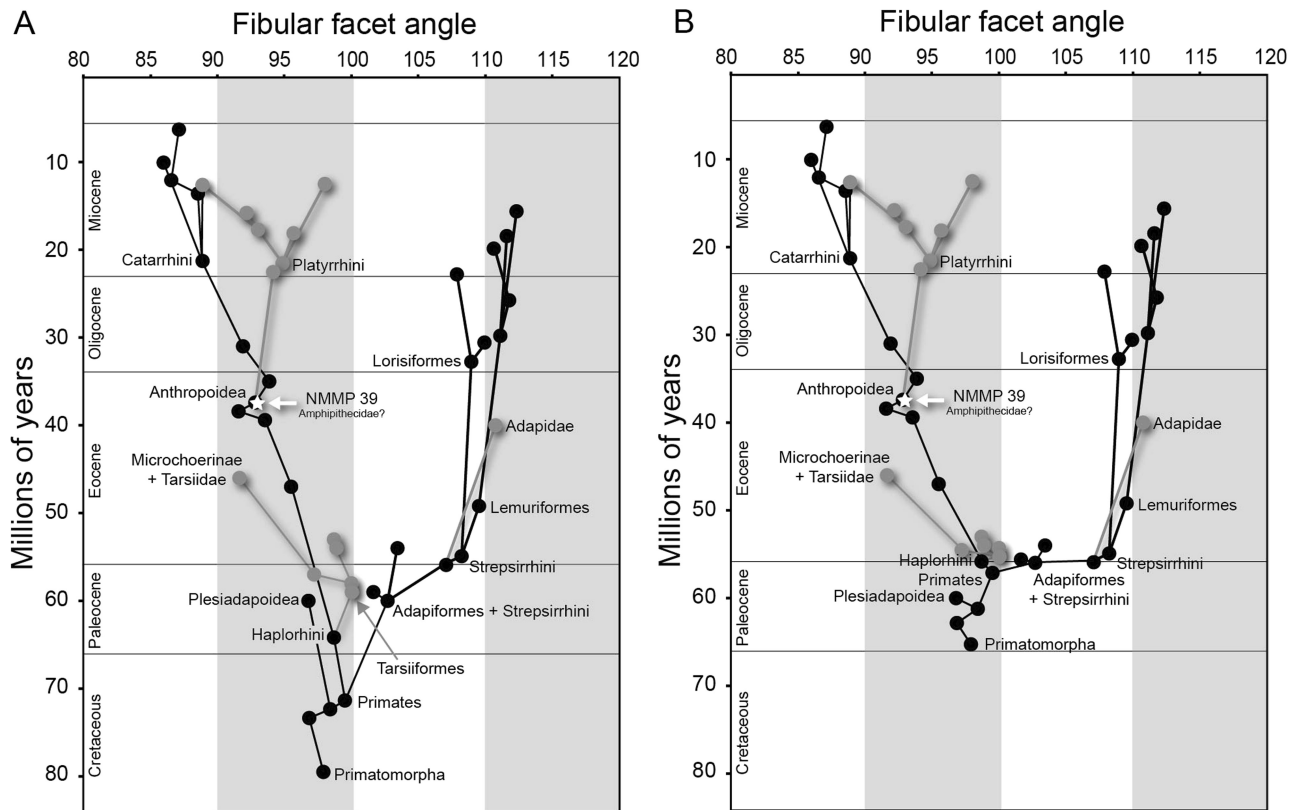


Fig. 11. Changes in fibular facet orientation over the course of primate evolution. (A) Mean ancestral reconstructions (based on living and extinct taxa) for selected euarchontan clades plotted against their ages in our time-scaled supertree; (B) same as in A but with oldest nodes arbitrarily adjusted to be consistent with a latest Paleocene origin of crown primates.

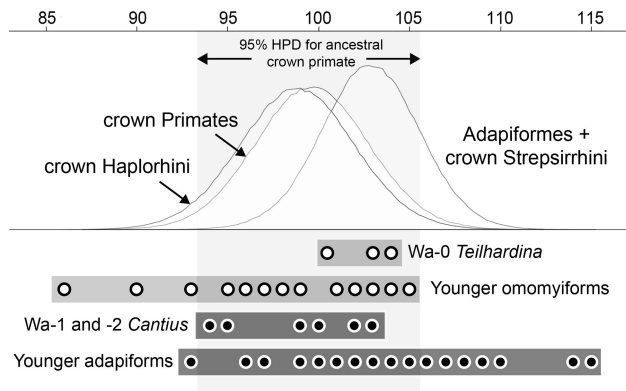


Fig. 12. Above, 95% HPDs of the Bayesian ancestral reconstructions (based on living and extinct taxa) for the crown primate, crown haplorhine, and adapiform+crown strepsirrhine nodes; below, fibular facet orientation in the oldest representatives of the omomyiform (*Teilhardina*) and adapiform (*Cantius*) clades, compared with the distribution of values in later omomyiforms and adapiforms (including younger *Cantius* species). Wa-0, Wa-1, Wa-2 refers to the earliest intervals of the early Eocene Wasatchian Land Mammal Age in North America.

high slopes, but two of the lines early in the primate tree are much closer to horizontal, suggesting a rapid change in fibular facet angle: 1) the line connecting last common ancestor (LCA) of a) *Teilhardina brandti* and all tarsii-forms aside from *Teilhardina belgica*, and b) of anaptomorphines, microchoerines, and tarsiids (slope of 0.35), and 2) the line connecting the LCA of a) adapiforms + strepsirrhines and b) of adapids + crown strepsirrhines (slope of 0.93). Both of these changes are reconstructed as having occurred in the later part of the Paleocene, before the first appearances of haplorhines and strepsirrhines in the fossil record. When the basal primate nodes are adjusted to fit a latest Paleocene, rather than a Late Cretaceous, origin for crown Primates (Fig. 11B), these early changes in fibular facet orientation become even more dramatic; this temporal scenario would require that this fundamental change in strepsirrhine pedal morphology occurred over a geologically very brief period of time, with very little change thereafter. The slope between the crown haplorhine node and that for Eosimiidae + later anthropoids is 5.38 on our time-scaled supertree, suggesting a fairly gradual change from the ancestral crown primate and crown haplorhine condition along the anthropoid stem lineage that would not change dramatically if crown primates and crown haplorhines appeared near the Paleocene-Eocene boundary.

There are, however, some paradoxical patterns among the oldest fossil primates that complicate this simple scenario. Gebo (2011) argued that "...all strepsirrhines, living or extinct, possess [the sloping fibular facet]. This includes taxa such as the primitive adapiform *Donrussellia* (Gebo et al., 2001) or the oldest adapiform (*Cantius*; Gebo et al., 1991)" (p. 325). We have not been able to calculate fibular facet orientation in *Donrussellia*, but we did calculate this angle in 17 specimens of early Eocene *Cantius*; these range from 93° to 118°, easily exceeding the entire 95% HPD of our estimate for the ancestral crown primate condition. Intriguingly, the oldest species of *Cantius* in our sample (Wa1-2 *Cantius ralstoni*, Wa2-3 *Cantius mckennai*, and Wa4-5 *Cantius trigonodus*) have average values of 99.8°, 96.4°, and 98°, respectively—that is, very close to, and in the case of *C.*

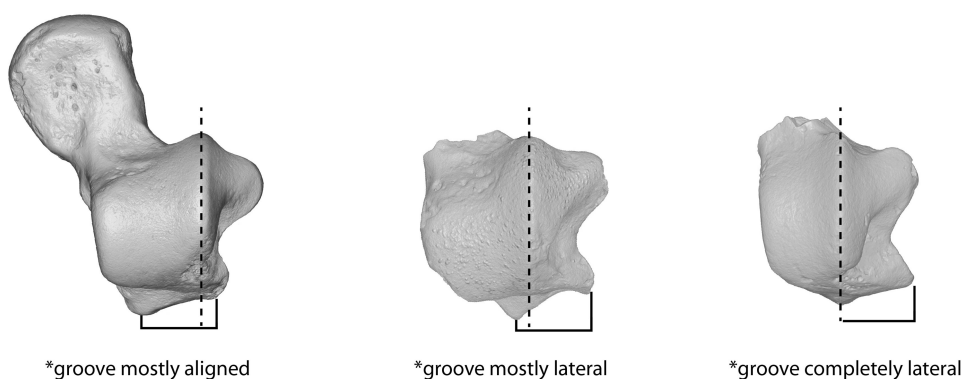
mckennai, even lower than, the value expected for the ancestral crown haplorhine (Fig. 12). The phylogenetically most basal notharctine, *Pelycodus jarrovii* (Gunnell, 2002), has a value of 99°—again, indistinguishable from our estimate for the ancestral crown haplorhine.

If notharctines are monophyletic as generally assumed (Godinot, 1998; Gunnell, 2002), the low values in the oldest and most basal taxa might indicate that high fibular facet angles (i.e., more gently sloping fibular facets) evolved independently in later notharctines and later strepsirrhines, and that the sloping fibular facet might not, by itself, constitute unambiguous evidence for inclusion of notharctines as stem strepsirrhines, regardless of the reality of such a clade. The Bayesian ancestral reconstruction for the common ancestor of Notharctinae, taking into account the relationships proposed by Gunnell (2002) is 101.6° (Table 9), which is on the high end of the ancestral 95% HPD for the crown primate; in light of this, lower values among some species of *Cantius* might represent reversals within that clade, or simply natural intraspecific variation in species that closely approximate the ancestral primate condition. We also note that other recent phylogenetic analyses (Marivaux, 2006; Bajpai et al., 2008; Ni et al., 2009; Boyer et al., 2010;) differ from ours in nesting *Cantius* deep within an adapiform clade rather than placing it as a relatively basal form; if these topologies are correct, then the low values in *Cantius* would be unambiguous convergences with the ancestral haplorhine condition.

In contrast to early *Cantius*, the mean and range of values for the younger notharctine *Notharctus* overlap substantially with more derived strepsirrhines (Tables 1, 2, 8, and 9; Figs. 1 and 4). The timing of speciation events during notharctine evolution is relatively well-constrained (Gunnell, 2002) and implies that a transition from a mean value of 98–100° (in *Cantius*) to 108° (in *Notharctus*) happened in no more than about 7 million years. Why would multiple lineages evolve greater fibular facet angles at roughly the same time? If early euprimate diversification is explained by environmental changes that proceeded after the initial morphological changes establishing the euprimate morphotype (e.g., Sussman, 1991), then it is easy to imagine multiple lineages of early euprimates responding similarly to such selection pressures in parallel. The sloping facet of *Notharctus* might have been gradually increased as part of a pedal complex that allowed these species to negotiate habitat structures that required the locomotor modes so characteristic of lemuriforms today, in which inverted foot postures on small diameter supports are typical and mobility in abduction and adduction is thereby selected for (Gebo, 1993, 2011). If notharctines followed the lemuriform (and platyrrhine) pattern of increasing fibular facet orientation with increasing body size, this change might reflect an increased dependence on inverted and abducted foot postures as notharctines got bigger in the late Wasatchian and early Bridgerian and were obliged to rely on supports of relatively smaller diameter.

We continue to refine and expand our morphological character matrix through careful examination of different elements (e.g., Patel et al., 2012), and in the current iteration the dataset supports the paraphyly of adapiforms with respect to crown strepsirrhines, with notharctines and asiadapines being basal, and adapids emerging as closer relatives of crown strepsirrhines (as envisioned by Beard et al., 1988). We consider this arrangement (rather than one with adapiforms as haplorrhines) to provide a better explanation for the sequence of pedal character

A. Dorsal view with rotation around proximodistal axis until axis of arc of lateral rim is parallel to page



B. Standard dorsal view



C. Standard proximal view (with lateral tibial facet highlighted)

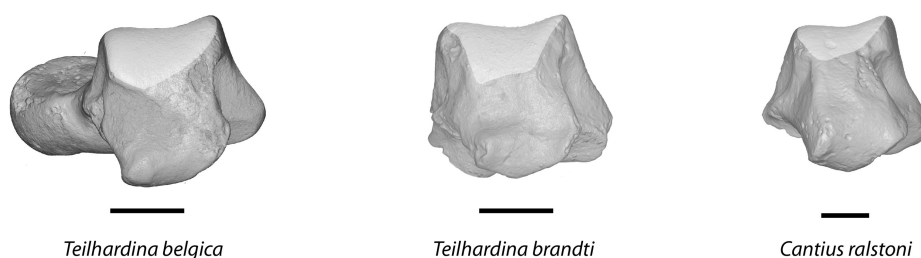


Fig. 13. *Teilhardina belgica* IRSNB M1235 (left); *Teilhardina brandti* USNM 540329 (center); *Cantius ralstoni* UM 87475 (reversed at right) showing differences in fibular facet groove position relative to tibial facet. Row A is the most relevant view for assessing this feature. The view is standardized relative to the axis of rotation dictated by the arc of the lateral trochlear rim. The subtle differences among various prosimian taxa in the configuration of this area make our interpretation subject to future finds of additional *T. brandti* specimens as well more comprehensive and repeatable quantification of this feature among primates.

evolution along the strepsirrhine stem lineage. For instance, the *Cantius* specimens with acute fibular facet angles nevertheless have laterally placed grooves for the tendon of flexor hallucis longus, somewhat trapezoidal (rather than rectangular) trochlear surfaces, and a curvilinear arc to the trochlea in dorsal view (Fig. 13) consistent with their placement as stem strepsirrhines (Dagosto, 1988), rather than stem haplorhines.

Omomyiforms are largely similar to *Tarsius* and platyrrhines in their fibular facet slope, but again, the most notable exceptions are the oldest known representatives, *Teilhardina brandti* (100–103°) and *Teilhardina belgica* (104°), with values that are on the high end of our ancestral estimate for crown primates (Fig. 11)—and higher than the ancestral estimate for Notharctinae. Other omomyiforms that have values higher than 100° are four specimens of *Hemiacodon*, one specimen of *Absarokius*, and one of *Shoshonius*. Interestingly, both species of *Teilhardina* differ somewhat from later

omomyiforms in the outline of the astragalar trochlea, having relatively elongate lateral and short medial trochlear keels (Gebo et al., 2012).

Recognition that the earliest known omomyiform and adapiform tali are indistinguishable in a feature long marshaled as evidence for these two groups being on separate haplorhine and strepsirrhine sides of the primate tree, respectively (see Gebo et al., 2012, their Table 12) has led us to look more carefully at other aspects of morphology. Unlike all other omomyiforms in our sample, *Teilhardina brandti* (USNM 540329) appears to have a groove for the tendon of flexor hallucis longus that is mostly lateral to the posterior aspect of the astragalar trochlea (Fig. 13). To the best of our knowledge, this is the only omomyiform that shows this morphology. If *T. brandti* is more basal in primate phylogeny than previously thought, a laterally placed groove for the tendon of flexor hallucis longus might be the primitive condition for primates, which would not be surprising as the groove is

also lateral to the trochlea in *Ptilocercus*, *Cynocephalus*, and plesiadapiforms; however, this would again reduce support for the monophyly of adapiforms and extant strepsirrhines with respect to haplorhines.

Cantius and *Teilhardina* are thus important examples of mosaic expression of the suite of features often argued to reflect strepsirrhine synapomorphies. This helps in considering both the phylogenetic and functional significance of these features. For instance, early *Cantius* clearly exhibit some features necessitating conjunct abduction–adduction with dorsiflexion–plantarflexion (see above discussion; Fig. 13) but lack the sloping facet. This may suggest that the sloping facet is more important for helping in weight-bearing, than permitting abduction–adduction. Likewise, in *T. brandti*, the lateral positioning of the groove for flexor fibularis suggests inverted and abducted foot postures, but the straight trochlear rims suggest against conjunct abduction–dorsiflexion.

While this study was mainly designed to evaluate the strepsirrhine-haplorhine dichotomy in fibular facet orientation, it has revealed fibular facet orientation to be functionally and phylogenetically informative at multiple levels within the primate tree. The low ancestral values for crown anthropoids (92.8°) and crown catarrhines (88.9°) are also derived conditions relative to that of the ancestral crown primate; this has not been fully appreciated and is not captured by the binary “straight-sided” versus “sloping” states typically used in phylogenetic analyses (Dagosto and Gebo, 1994; Ross et al., 1998). Interestingly, the controversial astragalus NMMP 39 from the middle Eocene of Myanmar (Marivaux et al., 2003), which has been interpreted as either anthropoid-like and supporting the anthropoid affinities for Amphipithecidae (Dagosto et al., 2010; Marivaux et al., 2003, 2010) or not (Gunnell and Ciochon, 2008), plots almost directly on top of the estimate for the ancestral crown anthropoid, given its age (~37 Ma) (Fig. 11).

The extremely acute values for catarrhines are due to asymmetry of the trochlear surface, in which the lateral keel is distinctly elevated relative to the medial keel (Seiffert and Simons, 2001, their Table 4). This configuration was previously interpreted as one aspect of stem catarrhines’ evolutionary solution to facilitate pedal inversion (and use of small-diameter supports) given their phylogenetically constrained pedal *bauplan* (Seiffert and Simons, 2001). If the preceding discussion outlining the functional demands on the foot during small-diameter support use is correct, then Seiffert and Simons (2001) scenario is only likely to be feasible in animals that do not 1) typically use inclined/vertical supports and abducted foot postures where a large medial tibial facet would be additionally important for transmitting body weight through a robust medial malleolus as it likely does in strepsirrhines (e.g., Gebo, 2011); 2) use postures where a large component of body weight is transmitted through the crurotarsal joints (and in which the talofibular facet should be oriented to help transmit this weight—as in strepsirrhines); or 3) benefit from mobility in abduction–adduction at the crurotarsal joint. In other words this configuration seems more likely to aid in inversion as used in antipronograde postures. Alternatively, this configuration may reflect a wide pronograde foot-stance in which the ankle is lateral to the knee, such that the tibia and fibula are slightly abducted. In such a posture, physiological inversion of the foot at the crurotarsal joint through reduction of the medial ridge of the lateral tibial facet could promote a flush contact

between the plantar aspect of the foot and a flat substrate, and would reduce the potential for laterally directed shear at the crurotarsal joint (which may also diminish the need for a large medial malleolus and medial tibial facet). The steep facet and reduced medial ridge of the lateral tibial facet in callitrichids and fossil plesiadapiforms (Boyer and Bloch, 2008; Boyer, 2009) probably reflects use of a wide foot stance on large-diameter tree trunks, for example. More habitual use of a wide foot stance on flat ground may also explain why a steep fibular facet (due to an enlarged lateral trochlear rim) is more pronounced in terrestrial cercopithecoids than in arboreal ones (Strasser, 1988).

Among anthropoids, hylobatids and callitrichids depart from the general trends seen in their respective clades. Hylobatids have elevated mean values compared to other catarrhines (Tables 1 and 2), and this has an important influence on ancestral state reconstruction when only extant taxa are considered (Table 8); within species they exhibit an exceptional degree of variation, possibly related to an emphasis on forelimb-dominated locomotion and relaxed selection on their pedal morphology. As discussed above, platyrrhines as a group (like strepsirrhines) exhibit a strong relationship between fibular facet orientation and measures of absolute size (Table 6). Without considering details of callitrichid behavior, the correlation between facet angle and size leads to the expectation that small-bodied callitrichids should have particularly acute facet angles. However, we suggest that more than allometry explains the difference between callitrichids and other platyrrhines. It seems to us that their highly acute facet angles are functionally related to their adaptive strategy of using large diameter, vertical supports via claw-clinging with feet that are widely spaced, and in which the hallux is habitually adducted and not heavily relied upon (Szalay and Dagosto, 1988).

SUMMARY

We comprehensively calculated astragalus fibular facet orientation on 304 specimens of extant fossil euarchontans using 3D digital models. We found that previous characterizations of a steeper slope (more acute angle) in haplorhines and a shallower slope (less acute angle) in strepsirrhines was accurate, with the exception of certain key fossil taxa including the earliest euprimates *Teilhardina* and *Cantius*. Additionally lemuriforms and platyrrhines (with locomotor styles characterized mainly by variations on arboreal quadrupedalism and leaping) show significant correlations between body mass proxies and facet angle, supporting a functional association between facet slope and relative support size as suggested by previous authors. Ancestral state reconstruction shows that a facet slope of around 97–99° can be considered primitive for Euarchonta and Euprimates, and that this value was retained by basal haplorhines. Strepsirrhines and at least one lineage of adapiforms independently rapidly evolved a more sloping facet and then changed little thereafter. Anthropoid lineages show trends toward the evolution of steeper slopes through time, with cercopithecoids and callitrichids having the most acute angles (steepest facet). Haplorhine-like fibular facet slopes in the oldest and most primitive notharctine *Cantius* indicate that this feature is not a synapomorphy uniting all known adapiforms with strepsirrhines. Finally, this study has revealed previously unrecognized mosaicism in an osteological complex known for its high functional and phylogenetic valence. This

suggests that more work is needed to understand the functional-adaptive significance of variation in the crurotarsal complex, and what it implies about the pattern of evolution of primates.

ACKNOWLEDGMENTS

The authors thank A. Persaud and J. Pulinat for their help in collecting data while they were honors students at Brooklyn College, CUNY. They thank the American Museum of Natural History for loans of fossil and extant primates; K.D. Rose for a loan of *Cantius* and Vastan primate specimens; the University of Michigan for a loan of *Cantius*

specimens; T. Smith for a loan of *Teilhardina* specimens; K.C. Beard for loan of eosimiids; DPC for a loan of fossil anthropoids; A. Su for use of scanned hominoid ankles; and NYCEP (including E. Delson, W. Harcourt-Smith; and L. Tallman) for access to scans of hylobatids and *Homo*. Stephen Chester paid for scanning of *Ptilocercus* specimens and those of some plesiadapiforms and kindly allowed us to use models generated from these scans in this study. The AMNH MIF (J. Thostenson and M. Hill) supported microCT scanning and poster printing. I. Wallace executed and processed additional scans at Stony Brook University's Center for Biotechnology. J. Butler and J. LoVoi processed scans.

Appendix: Individual Specimen Data.

TABLE A1.

Specimen	Infraorder	Superfamily	Higher taxon	Species ID	Scanner	Scan res. (mm)	Fib (degrees)	Ect (mm ²)	Troch (mm)
AMNH 187963	Haplorhini	Anthropoidea	Aotidae	<i>Aotus azarae</i>	VivaCT 75	0.0205	91.99	19.76	5.28
AMNH 211482	Haplorhini	Anthropoidea	Aotidae	<i>Aotus azarae boliviensis</i>	VivaCT 75	0.0205	97.46	25.33	5.38
AMNH 94992	Haplorhini	Anthropoidea	Aotidae	<i>Aotus infulatus</i>	VivaCT 75	0.0205	99.17	17.66	4.84
AMNH 201647	Haplorhini	Anthropoidea	Aotidae	<i>Aotus trivirgatus</i>	VivaCT 75	0.0205	91.15	18.35	5.10
AMNH 215056	Haplorhini	Anthropoidea	Aotidae	<i>Aotus trivirgatus</i>	VivaCT 75	0.0205	95.62	24.32	5.97
AMNH 239851	Haplorhini	Anthropoidea	Aotidae	<i>Aotus trivirgatus</i>	VivaCT 75	0.0205	98.66	19.64	5.17
AMNH 211513	Haplorhini	Anthropoidea	Atelidae	<i>Alouatta caraya</i>	VivaCT 75	0.039	102.63	78.86	10.77
AMNH 211525	Haplorhini	Anthropoidea	Atelidae	<i>Alouatta caraya</i>	VivaCT 75	0.039	95.14	77.43	10.34
AMNH 211585	Haplorhini	Anthropoidea	Atelidae	<i>Alouatta caraya</i>	VivaCT 75	0.039	95.78	54.82	9.63
SBU NA117	Haplorhini	Anthropoidea	Atelidae	<i>Alouatta</i> sp.	VivaCT 75	0.039	98.40	77.39	9.20
SBU NA113	Haplorhini	Anthropoidea	Atelidae	<i>Alouatta</i> sp.	VivaCT 75	0.039	97.69	51.23	8.39
SBU NA118	Haplorhini	Anthropoidea	Atelidae	<i>Alouatta</i> sp.	VivaCT 75	0.039	98.40	60.57	10.16
AMNH 259	Haplorhini	Anthropoidea	Atelidae	<i>Ateles belzebuth</i>	VivaCT 75	0.039	95.71	92.20	12.90
AMNH 188140	Haplorhini	Anthropoidea	Atelidae	<i>Ateles fusciceps</i>	VivaCT 75	0.039	107.70	110.20	12.90
AMNH 172985	Haplorhini	Anthropoidea	Atelidae	<i>Ateles geoffroyi</i>	VivaCT 75	0.039	98.44	118.00	13.19
SBU NA10	Haplorhini	Anthropoidea	Atelidae	<i>Ateles</i> sp.	VivaCT 75	0.039	99.40	58.83	10.93
SBU NA13	Haplorhini	Anthropoidea	Atelidae	<i>Ateles</i> sp.	VivaCT 75	0.039	98.17	102.06	12.04
SBU NA18	Haplorhini	Anthropoidea	Atelidae	<i>Ateles</i> sp.	VivaCT 75	0.039	94.25	86.91	11.86
AMNH 188142	Haplorhini	Anthropoidea	Atelidae	<i>Lagothrix lagotricha</i>	VivaCT 75	0.039	100.99	52.03	10.65
AMNH 188156	Haplorhini	Anthropoidea	Atelidae	<i>Lagothrix lagotricha</i>	VivaCT 75	0.039	103.43	63.53	10.30
AMNH 183289 (L)	Haplorhini	Anthropoidea	Callitrichidae	<i>Callimico goeldi</i>	VivaCT 75	0.0205	83.80	11.18	4.32
AMNH 183289 (R)	Haplorhini	Anthropoidea	Callitrichidae	<i>Callimico goeldi</i>	VivaCT 75	0.0205	84.50	11.19	4.41
SBU Ncm01	Haplorhini	Anthropoidea	Callitrichidae	<i>Callimico goeldi</i>	VivaCT 75	0.03	91.93	12.15	4.50
AMNH 133698	Haplorhini	Anthropoidea	Callitrichidae	<i>Callithrix jacchus</i>	v/tome/x	0.02652304	89.54	5.57	3.10
AMNH 133702	Haplorhini	Anthropoidea	Callitrichidae	<i>Callithrix jacchus</i>	v/tome/x	0.02652304	90.65	6.25	3.58
SBU NC01	Haplorhini	Anthropoidea	Callitrichidae	<i>Cebuella pygmaea</i>	uCT 40	0.018	82.87	2.71	2.13
AMNH 244101	Haplorhini	Anthropoidea	Callitrichidae	<i>Cebuella pygmaea</i>	uCT 40	0.018	80.75	2.90	2.26
AMNH 185347	Haplorhini	Anthropoidea	Callitrichidae	<i>Leontopithecus rosalia</i>	v/tome/x	0.02652304	88.43	10.54	4.46
AMNH 207726	Haplorhini	Anthropoidea	Callitrichidae	<i>Saguinus midas</i>	v/tome/x	0.02652304	87.76	11.05	4.25
AMNH 266481	Haplorhini	Anthropoidea	Callitrichidae	<i>Saguinus midas</i>	v/tome/x	0.02652304	91.49	14.40	4.64
AMNH 97316	Haplorhini	Anthropoidea	Callitrichidae	<i>Saguinus midas</i>	v/tome/x	0.02652304	81.92	9.84	3.88
AMNH 188177	Haplorhini	Anthropoidea	Callitrichidae	<i>Saguinus mystax</i>	v/tome/x	0.02652304	81.34	6.36	3.38
AMNH 188174	Haplorhini	Anthropoidea	Callitrichidae	<i>Saguinus mystax</i>	v/tome/x	0.02652304	89.70	7.32	3.53
AMNH 188177	Haplorhini	Anthropoidea	Callitrichidae	<i>Saguinus mystax</i>	v/tome/x	0.02652304	81.05	7.12	3.58
SBU NSg06	Haplorhini	Anthropoidea	Callitrichidae	<i>Saguinus oedipus</i>	uCT 40	0.018	85.80	8.89	3.86
AMNH 133606	Haplorhini	Anthropoidea	Cebidae	<i>Cebus apella</i>	VivaCT 75	0.025	93.22	44.18	8.86
AMNH 133608	Haplorhini	Anthropoidea	Cebidae	<i>Cebus apella</i>	VivaCT 75	0.025	87.16	33.48	7.84
AMNH 133647	Haplorhini	Anthropoidea	Cebidae	<i>Cebus apella</i>	VivaCT 75	0.025	87.57	35.38	7.55
SBU Ncb04	Haplorhini	Anthropoidea	Cebidae	<i>Cebus</i> sp.	VivaCT 75	0.035	89.42	45.68	7.27
SBU Ncb11	Haplorhini	Anthropoidea	Cebidae	<i>Cebus</i> sp.	VivaCT 75	0.035	94.62	31.62	7.04
SBU Ncb5	Haplorhini	Anthropoidea	Cebidae	<i>Cebus</i> sp.	VivaCT 75	0.035	91.08	32.70	7.06
AMNH 209934	Haplorhini	Anthropoidea	Cebidae	<i>Saimiri b. boliviensis</i>	VivaCT 75	0.0205	92.90	20.86	4.73
AMNH 211650	Haplorhini	Anthropoidea	Cebidae	<i>Saimiri b. boliviensis</i>	VivaCT 75	0.0205	92.25	15.90	4.37
AMNH 211651	Haplorhini	Anthropoidea	Cebidae	<i>Saimiri b. boliviensis</i>	VivaCT 75	0.0205	90.19	15.86	4.20
AMNH 188090	Haplorhini	Anthropoidea	Cebidae	<i>Saimiri sciureus</i>	VivaCT 75	0.0205	96.48	16.61	4.44
SBU NSm06	Haplorhini	Anthropoidea	Cebidae	<i>Saimiri</i> sp.	uCT 40	0.018	96.91	14.35	4.49
MCZ 34714	Haplorhini	Anthropoidea	Cercopithecoidea	<i>Macaca fascicularis</i>	VivaCT 75	0.0779	84.90	55.60	9.39
MCZ 35602	Haplorhini	Anthropoidea	Cercopithecoidea	<i>Macaca fascicularis</i>	VivaCT 75	0.0779	83.50	67.43	10.15
MCZ 35729	Haplorhini	Anthropoidea	Cercopithecoidea	<i>Macaca fascicularis</i>	VivaCT 75	0.0779	76.60	57.10	9.29
MCZ 35736	Haplorhini	Anthropoidea	Cercopithecoidea	<i>Macaca fascicularis</i>	VivaCT 75	0.0779	83.60	48.13	8.64
MCZ 35631	Haplorhini	Anthropoidea	Cercopithecoidea	<i>Macaca nemestrina</i>	VivaCT 75	0.0779	82.11	68.20	10.16
MCZ 35670	Haplorhini	Anthropoidea	Cercopithecoidea	<i>Macaca nemestrina</i>	VivaCT 75	0.0779	85.77	101.06	11.58
MCZ 35687	Haplorhini	Anthropoidea	Cercopithecoidea	<i>Macaca nemestrina</i>	VivaCT 75	0.0779	83.67	61.77	9.57
MCZ 37327	Haplorhini	Anthropoidea	Cercopithecoidea	<i>Nasalis larvatus</i>	Locus SP	0.044883	82.32	163.86	14.18
MCZ 37328	Haplorhini	Anthropoidea	Cercopithecoidea	<i>Nasalis larvatus</i>	Locus SP	0.044883	79.03	168.26	14.84
MCZ 41557	Haplorhini	Anthropoidea	Cercopithecoidea	<i>Nasalis larvatus</i>	Locus SP	0.044883	86.14	191.45	15.31
MCZ 41561	Haplorhini	Anthropoidea	Cercopithecoidea	<i>Nasalis larvatus</i>	Locus SP	0.044883	78.59	169.76	15.18
AMNH 106599	Haplorhini	Anthropoidea	Cercopithecoidea	<i>Presbytis melalophos</i>	v/tome/x	0.06325	87.66	76.82	10.85
AMNH 17405	Haplorhini	Anthropoidea	Cercopithecoidea	<i>Semnopithecus entellus</i>	v/tome/x	0.06325	84.77	79.92	11.58
MCZ 35618	Haplorhini	Anthropoidea	Cercopithecoidea	<i>Trachypithecus cristatus</i>	VivaCT 75	0.0779	90.61	72.24	9.39
MCZ 35688	Haplorhini	Anthropoidea	Cercopithecoidea	<i>Trachypithecus cristatus</i>	VivaCT 75	0.0779	87.73	60.98	9.32
MCZ 37670	Haplorhini	Anthropoidea	Cercopithecoidea	<i>Trachypithecus cristatus</i>	VivaCT 75	0.0779	84.85	73.86	10.72
AMNH 11297	Haplorhini	Anthropoidea	Cercopithecoidea	<i>Trachypithecus obscurus</i>	VivaCT 75	0.0779	84.31	61.88	10.46
AMNH 11092f	Haplorhini	Anthropoidea	Hominoidea	<i>Hoolock hoolock</i>	Cyberware	na	88.04	70.60	9.48

TABLE A1. Continued

Specimen	Infraorder	Superfamily	Higher taxon	Species ID	Scanner	Scan res. (mm)	Fib (degrees)	Ect (mm ²)	Troch (mm)
AMNH 112720	Haplorhini	Anthropoidea	Hominoidea	<i>Hoolock hoolock</i>	Cyberware	na	102.07	59.40	9.28
AMNH 80068	Haplorhini	Anthropoidea	Hominoidea	<i>Hoolock hoolock</i>	Cyberware	na	87.52	74.60	10.30
AMNH 83419	Haplorhini	Anthropoidea	Hominoidea	<i>Hoolock hoolock</i>	Cyberware	na	90.75	65.44	9.59
AMNH 83425	Haplorhini	Anthropoidea	Hominoidea	<i>Hoolock hoolock</i>	Cyberware	na	84.05	58.80	8.91
AMNH 112676	Haplorhini	Anthropoidea	Hominoidea	<i>Hoolock hoolock</i>	Cyberware	na	86.60	71.49	10.24
AMNH 834243	Haplorhini	Anthropoidea	Hominoidea	<i>Hoolock hoolock</i>	Cyberware	na	90.58	64.17	9.67
MCZ 17684	Haplorhini	Anthropoidea	Hominoidea	<i>Gorilla gorilla</i>	medical CT	0.1875	85.01	502.46	24.10
MCZ 20038	Haplorhini	Anthropoidea	Hominoidea	<i>Gorilla gorilla</i>	medical CT	0.1875	84.79	748.54	29.60
MCZ 29048	Haplorhini	Anthropoidea	Hominoidea	<i>Gorilla gorilla</i>	medical CT	0.1875	84.91	769.57	28.90
MCZ 57482	Haplorhini	Anthropoidea	Hominoidea	<i>Gorilla gorilla</i>	medical CT	0.1875	83.32	658.90	28.20
HTB 1710	Haplorhini	Anthropoidea	Hominoidea	<i>Gorilla gorilla</i>	Locus SP	0.045823	76.03	423.60	24.80
AMNH hss 98-315F (L)	Haplorhini	Anthropoidea	Hominoidea	<i>Homo sapiens</i>	Cyberware	na	97.76	527.70	27.14
AMNH hss 98-318m (L)	Haplorhini	Anthropoidea	Hominoidea	<i>Homo sapiens</i>	Cyberware	na	101.28	702.41	32.15
AMNH hss 98-322F (L)	Haplorhini	Anthropoidea	Hominoidea	<i>Homo sapiens</i>	Cyberware	na	96.22	606.10	30.03
AMNH hss 98-339m (L)	Haplorhini	Anthropoidea	Hominoidea	<i>Homo sapiens</i>	Cyberware	na	93.44	709.35	30.18
AMNH hss 98-350m (L)	Haplorhini	Anthropoidea	Hominoidea	<i>Homo sapiens</i>	Cyberware	na	94.03	763.99	31.12
AMNH 119601	Haplorhini	Anthropoidea	Hominoidea	<i>Hylobates lar</i>	v/tome/x	0.041556	100.68	57.16	7.92
AMNH 146725	Haplorhini	Anthropoidea	Hominoidea	<i>Hylobates lar</i>	v/tome/x	0.041556	99.37	53.32	7.35
MCZ 41415	Haplorhini	Anthropoidea	Hominoidea	<i>Hylobates lar</i>	VivaCT 75	0.0779	101.70	74.24	9.81
MCZ 41424	Haplorhini	Anthropoidea	Hominoidea	<i>Hylobates lar</i>	VivaCT 75	0.0779	94.33	68.03	9.23
MCZ 41427	Haplorhini	Anthropoidea	Hominoidea	<i>Hylobates lar</i>	VivaCT 75	0.0779	100.06	58.75	9.06
NMNH 176227	Haplorhini	Anthropoidea	Hominoidea	<i>Pan troglodytes</i>	Locus SP	0.044965	94.16	335.26	18.68
NMNH 176229	Haplorhini	Anthropoidea	Hominoidea	<i>Pan troglodytes</i>	Locus SP	na	89.12	380.76	19.63
NMNH 220062	Haplorhini	Anthropoidea	Hominoidea	<i>Pan troglodytes</i>	Locus SP	na	87.21	344.75	20.74
AMNH 89354	Haplorhini	Anthropoidea	Hominoidea	<i>Pan troglodytes</i>	Locus SP	0.044883	88.76	333.79	17.70
AMNH 89426	Haplorhini	Anthropoidea	Hominoidea	<i>Pan troglodytes</i>	Locus SP	0.044883	82.16	321.03	17.89
NMNH 142169	Haplorhini	Anthropoidea	Hominoidea	<i>Pongo pygmaeus</i>	Locus SP	na	78.32	248.64	20.01
NMNH 142170	Haplorhini	Anthropoidea	Hominoidea	<i>Pongo pygmaeus</i>	Locus SP	0.044965	86.15	271.51	19.50
NMNH 143596	Haplorhini	Anthropoidea	Hominoidea	<i>Pongo pygmaeus</i>	Locus SP	0.044965	86.80	247.93	18.90
NMNH 143597	Haplorhini	Anthropoidea	Hominoidea	<i>Pongo pygmaeus</i>	Locus SP	0.044965	84.82	223.56	16.74
NMNH 145302	Haplorhini	Anthropoidea	Hominoidea	<i>Pongo pygmaeus</i>	Locus SP	0.044965	73.33	251.70	18.94
AMNH 106581	Haplorhini	Anthropoidea	Hominoidea	<i>Symphalangus syndactylus</i>	Cyberware	na	94.90	na	12.34
AMNH 106583	Haplorhini	Anthropoidea	Hominoidea	<i>Symphalangus syndactylus</i>	v/tome/x	0.041556	87.80	79.47	11.25
AMNH 106584	Haplorhini	Anthropoidea	Hominoidea	<i>Symphalangus syndactylus</i>	Cyberware	na	98.66	87.44	11.70
AMNH 201122	Haplorhini	Anthropoidea	Pitheciidae	<i>Cacajao calvus</i>	VivaCT 75	0.035	97.84	41.28	6.83
AMNH 70192	Haplorhini	Anthropoidea	Pitheciidae	<i>Cacajao c. rubicundus</i>	VivaCT 75	0.035	94.42	39.80	7.78
SBU NCj1	Haplorhini	Anthropoidea	Pitheciidae	<i>Cacajao sp.</i>	VivaCT 75	0.039	103.97	40.21	8.75
AMNH 211491	Haplorhini	Anthropoidea	Pitheciidae	<i>Callicebus donacophilus</i>	VivaCT 75	0.0205	96.61	16.38	5.33
AMNH 211490	Haplorhini	Anthropoidea	Pitheciidae	<i>Callicebus d. donacophilus</i>	VivaCT 75	0.0205	100.13	19.32	5.42
AMNH 210393	Haplorhini	Anthropoidea	Pitheciidae	<i>Callicebus moloch</i>	VivaCT 75	0.0205	95.88	22.77	5.43
AMNH 244363	Haplorhini	Anthropoidea	Pitheciidae	<i>Callicebus moloch</i>	VivaCT 75	0.0205	95.87	19.07	5.20
AMNH 94977	Haplorhini	Anthropoidea	Pitheciidae	<i>Callicebus moloch</i>	VivaCT 75	0.0205	97.46	15.78	4.54
AMNH 95760	Haplorhini	Anthropoidea	Pitheciidae	<i>Chiropotes albinosus</i>	VivaCT 75	0.035	86.77	51.13	8.66
AMNH 96123	Haplorhini	Anthropoidea	Pitheciidae	<i>Chiropotes satanus</i>	VivaCT 75	0.035	94.43	29.46	7.05
AMNH 202373	Haplorhini	Anthropoidea	Pitheciidae	<i>Pithecia hirsuta</i>	VivaCT 75	0.035	94.90	34.80	7.47
AMNH 187978	Haplorhini	Anthropoidea	Pitheciidae	<i>Pithecia monachus</i>	VivaCT 75	0.035	95.95	37.60	7.95
AMNH 149149 (R)	Haplorhini	Anthropoidea	Pitheciidae	<i>Pithecia pithecia</i>	VivaCT 75	0.035	99.77	26.15	6.33
AMNH 106754 (L)	Haplorhini	Tarsiiformes	Tarsiidae	<i>Tarsius b. borneanus</i>	VivaCT 75	0.0205	93.19	4.88	3.36
AMNH 106754 (R)	Haplorhini	Tarsiiformes	Tarsiidae	<i>Tarsius b. borneanus</i>	VivaCT 75	0.0205	93.91	4.82	3.15
AMNH 109367	Haplorhini	Tarsiiformes	Tarsiidae	<i>Tarsius spectrum</i>	VivaCT 75	0.0205	92.67	4.53	3.11
AMNH 109369	Haplorhini	Tarsiiformes	Tarsiidae	<i>Tarsius spectrum</i>	VivaCT 75	0.0205	89.58	4.75	3.11
AMNH 203296	Haplorhini	Tarsiiformes	Tarsiidae	<i>Tarsius syrichta</i>	VivaCT 75	0.0205	97.07	4.70	3.20
DPC 0127	Haplorhini	Tarsiiformes	Tarsiidae	<i>Tarsius syrichta</i>	uCT 40	0.018	99.12	4.85	3.20
AMNH 100640	Strepsirrhini	Lemuriformes	Cheirogaleidae	<i>Cheirogaleus major</i>	VivaCT 75	0.0205	117.00	9.69	3.97
DPC 031	Strepsirrhini	Lemuriformes	Cheirogaleidae	<i>Cheirogaleus medius</i>	v/tome/x	0.0130268	114.75	4.51	2.86
DPC 0142	Strepsirrhini	Lemuriformes	Cheirogaleidae	<i>Cheirogaleus medius</i>	uCT 40	0.015	110.76	3.88	2.61
DPC 1023	Strepsirrhini	Lemuriformes	Cheirogaleidae	<i>Cheirogaleus medius</i>	uCT 40	0.015	105.47	4.03	2.89
AMNH 174415	Strepsirrhini	Lemuriformes	Cheirogaleidae	<i>Microcebus griseorufus</i>	uCT 40	0.01	100.70	1.92	1.71
AMNH 174430	Strepsirrhini	Lemuriformes	Cheirogaleidae	<i>Microcebus griseorufus</i>	uCT 40	0.01	101.58	1.89	1.62
AMNH 174431	Strepsirrhini	Lemuriformes	Cheirogaleidae	<i>Microcebus griseorufus</i>	uCT 40	0.01	105.92	1.90	1.66
AMNH 174471	Strepsirrhini	Lemuriformes	Cheirogaleidae	<i>Microcebus griseorufus</i>	uCT 40	0.01	106.16	1.93	1.65
AMNH 174383	Strepsirrhini	Lemuriformes	Cheirogaleidae	<i>Microcebus griseorufus</i>	uCT 40	0.01	97.20	1.93	1.67
AMNH 174472	Strepsirrhini	Lemuriformes	Cheirogaleidae	<i>Microcebus griseorufus</i>	uCT 40	0.01	106.25	1.72	1.69
AMNH 174423	Strepsirrhini	Lemuriformes	Cheirogaleidae	<i>Microcebus griseorufus</i>	uCT 40	0.01	102.50	2.22	1.73
AMNH 174428	Strepsirrhini	Lemuriformes	Cheirogaleidae	<i>Microcebus griseorufus</i>	uCT 40	0.01	101.17	1.79	1.69
AMNH 174500	Strepsirrhini	Lemuriformes	Cheirogaleidae	<i>Microcebus griseorufus</i>	uCT 40	0.01	105.35	2.41	1.96
AMNH 185627	Strepsirrhini	Lemuriformes	Cheirogaleidae	<i>Microcebus griseorufus</i>	uCT 40	0.01	104.21	1.81	1.69
DPC 0137	Strepsirrhini	Lemuriformes	Cheirogaleidae	<i>Mirza coquereli</i>	uCT 40	0.015	106.90	6.04	3.23
DPC 1139	Strepsirrhini	Lemuriformes	Cheirogaleidae	<i>Mirza coquereli</i>	uCT 40	0.015	109.70	5.46	3.16
AMNH 185643	Strepsirrhini	Lemuriformes	Daubentoniidae	<i>Daubentonia madagascariensis</i>	VivaCT 75	0.039	109.88	33.19	6.61
AMNH 170461	Strepsirrhini	Lemuriformes	Indriidae	<i>Avahi laniger</i>	VivaCT 75	0.035	110.87	21.61	5.10
AMNH 100504	Strepsirrhini	Lemuriformes	Indriidae	<i>Indri indri</i>	VivaCT 75	0.039	114.97	58.26	9.38
AMNH 208992	Strepsirrhini	Lemuriformes	Indriidae	<i>Indri indri</i>	VivaCT 75	0.039	110.64	61.90	9.72
AMNH 100633	Strepsirrhini	Lemuriformes	Indriidae	<i>Propithecus diadema</i>	VivaCT 75	0.035	117.35	73.45	10.93
AMNH 208991 (L)	Strepsirrhini	Lemuriformes	Indriidae	<i>Propithecus verreauxi</i>	VivaCT 75	0.025	113.92	37.76	8.16
AMNH 170471	Strepsirrhini	Lemuriformes	Indriidae	<i>Propithecus verreauxi</i>	VivaCT 75	0.039	110.29	28.67	7.66
AMNH 170474	Strepsirrhini	Lemuriformes	Indriidae	<i>Propithecus verreauxi</i>	VivaCT 75	0.025	116.72	35.51	7.74
AMNH 208989	Strepsirrhini	Lemuriformes	Indriidae	<i>Propithecus verreauxi</i>	VivaCT 75	0.035	113.79	33.44	7.10
AMNH 208991 (R)	Strepsirrhini	Lemuriformes	Indriidae	<i>Propithecus verreauxi</i>	VivaCT 75	0.025	110.38	36.24	8.30
AMNH 170491	Strepsirrhini	Lemuriformes	Indriidae	<i>Propithecus v. verreauxi</i>	VivaCT 75	0.039	109.57	32.89	8.02
DPC 095	Strepsirrhini	Lemuriformes	Lemuridae	<i>Eulemur sp.</i>	VivaCT 75	0.0205	116.24	22.74	6.03
AMNH 170708	Strepsirrhini	Lemuriformes	Lemuridae	<i>Eulemur fulvus</i>	VivaCT 75	0.025	113.26	21.79	5.38
AMNH 170717	Strepsirrhini	Lemuriformes	Lemuridae	<i>Eulemur fulvus</i>	VivaCT 75	0.025	112.48	25.37	5.44
AMNH 170728	Strepsirrhini	Lemuriformes	Lemuridae	<i>Eulemur fulvus</i>	VivaCT 75	0.025	111.33	29.10	6.15
AMNH 170764 (L)	Strepsirrhini	Lemuriformes	Lemuridae	<i>Eulemur fulvus</i>	VivaCT 75	0.025	116.57	29.22	5.50
AMNH 170764 (R)	Strepsirrhini	Lemuriformes	Lemuridae	<i>Eulemur fulvus</i>	VivaCT 75	0.025	116.51	29.23	5.73
AMNH 31254	Strepsirrhini	Lemuriformes	Lemuridae	<i>Eulemur fulvus</i>	VivaCT 75	0.035	110.13	28.60	6.71
AMNH 17403	Strepsirrhini	Lemuriformes	Lemuridae	<i>Eulemur mongoz</i>	VivaCT 75	0.035	114.95	22.46	5.49
AMNH 170680	Strepsirrhini	Lemuriformes	Lemuridae	<i>Hapalemur g. griseus</i>	VivaCT 75	0.0205	115.13	16.22	5.02

TABLE A1. Continued

Specimen	Infraorder	Superfamily	Higher taxon	Species ID	Scanner	Scan res. (mm)	Fib (degrees)	Ect (mm ²)	Troch (mm)
AMNH 170689	Strepsirrhini	Lemuriformes	Lemuridae	<i>Hapalemur g. griseus</i>	VivaCT 75	0.0205	113.13	14.06	4.80
AMNH 61589	Strepsirrhini	Lemuriformes	Lemuridae	<i>Hapalemur g. griseus</i>	VivaCT 75	0.0205	110.83	11.54	4.68
AMNH 170739	Strepsirrhini	Lemuriformes	Lemuridae	<i>Lemur catta</i>	VivaCT 75	0.035	114.46	30.65	7.83
AMNH 170765 (L)	Strepsirrhini	Lemuriformes	Lemuridae	<i>Lemur catta</i>	VivaCT 75	0.025	109.78	25.52	6.36
AMNH 170765 (R)	Strepsirrhini	Lemuriformes	Lemuridae	<i>Lemur catta</i>	VivaCT 75	0.025	115.21	24.92	6.42
AMNH 22912	Strepsirrhini	Lemuriformes	Lemuridae	<i>Lemur catta</i>	VivaCT 75	0.035	108.21	25.08	6.33
AMNH 100512	Strepsirrhini	Lemuriformes	Lemuridae	<i>Varecia variegata</i>	VivaCT 75	0.035	111.04	37.77	8.44
AMNH 201384	Strepsirrhini	Lemuriformes	Lemuridae	<i>Varecia variegata</i>	VivaCT 75	0.035	110.77	38.67	7.93
DPC 049	Strepsirrhini	Lemuriformes	Lemuridae	<i>Varecia variegata</i>	VivaCT 75	0.0205	109.96	36.41	7.55
AMNH 170556	Strepsirrhini	Lemuriformes	Lepilemuridae	<i>Lepilemur m. leucopus</i>	VivaCT 75	0.0205	111.40	11.92	4.51
AMNH 170559	Strepsirrhini	Lemuriformes	Lepilemuridae	<i>Lepilemur m. leucopus</i>	VivaCT 75	0.0205	117.58	11.26	4.26
AMNH 170560	Strepsirrhini	Lemuriformes	Lepilemuridae	<i>Lepilemur m. leucopus</i>	VivaCT 75	0.0205	114.11	12.59	4.69
AMNH 170565	Strepsirrhini	Lemuriformes	Lepilemuridae	<i>Lepilemur m. leucopus</i>	VivaCT 75	0.0205	108.74	9.90	3.84
AMNH 170568	Strepsirrhini	Lemuriformes	Lepilemuridae	<i>Lepilemur m. leucopus</i>	VivaCT 75	0.0205	115.42	14.06	4.84
AMNH 170569	Strepsirrhini	Lemuriformes	Lepilemuridae	<i>Lepilemur m. leucopus</i>	VivaCT 75	0.0205	115.50	11.79	4.22
AMNH 269914	Strepsirrhini	Lorisiformes	Galagidae	<i>Euticus elegantulus</i>	uCT 40	0.015	102.01	7.67	3.49
AMNH 241127	Strepsirrhini	Lorisiformes	Galagidae	<i>Euticus elegantulus</i>	uCT 40	0.018	105.60	7.29	3.62
AMNH 119521	Strepsirrhini	Lorisiformes	Galagidae	<i>Galago senagalensis</i>	VivaCT 75	0.0205	112.65	6.05	3.10
AMNH 35445	Strepsirrhini	Lorisiformes	Galagidae	<i>Galago senagalensis</i>	VivaCT 75	0.0205	109.51	6.05	3.27
AMNH 83299	Strepsirrhini	Lorisiformes	Galagidae	<i>Galago senagalensis</i>	uCT 40	0.015	104.96	6.87	3.43
AMNH 87064	Strepsirrhini	Lorisiformes	Galagidae	<i>Galago senagalensis</i>	uCT 40	0.015	108.61	6.01	3.35
AMNH 70410	Strepsirrhini	Lorisiformes	Galagidae	<i>Galago sp.</i>	VivaCT 75	0.0205	113.19	6.45	3.12
AMNH 212956	Strepsirrhini	Lorisiformes	Galagidae	<i>Galagoides demidoff</i>	uCT 40	0.01	111.08	2.77	2.00
AMNH 241121 (L)	Strepsirrhini	Lorisiformes	Galagidae	<i>Galagoides demidoff</i>	uCT 40	0.01	111.20	3.11	2.21
AMNH 241121 (R)	Strepsirrhini	Lorisiformes	Galagidae	<i>Galagoides demidoff</i>	uCT 40	0.01	110.72	3.36	2.23
AMNH 212957	Strepsirrhini	Lorisiformes	Galagidae	<i>Galagoides demidoff</i>	uCT 40	0.015	112.08	3.14	2.11
AMNH 215180	Strepsirrhini	Lorisiformes	Galagidae	<i>Galagoides demidoff</i>	uCT 40	0.015	118.42	3.08	2.22
AMNH 150413	Strepsirrhini	Lorisiformes	Galagidae	<i>Galagoides demidoff</i>	uCT 40	0.015	115.00	2.94	2.07
AMNH 187364 (L)	Strepsirrhini	Lorisiformes	Galagidae	<i>Otolemur crassicaudatus</i>	VivaCT 75	0.0205	107.22	13.97	4.23
AMNH 187364 (R)	Strepsirrhini	Lorisiformes	Galagidae	<i>Otolemur crassicaudatus</i>	VivaCT 75	0.0205	108.35	13.80	4.25
AMNH 216240	Strepsirrhini	Lorisiformes	Galagidae	<i>Otolemur crassicaudatus</i>	VivaCT 75	0.0205	111.92	18.30	4.35
AMNH 80801 (L)	Strepsirrhini	Lorisiformes	Galagidae	<i>Otolemur crassicaudatus</i>	VivaCT 75	0.025	108.79	21.38	5.76
AMNH 80801 (R)	Strepsirrhini	Lorisiformes	Galagidae	<i>Otolemur crassicaudatus</i>	VivaCT 75	0.025	108.16	19.10	5.37
AMNH 207949	Strepsirrhini	Lorisiformes	Lorisidae	<i>Arctocebus calabarensis</i>	uCT 40	0.018	110.81	3.53	2.76
AMNH 212576	Strepsirrhini	Lorisiformes	Lorisidae	<i>Arctocebus calabarensis</i>	uCT 40	0.015	114.31	3.88	2.91
AMNH 150038	Strepsirrhini	Lorisiformes	Lorisidae	<i>Loris tardigradus</i>	uCT 40	0.018	110.98	5.32	3.34
AMNH 165931	Strepsirrhini	Lorisiformes	Lorisidae	<i>Loris tardigradus</i>	uCT 40	0.018	108.10	4.58	3.03
AMNH 34257 (L)	Strepsirrhini	Lorisiformes	Lorisidae	<i>Loris tardigradus</i>	uCT 40	0.015	107.66	2.88	2.35
AMNH 34257 (R)	Strepsirrhini	Lorisiformes	Lorisidae	<i>Loris tardigradus</i>	uCT 40	0.015	108.23	2.83	2.30
AMNH 102027	Strepsirrhini	Lorisiformes	Lorisidae	<i>Nycticebus coucang</i>	VivaCT 75	0.0205	113.30	6.61	3.97
AMNH 16591	Strepsirrhini	Lorisiformes	Lorisidae	<i>Nycticebus coucang</i>	VivaCT 75	0.0205	113.54	6.43	3.43
AMNH 90381	Strepsirrhini	Lorisiformes	Lorisidae	<i>Nycticebus coucang</i>	VivaCT 75	0.0205	108.52	5.83	3.62
AMHN 269851	Strepsirrhini	Lorisiformes	Lorisidae	<i>Perodicticus potto</i>	VivaCT 75	0.0205	108.47	10.93	4.63
AMNH 269907	Strepsirrhini	Lorisiformes	Lorisidae	<i>Perodicticus potto</i>	VivaCT 75	0.0205	109.28	13.51	5.04
AMNH 184579	Strepsirrhini	Lorisiformes	Lorisidae	<i>Perodicticus potto</i>	VivaCT 75	0.0205	116.05	8.61	4.54
AMNH 52698	Strepsirrhini	Lorisiformes	Lorisidae	<i>Perodicticus potto</i>	VivaCT 75	0.0205	110.43	10.41	4.38
AMNH 52708	Strepsirrhini	Lorisiformes	Lorisidae	<i>Perodicticus potto</i>	VivaCT 75	0.0205	112.17	11.17	4.28
AMNH 86898	Strepsirrhini	Lorisiformes	Lorisidae	<i>Perodicticus potto</i>	VivaCT 75	0.0205	116.74	8.79	3.77
Fossil Primates									
MACN 362	Haplorhini	Anthropoidea	Cebidae	<i>Dolichopithecus</i>	v/tome/x	0.03001786	94.40	na	na
UCMP 38762	Haplorhini	Anthropoidea	Pitheciidae	<i>Cebupithecia</i>	VivaCT 75	0.0205	102.76	21.57	5.30
DPC 1301	Haplorhini	Anthropoidea	Propliopithecidae	<i>Aegyptopithecus zeuxis</i>	v/tome/x	0.03770107	86.36	53.15	9.62
DPC 3052	Haplorhini	Anthropoidea	Propliopithecidae	<i>Aegyptopithecus zeuxis</i>	v/tome/x	0.03230916	96.70	na	9.02
DPC 24776	Haplorhini	Anthropoidea	Oligopithecidae	<i>Catopithecus brouni</i>	uCT 40	0.018	95.96	12.92	4.27
DPC 1130	Haplorhini	Anthropoidea	Parapithecidae	"Parapithecid"	v/tome/x	0.03083936	79.39	26.64	5.91
DPC 3054	Haplorhini	Anthropoidea	Parapithecidae	<i>Apidium</i>	v/tome/x	0.02192416	93.12	na	5.14
DPC 5027	Haplorhini	Anthropoidea	Parapithecidae	<i>Apidium</i>	v/tome/x	0.03230916	79.68	15.50	4.74
DPC 5416	Haplorhini	Anthropoidea	Parapithecidae	<i>Apidium</i>	v/tome/x	0.02119616	83.22	18.07	5.05
DPC 1001	Haplorhini	Anthropoidea	Parapithecidae	<i>Parapithecus grangeri</i>	v/tome/x	0.03230916	83.17	15.15	4.76
DPC 15417	Haplorhini	Anthropoidea	Parapithecidae	<i>Proteopithecus sylviae</i>	uCT 40	0.018	95.10	8.25	3.69
IVPP v11849	Haplorhini	Anthropoidea	Eosimiidae	<i>Eosimias sinensis</i>	v/tome/x	0.00672885	95.87	3.50	2.38
IVPP v11855	Haplorhini	Anthropoidea	Eosimiidae	<i>Eosimias sinensis</i>	v/tome/x	0.00736095	92.88	3.84	2.37
IVPP v12303	Haplorhini	Anthropoidea	Eosimiidae	<i>Eosimias sinensis</i>	v/tome/x	0.00633392	97.24	3.50	2.20
NMMP 39	?	?	?	<i>Pondaungia (?)</i>	VivaCT 75	0.035	93.00	34.51	7.45
AMNH 12613	Haplorhini	Tarsiiformes	Omomyiformes	<i>Hemiacodon gracilis</i>	uCT 40	0.015	102.68	7.40	3.47
AMNH 29160	Haplorhini	Tarsiiformes	Omomyiformes	<i>Hemiacodon gracilis?</i>	v/tome/x	0.01751564	101.21	na	3.49
AMNH 29163	Haplorhini	Tarsiiformes	Omomyiformes	<i>Hemiacodon gracilis?</i>	v/tome/x	0.01751564	101.30	6.07	3.20
AMNH 29185	Haplorhini	Tarsiiformes	Omomyiformes	<i>Hemiacodon gracilis?</i>	v/tome/x	0.01751564	102.82	6.25	3.13
UCM 57458	Haplorhini	Tarsiiformes	Omomyiformes	<i>Hemiacodon gracilis</i>	v/tome/x	0.01706327	98.90	6.34	3.56
BFI P79	Haplorhini	Tarsiiformes	Omomyiformes	<i>Necrolemur sp.</i>	uCT 40	0.01	85.50	6.01	2.59
UM 38321	Haplorhini	Tarsiiformes	Omomyiformes	<i>Omomys carteri</i>	uCT 40	0.018	98.66	4.95	2.79
UM 98648	Haplorhini	Tarsiiformes	Omomyiformes	<i>Omomys carteri</i>	uCT 40	0.018	96.74	4.71	2.76
SDSNH 69378	Haplorhini	Tarsiiformes	Omomyiformes	<i>Ourayia uintensis</i>	VivaCT 75	0.0205	97.58	23.52	5.84
CM 70905	Haplorhini	Tarsiiformes	Omomyiformes	<i>Ourayia uintensis</i>	VivaCT 75	0.0205	90.06	16.89	4.89
CM 67297	Haplorhini	Tarsiiformes	Omomyiformes	<i>Shoshonius cooperi</i>	v/tome/x	0.00579413	96.77	2.77	1.90
CM 69756	Haplorhini	Tarsiiformes	Omomyiformes	<i>Shoshonius cooperi</i>	v/tome/x	0.01215219	95.77	3.23	2.09
UCM 64159	Haplorhini	Tarsiiformes	Omomyiformes	<i>Shoshonius ?</i>	v/tome/x	0.0116881	102.20	2.14	1.85
IRSNB M 1235	Haplorhini	Tarsiiformes	Omomyiformes	<i>Teilhardina belgica</i>	v/tome/x	0.00535529	103.23	1.45	1.63
USNM 540329	Haplorhini	Tarsiiformes	Omomyiformes	<i>Teilhardina brandti</i>	v/tome/x	0.00520299	103.72	1.36	1.77
USNM 539577	Haplorhini	Tarsiiformes	Omomyiformes	<i>Teilhardina brandti</i>	v/tome/x	0.00525944	100.20	1.47	1.91
AMNH 88817	Haplorhini	Tarsiiformes	Omomyiformes	<i>Tetonius sp.</i>	v/tome/x	0.007727105	99.17	2.83	2.03
AMNH 88818	Haplorhini	Tarsiiformes	Omomyiformes	<i>Tetonius sp.</i>	v/tome/x	0.01545421	95.50	2.25	1.86
UCM 56853	Haplorhini	Tarsiiformes	Omomyiformes	<i>Anemorhysis pearcei</i>	uCT 40	0.01	96.02	2.08	1.63
UCM 93768	Haplorhini	Tarsiiformes	Omomyiformes	<i>Anemorhysis pearcei</i>	v/tome/x	0.01115877	92.80	2.32	1.79
UCM 60901	Haplorhini	Tarsiiformes	Omomyiformes	<i>Anemorhysis pearcei</i>	uCT 40	0.01	98.60	na	1.64
UCM 62681	Haplorhini	Tarsiiformes	Omomyiformes	<i>Absarokius abbotti</i>	v/tome/x	0.0116881	103.60	3.83	2.27
UCM 64160	Haplorhini	Tarsiiformes	Omomyiformes	<i>Washakius insignis</i>	v/tome/x	0.0116881	96.90	3.35	2.24

TABLE A1. Continued

Specimen	Infraorder	Superfamily	Higher taxon	Species ID	Scanner	Scan res. (mm)	Fib (degrees)	Ect (mm ²)	Troch (mm)
UM 99074	Haplorhini	Tarsiiformes	Omomyiformes	<i>Washakius insignis</i>	uCT 40	0.01	96.80	3.23	2.09
UCM 72230	Haplorhini	Tarsiiformes	Omomyiformes	?	v/tome/x	0.0116881	106.00	2.20	1.80
ECA 1379	Strepsirrhini	Adapiformes	Adapinae	<i>Adapis parisiensis</i>	uCT 40	0.018	105.53	14.32	5.13
ECA 7377	Strepsirrhini	Adapiformes	Adapinae	<i>Adapis parisiensis</i>	uCT 40	0.018	105.74	13.32	4.86
ESC 936	Strepsirrhini	Adapiformes	Adapinae	<i>Adapis parisiensis</i>	uCT 40	0.018	113.98	12.60	4.46
MaPhQ 1390	Strepsirrhini	Adapiformes	Adapinae	<i>Adapis parisiensis</i>	uCT 40	0.018	109.72	18.98	4.94
MaPhQ nn	Strepsirrhini	Adapiformes	Adapinae	<i>Adapis parisiensis</i>	uCT 40	0.018	110.31	16.60	4.98
ROS 106	Strepsirrhini	Adapiformes	Adapinae	<i>Adapis parisiensis</i>	uCT 40	0.018	108.14	15.45	4.65
ROS 2708	Strepsirrhini	Adapiformes	Adapinae	<i>Adapis parisiensis</i>	uCT 40	0.018	108.95	17.75	4.61
ROS 290	Strepsirrhini	Adapiformes	Adapinae	<i>Adapis parisiensis</i>	uCT 40	0.018	109.55	na	4.53
QE 496	Strepsirrhini	Adapiformes	Adapinae	<i>Leptadapis magnus</i>	uCT 40	0.03	104.32	82.23	10.66
NMB QE 261	Strepsirrhini	Adapiformes	Adapinae	<i>Leptadapis magnus</i>	VivaCT 75	0.0205	108.61	62.53	8.70
MNH QU 11001	Strepsirrhini	Adapiformes	Adapinae	<i>Leptadapis magnus</i>	VivaCT 75	0.03	106.00	74.99	9.91
GU 747	Strepsirrhini	Adapiformes	Asiadapinae	<i>Asiadapis cambayensis</i>	uCT 40	0.015	100.37	6.88	3.17
GU 1641	Strepsirrhini	Adapiformes	Asiadapinae	<i>Marcgodinotius indicus</i>	uCT 40	0.015	105.57	3.60	2.07
GU 748	Strepsirrhini	Adapiformes	Asiadapinae	<i>Marcgodinotius indicus</i>	uCT 40	0.015	106.91	3.25	1.96
GU 749	Strepsirrhini	Adapiformes	Asiadapinae	<i>Marcgodinotius indicus</i>	uCT 40	0.015	109.71	3.71	2.10
DPC 21445C	Strepsirrhini	Adapiformes	Caenopithecinae	<i>Afradapis longicristatus</i>	uCT 40	0.01	116.39	18.96	5.51
USGS 16469	Strepsirrhini	Adapiformes	Nothartinae	<i>Cantius abditus</i>	v/tome/x	0.02649841	105.42	32.97	6.04
USGS 16583	Strepsirrhini	Adapiformes	Nothartinae	<i>Cantius abditus</i>	v/tome/x	0.03458816	102.38	31.70	6.42
USGS 21769	Strepsirrhini	Adapiformes	Nothartinae	<i>Cantius abditus</i>	v/tome/x	0.03458801	92.73	na	6.49
USGS 21772	Strepsirrhini	Adapiformes	Nothartinae	<i>Cantius abditus</i>	v/tome/x	0.02589531	99.82	na	6.25
USGS 21825A	Strepsirrhini	Adapiformes	Nothartinae	<i>Cantius abditus</i>	v/tome/x	0.03508375	106.96	30.86	6.08
USGS 6784	Strepsirrhini	Adapiformes	Nothartinae	<i>Cantius abditus</i>	v/tome/x	0.03458801	103.35	na	6.03
USGS 21761	Strepsirrhini	Adapiformes	Nothartinae	<i>Cantius mckennai</i>	v/tome/x	0.02649841	93.70	na	4.83
USGS 25029	Strepsirrhini	Adapiformes	Nothartinae	<i>Cantius mckennai</i>	v/tome/x	0.03269319	99.10	15.80	4.87
UF 254999	Strepsirrhini	Adapiformes	Nothartinae	<i>Cantius ralstoni</i>	v/tome/x	0.02589531	101.65	na	3.39
UM 87475	Strepsirrhini	Adapiformes	Nothartinae	<i>Cantius ralstoni</i>	v/tome/x	0.020735	94.68	15.18	4.34
USGS 21759	Strepsirrhini	Adapiformes	Nothartinae	<i>Cantius ralstoni</i>	v/tome/x	0.02649841	99.60	na	4.21
USGS 21831	Strepsirrhini	Adapiformes	Nothartinae	<i>Cantius ralstoni</i>	v/tome/x	0.02649841	103.18	na	4.37
USGS 21832	Strepsirrhini	Adapiformes	Nothartinae	<i>Cantius trigonodus</i>	v/tome/x	0.02649841	97.28	22.74	5.71
USGS 4724	Strepsirrhini	Adapiformes	Nothartinae	<i>Cantius trigonodus</i>	v/tome/x	0.03458816	103.12	na	4.85
USGS 5900	Strepsirrhini	Adapiformes	Nothartinae	<i>Cantius trigonodus</i>	v/tome/x	0.03458816	96.59	na	5.89
UCM 75066	Strepsirrhini	Adapiformes	Nothartinae	<i>Cantius trigonodus</i> ?	v/tome/x	0.02658225	101.00	18.21	5.33
UCM 76718	Strepsirrhini	Adapiformes	Nothartinae	<i>Cantius trigonodus</i> ?	v/tome/x	0.02658225	92.50	na	5.16
UCM 60918	Strepsirrhini	Adapiformes	Nothartinae	<i>Pelycodus</i> sp.?	v/tome/x	0.03920557	103.40	36.89	6.94
UCM 60920	Strepsirrhini	Adapiformes	Nothartinae	<i>Pelycodus</i> sp.?	v/tome/x	0.04202774	107.90	45.56	7.35
UCM 62671	Strepsirrhini	Adapiformes	Nothartinae	<i>Pelycodus</i> sp.?	v/tome/x	0.03920557	95.60	38.41	7.21
USGS 16468	Strepsirrhini	Adapiformes	Nothartinae	<i>Cantius frugivorus</i>	v/tome/x	0.03458801	110.43	na	5.46
AMNH 11478	Strepsirrhini	Adapiformes	Nothartinae	<i>Notharctus tenebrosus</i>	v/tome/x	0.02824787	108.51	na	7.00
AMNH 11478	Strepsirrhini	Adapiformes	Nothartinae	<i>Notharctus tenebrosus</i>	v/tome/x	0.02824787	109.22	33.12	7.08
AMNH 12570	Strepsirrhini	Adapiformes	Nothartinae	<i>Notharctus pugni</i>	v/tome/x	0.03090209	105.84	36.94	6.86
AMNH 129382	Strepsirrhini	Adapiformes	Nothartinae	<i>Notharctus tenebrosus</i>	v/tome/x	0.032153	101.43	28.67	6.30
AMNH 13024	Strepsirrhini	Adapiformes	Nothartinae	<i>Notharctus tenebrosus</i>	v/tome/x	0.02925508	106.99	na	7.12
AMNH 131955	Strepsirrhini	Adapiformes	Nothartinae	<i>Notharctus tenebrosus</i>	v/tome/x	0.03012555	108.98	23.61	6.20
AMNH11474	Strepsirrhini	Adapiformes	Nothartinae	<i>Notharctus tenebrosus</i>	uCT 40	0.03	108.01	28.09	6.12
UCM 65789	Strepsirrhini	Adapiformes	Nothartinae	<i>Notharctus tenebrosus</i>	v/tome/x	0.04202774	116.00	36.70	7.07
UCM 68994	Strepsirrhini	Adapiformes	Nothartinae	<i>Notharctus tenebrosus</i>	v/tome/x	0.04202774	107.70	na	7.93
UCM 70032	Strepsirrhini	Adapiformes	Nothartinae	<i>Notharctus tenebrosus</i>	v/tome/x	0.04202774	105.10	52.85	8.40
USGS 21782	Strepsirrhini	Adapiformes	Nothartinae	<i>Pelycodus jarrovii</i>	v/tome/x	0.03508375	99.09	na	7.96
AMNH 140725	Strepsirrhini	Adapiformes	Nothartinae	<i>Cantius nuniensis</i>	v/tome/x	0.03090209	117.72	na	6.86
AMNH 131763	Strepsirrhini	Adapiformes	Nothartinae	<i>Smilodectes gracilis</i>	v/tome/x	0.03090204	107.08	29.19	6.71
AMNH 131774	Strepsirrhini	Adapiformes	Nothartinae	<i>Smilodectes gracilis</i>	v/tome/x	0.03090204	109.07	29.06	6.93
Non-euprimate euarchontan outgroups									
UM 101963	stem-primates	Plesiadapiformes	Carpolestidae	<i>Carpolestes simpsoni</i>	uCT 40	0.01	98.20	2.51	2.08
USNM 442235	stem-primates	Plesiadapiformes	Paromomyidae	<i>Ignacius graybullianus</i>	uCT 40	0.01	90.55	2.67	2.07
UM 87990	stem-primates	Plesiadapiformes	Plesiadapidae	<i>Plesiadapis cookei</i>	uCT 40	0.018	100.41	17.30	5.14
UM 94816	stem-primates	Plesiadapiformes	Plesiadapidae	<i>Plesiadapis rex</i>	uCT 40	0.018	102.70	9.25	3.77
UNSM 15502	Non-primates	Non-primates	Dermoptera	<i>Cynocephalus volans</i>	VivaCT 75	0.0205	107.21	10.30	4.22
AMNH 207001	Non-primates	Non-primates	Dermoptera	<i>Cynocephalus volans</i>	VivaCT 75	0.0205	107.55	12.97	5.00
YPM 963	Non-primates	Non-primates	Dermoptera	<i>Cynocephalus volans</i>	uCT 40	0.018	111.08	5.02	3.12
USNM 481106	Non-primates	Non-primates	Ptilocercidae	<i>Ptilocercus lowii</i>	VivaCT 75	0.0205	93.84	1.45	1.45
USNM 488069	Non-primates	Non-primates	Ptilocercidae	<i>Ptilocercus lowii</i>	VivaCT 75	0.0205	96.36	1.46	1.47
USNM 488055	Non-primates	Non-primates	Ptilocercidae	<i>Ptilocercus lowii</i>	VivaCT 75	0.0205	97.69	1.47	1.43
AMNH 113135	Non-primates	Non-primates	Tupaiaidae	<i>Tupaia glis belangeri</i>	uCT 40	0.015	73.73	4.66	2.74
AMNH 215175	Non-primates	Non-primates	Tupaiaidae	<i>Tupaia</i> sp.	uCT 40	0.015	73.89	4.12	2.64
AMNH 215178	Non-primates	Non-primates	Tupaiaidae	<i>Tupaia</i> sp.	uCT 40	0.015	74.24	4.77	2.58

LITERATURE CITED

- Bajpai S, Kay RF, Williams BA, Das DP, Kapur VV, Tiwari BN. 2008. The oldest Asian record of Anthroproidea. *Proc Natl Acad Sci USA* 105:11093–11098.
- Beard KC, Dagosto M, Gebo DL, Godinot M. 1988. Interrelationships among primate higher taxa. *Nature* 331:712–714.
- Beard KC, Qi T, Dawson MR, Wang B, and Li C. 1994. A diverse new primate fauna from middle Eocene fissure-fillings in southeastern China. *Nature* 368:604–609.
- Bloch JI, Silcox MT, Boyer DM, Sargis EJ. 2007. New Paleocene skeletons and the relationship of plesiadapiforms to crown-clade primates. *Proc Natl Acad Sci USA* 104:1159–1164.
- Boyer DM, Patel BA, Larson SG, Stern JTT. 2007. Telemeasured electromyography of peroneus longus in *Varecia variegata* and *Eulemur rubriventer*: implications for the functional significance of a large peroneal process. *J Hum Evol* 53:119–134.
- Boyer DM. 2009. New cranial and postcranial remains of late Paleocene Plesiadapidae (“Plesiadapiformes,” Mammalia) from North America and Europe: description and evolutionary implications. *Stony Brook: Stony Brook University* 569 p.
- Boyer DM, and Bloch JI. 2008. Evaluating the mitten-gliding hypothesis for Paromomyidae and Micromomyidae (Mammalia, “Plesiadapiformes”) using comparative functional morphology of new Paleogene skeletons. In: Sargis EJ, and Dagosto M,

- editors. *Mammalian Evolutionary Morphology: A Tribute to Frederick S Szalay*. New York: Kluwer p 233–284.
- Boyer DM, Seiffert ER, Simons EL. 2010. Astragalar morphology of *Afradapis*, a large adapiform primate from the earliest late Eocene of Egypt. *Am J Phys Anthropol* 143:383–402.
- Charles-Dominique P. 1974. Ecology and feeding behaviour of five sympatric lorises in Gabon. In: Martin RD, Doyle GA, Walker AC, editors. *Prosimian biology*. London: Duckworth Co. Ltd. p 131–150.
- Dagosto M. 1985. The distal tibia of primates with special reference to the Omomyidae. *Int J Primatol* 6:45–75.
- Dagosto M. 1988. Implications of postcranial evidence for the origin of euprimates. *J Hum Evol* 17:35–56.
- Dagosto M. 1993. Postcranial anatomy and locomotor behavior in Eocene primates. In: Gebo DL, editor. *Postcranial adaptations in nonhuman primates*. DeKalb, IL: Northern Illinois University Press. p 199–219.
- Dagosto M, Gebo DL. 1994. Postcranial anatomy and the origin of the Anthropoidea. In: Fleagle JG, Kay RF, editors. *Anthropoid origins*. New York: Plenum Press. p 567–593.
- Dagosto M, Gebo DL, Beard KC, Ni X, Qi T. 2008. Primate tibiae from the middle Eocene Shanghuang fissure-fillings of eastern China. In: Sargis EJ, Dagosto M, editors. *Mammalian evolutionary morphology: a tribute to Frederick S. Szalay*. Dordrecht, The Netherlands: Springer. p 315–324.
- Dagosto M, Marivaux L, Gebo DL, Beard KC, Chaimanee Y, Jaeger JJ, Marandat B, Soe AN, Kyaw AA. 2010. The phylogenetic affinities of the Pondaung tali. *Am J Phys Anthropol* 143:223–234.
- Franzen JL, Gingerich PD, Habersetzer J, Hurum JH, von Koenigswald W, Smith BH. 2009. Complete primate skeleton from the middle Eocene of Messel in Germany: morphology and paleobiology. *PLoS ONE* 4:e5723.
- Gebo DL. 1987. Locomotor diversity in prosimian primates. *Am J Primatol* 13:271–281.
- Gebo DL. 1988. Foot morphology and locomotor adaptation in Eocene primates. *Folia Primatol* 50:3–41.
- Gebo DL. 1993. Functional morphology of the foot in primates. In: Gebo DL, editor. *Postcranial adaptations in nonhuman primates*. DeKalb, IL: Northern Illinois University Press. p 175–196.
- Gebo DL. 2011. Vertical clinging and leaping revisited: vertical support use as the ancestral condition of strepsirrhine primates. *Am J Phys Anthropol* 146:323–335.
- Gebo DL, Dagosto M, Beard KC, Qi T. 2001. Middle Eocene primate tarsals from China: implications for haplorhine evolution. *Am J Phys Anthropol* 116:88–107.
- Gebo DL, Dagosto M, Beard KC, Qi T, Wang J. 2000. The oldest known anthropoid postcranial fossils and the early evolution of higher primates. *Nature* 404:276–278.
- Gebo DL, Dagosto M, Rose KD. 1991. Foot morphology and evolution in early Eocene *Cantius*. *Am J Phys Anthropol* 86:51–73.
- Gebo DL, Smith T, Dagosto M. 2012. New postcranial elements for the earliest Eocene fossil primate *Teilhardina belgica*. *J Hum Evol* 63:205–218.
- Gingerich PD, Franzen JL, Habersetzer J, Hurum JH, Smith BH. 2010. *Darwinius masillae* is a haplorhine: reply to Williams et al. (2010). *J Hum Evol* 59:574–579.
- Godinot M. 1998. A summary of adapiform systematics and phylogeny. *Folia Primatol* 69 S1:218–249.
- Gunnell GF. 2002. Notharctine primates (Adapiformes) from the early to middle Eocene (Wasatchian–Bridgerian) of Wyoming: transitional species and the origins of *Notharctus* and *Smilodectes*. *J Hum Evol* 43:353–380.
- Gunnell GF, Ciochon RL. 2008. Revisiting primate postcrania from the Pondaung Formation of Myanmar. In: Fleagle JG, Gilbert CC, editors. *Elwyn Simons: a search for origins*. New York: Springer. p 211–228.
- Jacobs RL, Boyer DM, Patel BA. 2009. Comparative functional morphology of the primate peroneal process. *J Hum Evol* 57:721–731.
- Janečka JE, Miller W, Pringle TH, Wiens F, Zitzmann A, Helsen KM, Springer MS, Murphy WJ. 2007. Molecular and genomic data identify the closest living relative of primates. *Science* 318:792–794.
- Maiolino S, Boyer DM, Bloch JI, Gilbert CC, Groenke J. 2012. Evidence for a grooming claw in a North American adapiform primate: implications for anthropoid origins. *PLoS ONE* 7:e29135.
- Marivaux L. 2006. The eosimiid and amphipithecoid primates (Anthropoidea) from the Oligocene of the Bugti Hills (Balochistan, Pakistan): new insight into early higher primate evolution in South Asia. *Palaeovertebrata* 34:29–109.
- Marivaux L, Beard KC, Chaimanee Y, Dagosto M, Gebo DL, Guy F, Marandat B, Khaing K, Kyaw AA, Oo M et al. 2010. Talar morphology, phylogenetic affinities, and locomotor adaptation of a large-bodied amphipithecoid primate from the late middle Eocene of Myanmar. *Am J Phys Anthropol* 143:208–222.
- Marivaux L, Chaimanee Y, Ducrocq S, Marandat B, Sudre J, Soe AN, Tun ST, Htoon W, Jaeger J-J. 2003. The anthropoid status of a primate from the late middle Eocene Pondaung Formation (Central Myanmar): tarsal evidence. *Proc Natl Acad Sci USA* 100:13173–13178.
- Ni XJ, Meng J, Beard KC, Gebo DL, Wang YQ, Li CK. 2009. A new tarkadectine primate from the Eocene of Inner Mongolia, China: phylogenetic and biogeographic implications. *Proc R Soc B-Biol Sci* 277:247–256.
- Nunn CL. 2011. *The comparative approach in evolutionary anthropology and biology*. Chicago: University of Chicago Press.
- Orme CDL, Freckleton RP, Thomas G, Petzoldt T, Fritz SA, Isaac N, Pearse W. 2011. *caper: Comparative Analysis of Phylogenetics and Evolution in R*. Computer Program: Tracer v1.5.
- Pagel M, Meade A. 2011. *BayesTraits*. Reading, UK: University of Reading.
- Patel BA, Seiffert ER, Boyer DM, Jacobs RL, St. Clair EM, Simons EL. 2012. New primate first metatarsals from the Paleogene of Egypt and the origin of the anthropoid big toe. *J Hum Evol* 63:99–120.
- Rambaut A, Drummond A. 2009. Computer Program: Tracer v1.5.
- Roberts TE, Lanier HC, Sargis EJ, Olson LE. 2011. Molecular phylogeny of tree shrews (Mammalia: Scandentia) and the timescale of diversification in Southeast Asia. *Mol Phylogenet Evol* 60:358–372.
- Rose KD, Chester SGB, Dunn RH, Boyer DM, Bloch JI. 2011. New fossils of the oldest North American euprimate *Teilhardina brandti* (Omomyidae) from the Paleocene-Eocene Thermal Maximum. *Am J Phys Anthropol* 146:281–305.
- Ross C, Williams B, Kay RF. 1998. Phylogenetic analysis of anthropoid relationships. *J Hum Evol* 35:221–306.
- Sargis EJ. 2004. New views on tree shrews: the role of tupaiids in primate supraordinal relationships. *Evol Anthropol* 13:56–66.
- Seiffert ER, Perry JMG, Simons EL, Boyer DM. 2009. Convergent evolution of anthropoid-like adaptations in Eocene adapiform primates. *Nature* 461:1118–1121.
- Seiffert ER, Simons EL. 2001. Astragalar morphology of late Eocene anthropoids from the Fayum Depression (Egypt) and the origin of catarrhine primates. *J Hum Evol* 41:577–606.
- Springer MS, Meredith RW, Gates J, Emerling CA, Park J, Rabosky DL, Stadler T, Steiner C, Ryder OA, Janečka JE et al. 2012. Macroevolutionary dynamics and historical biogeography of primate diversification inferred from a species supermatrix. *PLoS ONE* 7:e49521.
- Strasser E. 1988. Pedal evidence for the origin and diversification of cercopithecoid clades. *J Hum Evol* 17:225–246.
- Sussman RW. 1991. Primate origins and the evolution of angiosperms. *Am J Primatol* 23:209–223.
- Szalay FS, Dagosto M. 1988. Evolution of hallucial grasping in the primates. *J Hum Evol* 17:1–33.
- Swofford DL. 1998. *PAUP* Phylogenetic analysis using parsimony (*and other methods)*, Version 4. Sunderland, MA: Sinauer Associates.
- Tornow MA. 2008. Systematic analysis of the Eocene primate family Omomyidae using gnathic and postcranial data. *Bull Peabody Mus Nat Hist* 49:43–129.
- Williams BA, Kay RF, Kirk EC. 2010. New perspectives on anthropoid origins. *Proc Natl Acad Sci USA* 107:4797–4804.
- Williams BA, Kay RF, Kirk EC, Ross CF. 2009. *Darwinius masillae* is a strepsirrhine: a reply to Franzen et al. (2009). *J Hum Evol* 59:567–573.